



ScuDo
Scuola di Dottorato ~ Doctoral School
WHAT YOU ARE, TAKES YOU FAR



Doctoral Dissertation
Doctoral Program in Civil and Environmental Engineering (32.th cycle)

Structural Health Monitoring Framework for Automatic Damage Detection based on IoT and Big Data Analytics

Application to a network of structures

Marzia Malavisi

* * * * *

Supervisors

Prof. Gabriele Bertagnoli, Supervisor
Prof. Fabio Di Trapani, Co-supervisor
Prof. Francesco Vaccarino, Co-supervisor

Doctoral Examination Committee:

Prof. Quaranta Giuseppe, University of "La Sapienza", Rome
Prof. Tubaldi Enrico, University of Strathclyde

Politecnico di Torino
March 31, 2020

This thesis is licensed under a Creative Commons License, Attribution - Noncommercial-NoDerivative Works 4.0 International: see www.creativecommons.org. The text may be reproduced for non-commercial purposes, provided that credit is given to the original author.

I hereby declare that, the contents and organisation of this dissertation constitute my own original work and does not compromise in any way the rights of third parties, including those relating to the security of personal data.

.....

Marzia Malavisi
Turin, March 31, 2020

Summary

Civil infrastructure facilities, such as bridges and tunnels, have a considerable impact on the economic, social and political growth of nowadays society. Such structural systems, due to their inherent vulnerability, may be affected by aging and degradation processes over time, which lead to a loss of the expected performances.

Structural Health Monitoring (SHM) has assumed a key role in the past two decades in the management of important civil infrastructures, since it could provide, on a continuous real-time basis, relevant information about the behavior of critical structures, recognizing unsafe conditions and predicting potential failures.

Nowadays, several techniques are available for recognizing damages in civil engineering structures, identifying any change in the intrinsic dynamic characteristics of a system. Indeed, a large number of damage identification algorithms have been developed over the years, from the simplest to the most sophisticated, capable of identifying even very small variations in the dynamic behavior of structures.

However, in most cases, the available techniques have been tested and applied to numerical case studies or, at best, to small structures with a limited number of devices. Moreover, no methodology has been developed to cope with the most critical aspects related to the need of monitoring a large number of structures, equipped with many sensors, and providing at the same time a monitoring service for reporting in real-time any anomaly in an automatic but reliable way.

This dissertation aims at providing a new methodology for the continuous and automatic monitoring of a large number of structures instrumented with many sensors, overcoming many of the issues related to the application and management of widespread monitoring systems. More in detail, this work has focused on the development and implementation of a data-based multi-level processing framework, adequate to extract relevant information about the behaviour of structures from continuous and long-term monitoring systems and automatically generate early-stage system health indicators without any detailed analysis of the monitored infrastructure. Furthermore, the multi-level approach, based on different levels of complexity, allows avoiding high computational costs and time while ensuring a robust and reliable damage detection service.

A numerical case study has been used for selecting the most reliable identification algorithm to be implemented in the monitoring framework. Afterwards, the robustness, reliability and efficiency of the proposed methodology have been validated through real case studies. Indeed, the multi-level approach has been applied for the long-term real-time monitoring of a significant number of structures under normal operating conditions. In particular, the implemented monitoring methodology was tested thanks to real damage scenarios occurred on two of the currently monitored structures. The first case study is a box composite highway bridge, strengthened by both internal and external prestressing, where all the features of the proposed methodology were applied and permitted to detect real damages occurred during the monitoring period. The second case study is a pre-stressed concrete bridge from the early 1965s, where real changes in structural stiffness were identified through the dynamic monitoring system in which the proposed methodology has been adopted.

The two significant case studies permitted to demonstrate both the usefulness and robustness of all the components included in the proposed methodology as well as the main advantages of the developed monitoring framework. The multilevel and data-driven method was in fact able to automatically generate system health indicators (effectively detecting structural damages) without any specific analysis on the monitored structures. Damage identification algorithms were combined with statistical analysis and machine learning approaches for detecting anomalous structural behaviours while avoiding high computational cost and time.

*I would like to dedicate
this thesis to my
brother*

*...the first step in our spiritual growth
has the form of a question...*

Contents

List of Tables	IX
List of Figures	X
1 Introduction	1
1.1 Research Context	1
1.2 Dynamic Monitoring	3
1.2.1 Experimental Modal Analysis	4
1.2.2 Operational Modal Analysis	5
1.3 Organization of Dissertation	7
2 State of Art	11
2.1 Structural Health Monitoring	11
2.2 Dynamic Monitoring	13
2.2.1 Frequency-based methods	15
2.2.2 Mode shape-based methods	16
2.2.3 Curvature-based methods	17
2.2.4 Other methods	18
2.2.5 Long-term dynamic monitoring	18
2.3 Research Objectives and Main Contribution	21
3 Dynamic Monitoring	25
3.1 Chapter Introduction	25
3.2 Signal Processing	26
3.2.1 Sampling frequency	27
3.2.2 Spectral leakage	28
3.3 Dynamic models	29
3.3.1 Spatial Model	29
3.3.2 Modal Model	30
3.3.3 State-Space Model	32
3.4 Theoretical background of OMA identification methods	34
3.4.1 Overview of OMA methods	34

3.4.2	Frequency Domain Methods	35
3.4.3	Time Domain Methods	41
3.5	Numerical case study	45
3.5.1	Numerical FEM Model	46
3.5.2	Results discussion	50
3.5.3	Final Considerations about OMA methods	56
4	Proposed Methodology	59
4.1	Chapter Introduction	59
4.2	Aim of the proposed Methodology	59
4.3	Monitoring system description	62
4.4	Acquisition and Storage Protocol	65
4.4.1	Thresholds definition - Principal Component Analysis (PCA) approach	70
4.4.2	Time-Window Size	74
4.4.3	Sudden Events Threshold	77
4.5	Multilevel damage detection procedure	80
4.5.1	First alert level - Sudden Events Threshold	85
4.5.2	Second alert level - Machine Learning Approach	85
4.5.3	Third alert level - Frequency in time	88
5	Continuous Monitoring - Case Studies 1	91
5.1	Chapter Introduction	91
5.2	Dynamic monitoring of a box composite highway bridge	91
5.3	Bridge Description	92
5.4	Monitoring System Description	95
5.4.1	Naming Convention	98
5.5	Preliminary analysis	100
5.6	Methodology	105
5.7	Monitoring Results	108
5.7.1	Statistical Analysis of Dynamic Signals	108
5.7.2	Environmental effects	110
5.7.3	Damage Detection	113
5.8	Final Remarks	126
6	Continuous Monitoring - Case Study 2	129
6.1	Chapter Introduction	129
6.1.1	Dynamic monitoring of a pre-stressed highway bridge	129
6.2	Bridge Description	130
6.3	Monitoring System Description	132
6.3.1	Naming Convention	134
6.4	Strengthening Works	135

6.5	Preliminary analysis	137
6.6	Monitoring Results	141
6.6.1	Statistical Analysis of Dynamic Signals	141
6.6.2	Monitoring during the strengthening works	144
6.7	Final Remarks	150
7	Conclusion	153
7.1	Main Outcomes	153

List of Tables

3.1	Natural Frequencies from FEM model	50
3.2	Natural Frequencies - PP results	52
3.3	Natural Frequencies - FDD results	53
3.4	Natural Frequencies - Cov-SSI results	55
3.5	Natural Frequencies - PolyMAX results	56
5.1	Geometric and mechanical characteristics of external pre-stressing tendons	93
5.2	Naming convention of all sensors installed on the bridge	100
5.3	Identified Natural Frequencies	101
5.4	Comparison between numerical and measured frequencies - odd sensors	103
5.5	Comparison between numerical and measured frequencies - even sen- sors	104
6.1	Naming convention of all the sensors installed on the bridge	136
6.2	Identified Natural Frequencies - Right spans	138
6.3	Identified Natural Frequencies - Left spans	138

List of Figures

1.1	Recent examples of bridge failures	2
1.2	Schematic description of the Experimental Modal Analysis method	4
1.3	Schematic description of the Operation Modal Analysis method . .	6
1.4	Organization of the dissertation	7
3.1	Aliased signal due to Undersampling	27
3.2	Quantization error	28
3.3	(a) Plan view and (b) elevation of the analyzed bridge	47
3.4	Cross-sections of the bridge: (a) A-A' section (b) B-B' section . . .	47
3.5	3D view of the FE model of the analyzed bridge	48
3.6	White noise signal used as input for the numerical model	48
3.7	Simulink block diagram used for simulating the system dynamics . .	49
3.8	Spectral envelope between the three measurement directions x, y and z: (a) Sensor located in the middle of the span; (b) Sensor located at left support	51
3.9	SVD diagram: (a) Sensor located at left support; (b) Both sensors (left support and middle of the span)	53
3.10	Comparison between different OMA identification methods: (a) Peak- Piking; (b) Frequency Domain Decomposition; (c) Covariance-driven Stochastic Subspace Identification Method; (d) PolyMAX	57
4.1	IoT Monitoring system overview	63
4.2	Acquisition and storage procedure	68
4.3	Principal Component Analysis. (a) PCA explanation in a two-dimensional feature space; (b) Projection of reconstruction error e_i	72
4.4	Principal Component Analysis example. (a) raw vibration data and corresponding STD values; (b) STD distribution	74
4.5	Boxplot of the InterQuartile Range (IQR)	78
4.6	InterQuartile Range (IQR) procedure	79
4.7	Proposed Multilevel damage detection procedure	83
4.8	Autoencoder architecture	86
4.9	Main processing steps of the third alert level - Evolution of natural frequencies	89

5.1	(a) Bridge 3D view. (b) Pictures of the bridge both under construction and in operating conditions.	93
5.2	Structural details of the bridge: plan view, elevation and two different cross-sections (at the bearings and on the centerline of the span).	94
5.3	External pre-stressing tendons layout. (a) External pre-stressing drawings; (b) picture of one anchorage of external tendons; (c) external tendons positioning inside the bridge.	95
5.4	Accelerometer coordinate system: (a) Signs convention; (b) Measurement axes (x, y, z) orientation	96
5.5	Sensor nodes positioning on the pre-stressing tendons	97
5.6	Tendons naming convention	98
5.7	Comparison between (a) Frequency Domain Decomposition and (b) Covariance-driven Stochastic Subspace Identification Method for frequency identification	101
5.8	Threshold values for one sensor installed on the structure	106
5.9	Acceleration time series collected from one sensor (a) during the night, (b) during the day.	108
5.10	Standard Deviation (STD) evolution in time.	109
5.11	Maximum and minimum acceleration values calculated over a time period of one month.	110
5.12	Correlation between temperature and frequency. (a) Temperature and Frequency evolution over time (b) Temperature vs Third natural frequency	111
5.13	Pearson Correlation Coefficient calculated for all the sensors	112
5.14	Third natural frequency evolution over time and relative histogram. (a) before removing the thermal influence (b) after removing the thermal influence	113
5.15	Sensors that exceeded the first level threshold during the earthquake (a) STD values, (b) Plan view	114
5.16	Frequency evolution over time - Section 2R	115
5.17	Acceleration time series collected during the earthquake (a) sensor 7L2, (b) sensor 2L2.	116
5.18	Reconstruction Error at the anomalous event - sensor 1L3	117
5.19	PSD calculated for tendon L3 before and after the anomalous event-Significant shift in fundamental frequency values	118
5.20	Frequency evolution over time - Section 1L - with zoom on sensor 1L3 which showed a significant shift in fundamental frequency values	118
5.21	Sensors that exceeded the T_{SE} threshold along the 3 measurements axes x, y, z. (a) Section 1, (b) Section 2	120

5.22	Inspections carried out in February 2018. (a) Inspected tendons, (b) localized increase in volume of the damaged tendon compared with safe one.	121
5.23	Sensors that exceeded the first level threshold during the tendon breakage (a) STD values, (b) Plan view	122
5.24	Acceleration time series related to the tendon breakage - Section 1 .	123
5.25	Acceleration time series related to the tendon breakage - Section 2 .	124
5.26	Broken tendon	124
5.27	Evolution of the STD values calculated for each sensor in the monitoring period from 01/10/2017 to 05/05/2018 - identification of three main events	125
6.1	Plan and elevation view of the monitored bridge	130
6.2	Cross-section of the monitored bridge	131
6.3	Bridge pictures	131
6.4	Damage evidences highlighted during visual inspections	132
6.5	Sensors positioning on the bridge - Plan and elevation view	133
6.6	Sensors positioning on the bridge - Cross-section	133
6.7	Sensors installed on the bridge	134
6.8	Measurement axes (x, y, z) orientation along the deck	134
6.9	External pre-stressing tendons installed for strengthening the structure	137
6.10	Comparison between (a) Frequency Domain Decomposition and (b) Covariance-driven Stochastic Subspace Identification Method for frequency identification	137
6.11	Results of the FDD analysis for the vertical and out-of-plane bending modes for L5 span	139
6.12	Comparison between PSD curves of some sensors installed on span L5 and L6 - axes x, y, z	140
6.13	Acceleration time series collected from one sensor (a) during the night, (b) during the day.	141
6.14	PDF of STD values collected along z axis during day and night hours - week and week-end	142
6.15	PDF of STD values collected from 01/06/2019 to 20/06/2019 - sensors L1.1 and L1.3; axes x, y, z	143
6.16	Boxplot of STD values along the z direction between 01/04/2019 and 30/04/2019; (a) sensors located at supports; (b) sensors located at mid-span	144
6.17	STD values along the z direction between 13/04/2019 and 25/04/2019; (a) sensors located at supports; (b) sensors located at mid-span	144
6.18	Reconstruction Error at the anomalous event - sensor L6.3	146
6.19	Frequency evolution over time at the reinforcement works	146
6.20	PSD calculated for the 3 measurement directions (x, y, z) before and after the strengthening works	147

6.21 Tilt measurements using a single axis of the accelerometer	148
6.22 Averaged acceleration data along y axis at the strengthening works	149
6.23 Deformed shape of the L6 span after the reinforcement works	150

Chapter 1

Introduction

1.1 Research Context

Civil infrastructure facilities, such as bridges and tunnels, have a considerable impact on the economic, social and political growth of nowadays society. Such structural systems, due to their inherent vulnerability, may be affected by aging and degradation processes, which can lead to a loss of functionality over time that turns into unsatisfactory structural performances under service loadings or accidental actions. The social and economic impact of structural deterioration of civil infrastructures is extraordinary high and highlights the importance of adequate maintenance, repair, and rehabilitation of structurally deficient systems.

Over the past few years, there have been a number of remarkable bridge failures, including the I-35W Mississippi River bridge which had a catastrophic breakdown during the evening rush hour on August 1, 2007, killing 13 people and injuring 145 and the most recent disaster of Polcevera Viaduct, in Italy, which failed on August 14, 2018, killing 43 people who were crossing the bridge at the time.

All these deadly incidents, mainly caused by structural deficiencies, lack of proper inspections and degradation, have significantly focused the attention of both designers and owners on the management and condition assessment of large infrastructures. To this end, a number of procedures, methodologies and tools have been implemented over the years in order to cope with the maintenance of the aforementioned existing structures.

Visual inspection techniques are the main methods currently used to evaluate the health of the majority of our infrastructures. However, the effectiveness of this kind of analysis is heavily influenced on the inspectors' experience and judgment and guarantees a very limited levels of accuracy, considering that only visible damages can be recognized.

A large study about the reliability of visual inspection for highway bridges has been conducted by Moore et al. [50], which have shown that this type of investigation does not consistently provide accurate results about the health state of



(a) Polcevera Viaduct

(b) I-35W Mississippi River bridge

Figure 1.1: Recent examples of bridge failures

a structure, despite being one of the predominant techniques used for assessing bridge conditions. This kind of non-destructive evaluation method is time consuming and cost inefficient and does not allow a continuous and effective inspection program, leaving a gap in knowledge about the performances and deterioration of infrastructures. In 2004, Phares et al. [54] investigated the accuracy and reliability of documentation generated during visual inspections, having the same bridge inspected independently by 100 experienced inspectors. A significant variability has been underlined by investigation results, proving the subjectivity of visual inspections and their poor reliability.

Structural Health Monitoring (SHM) is defined as the process of assessing the health state of a structure, detecting any change due to damage or deterioration as a function of time. SHM aims to provide, on a continuous real-time basis, relevant information about the behavior of critical infrastructures, recognizing unsafe conditions and predicting potential failures. SHM has gained the strong interest of the research engineering communities in the past two decades, thanks to the possibility of facilitating the routine inspection and maintenance activities and increasing at the same time the frequency and accuracy of the performed risk analysis. In particular, the structural behavior and the performances of a structure can be directly evaluated by processing real-time data collected by a network of sensors, which monitor the response of the structure under service loads. In this way, damage detection and characterization analysis can be performed in order to predict and assure the ongoing safety of the monitored system.

Sensors are the most elementary but at the same time fundamental elements of a SHM system. Indeed, they are installed in a structure to collect data about the most significant parameters able to describe the system response under stresses and loads, as well as some complementary information, such as environmental data (temperature, wind, etc...). A wide range of devices has been developed over the years to meet the needs of SHM. Depending on the purpose, the most used ones are fiber optic sensors, accelerometers, inclinometers, strain gauges, GPS sensors, etc..

The application of such devices on structures, combined with strong acquisition and process capabilities, allows the continuous assessment of the current state of system health and provides the possibility to evaluate the structural integrity after extreme events, such as earthquakes. However, despite all these undeniable advantages, SHM struggles to find a large-scale application mainly because of the high cost of the system devices, as well as the complex data management. In fact, installing and querying a large number of sensors, just like processing and archiving the enormous quantity of data generated, represents currently a big obstruction to the massive diffusion of monitoring systems.

Recently, thanks to the simple, yet efficient, design, Micro Electro-Mechanical Systems (MEMS) sensors, which have been initially employed for other applications, have demonstrated to be a suitable solution for SHM uses. MEMS devices have been employed since the 1990s for early-bird monitoring of civil infrastructures but only in recent years technology has improved considerably, leading to higher performances and limited costs. This allows designing inexpensive and distributed monitoring systems, easier to install and manage, in the view of creating a future in which each structure will be continuously and almost automatically monitored, from the construction until the end of its service life. The use of MEMS sensors for SHM applications finds consensus in the literature, with promising results about the reliability of these low-cost devices [16], [55], [7].

MEMS sensors may work in static and dynamic conditions, depending on the physical phenomenon to be observed and consequently on the parameters able to characterize it. Dynamic and static sensors, that is accelerometers and inclinometers, may be used for measuring vibration and displacement to which structures can be subjected. In particular, data collected by accelerometers are usually used to analyze the dynamic behaviour of a system subjected to varying load conditions over time (for example traffic load on a bridge). On the other hand, inclinometers allow measuring structural deflections or residual deformation on bridge-like structures, as well as the evolution of phenomena evolving slowly over time, such as the deformation of a tunnel section under a slope movement.

In this dissertation, different approaches for the analysis and interpretation of data acquired from dynamic SHM systems installed on civil infrastructures are presented. The implemented methodologies are then tested and applied for the analysis of data collected from a number of case studies, including highway bridges.

1.2 Dynamic Monitoring

Dynamic monitoring can be defined as the process of characterizing the behaviour of a structure through the study of vibrations induced by dynamic loads and/or ambient excitation on the system. Vibration-based techniques for SHM purposes have been studied since the early 1980s, mainly for applications to bridge

structures. In 1980 Richardson [59] presented an in-depth survey of the state of the art related to the damage detection approaches, based on modal analysis procedures. The survey showed that the application of vibration-based methodologies for civil structural monitoring was still at primordial levels, unlike industrial applications (for example for rotating machinery).

Dynamic methods are based on the awareness that structural changes caused by a damage result in a more or less noticeable change of the dynamic behavior of the structure itself. The basic idea is that modal parameters, such as frequencies, mode shapes etc., strongly depend of the physical properties of the system, namely mass, damping, and stiffness. As a consequence, any change in the physical properties of the structure will cause also changes in its modal properties. In view of these considerations, in the last decades the scientific community has focused its attention on the experimental identification of modal parameters, to get important insight about the dynamic performances of structures.

1.2.1 Experimental Modal Analysis

Experimental Modal Analysis (EMA) allows the identification of modal parameters from measurements of the vibration response of the structure subjected to controlled excitation forces. This type of analysis is carried out through a number of Forced Vibration Tests (FVT), which generate a vibration impact by means of shakers or hammers. EMA methods has gained more and more interest since the early 1970's, thanks to the introduction of the digital FFT processing [60]. The basic idea behind the EMA methods is that the response of a system exposed to an arbitrary vibration input can be obtained through the frequency response function multiplied by the input forcing function.

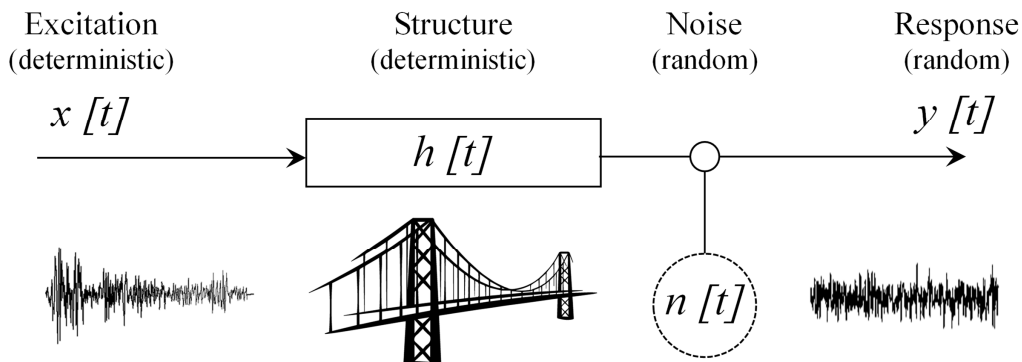


Figure 1.2: Schematic description of the Experimental Modal Analysis method

Figure 1.2 shows a schematic overview of the Input-Output approach. A random input force is applied to the system and causes all the modes of the structure to be

activated. As a consequence, the response is given by a linear combination of all the modes excited by the forcing function.

EMA has been extensively used over the years in different fields, especially automotive, industrial and aerospace engineering. However, the application of this methodology becomes more challenging in civil engineering, due to the larger size of the structures and the lower range of resonance frequencies. Indeed, it is extremely complex to apply a controlled and measurable input force to a civil structure, due to the high costs and dimensions of the necessary equipment. Furthermore, the analysis should be repeated over time, increasing even more the testing costs and considerably limiting the information about the structural behaviour between two consecutive tests.

1.2.2 Operational Modal Analysis

An attractive solution for the dynamic characterization of structures is offered by the Operational Modal Analysis (OMA), which allows avoiding the high costs and time-consuming EMA operations. OMA can be defined as *"the modal testing procedure that allows the experimental estimation of the modal parameters of the structure from measurements of the vibration response only"* [57]. In other words, OMA technique, also known as output-only approach, aims to use as input force the excitation given to the structure by all the loads (traffic, wind..) and ambient forces which act on the system under operating conditions. This means that the dynamic properties of the structure, mainly resonance frequencies, damping ratios and mode shapes, are extracted from the signal that represents the response of the system to a non-artificial and unknown input excitation. The advantages deriving from the use of this methodology are numerous, especially when dealing with civil engineering structures. First of all, OMA method is much less expensive than the traditional experimental modal analysis as there is no need to generate a known artificial input, which requires tests repeated over time using heavy and large dedicated equipment. Moreover, ambient modal identification can be performed quickly (also in real-time), since random excitation is freely available during operational conditions and tests do not interfere with the regular use of the structure. Figure 1.3 shows a schematic overview of OMA method.

As described in Figure 1.3, according to OMA methods, the structure, which is assumed to be deterministic, linear and time invariant, is excited by a random input, such as wind, traffic, rail irregularities ect... The measures output includes the response of the structure under the aforementioned input as well as a stochastic noise given by environmental effects and disturbances, instrument noise, discretization noise and so on.

One of the most important implications of OMA methods is the possibility of performing a reliable damage detection on civil infrastructures. In practice, this implies the permanent installation of a set of accelerometers on the structure and

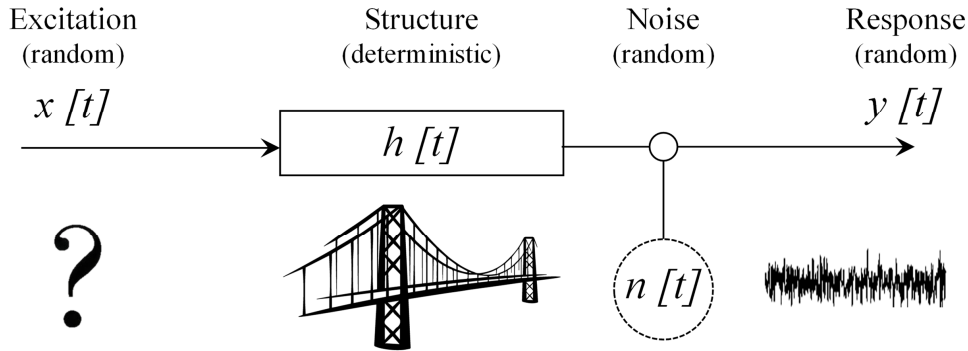


Figure 1.3: Schematic description of the Operation Modal Analysis method

the development of dedicated algorithms to extract modal parameters, in order to track their evolution over time. Unlike EMA methods, processing of data coming from environmental excitation is more challenging because of the unmeasured and unknown operational loads. Indeed, particular attention must be paid to signal noise and environmental influences on sensors output, in order to avoid the erroneous identification of the dynamic parameters. Therefore, the need of developing robust and powerful algorithms has become increasingly evident, with the aim of performing an automatic and reliable processing of a large number of data collected in real-time from the monitoring system, taking into account the environmental changes (temperature, wind, etc.) which can lead to variations in the dynamic response of the structure. In recent years, many steps forward have been made regarding the data processing topic but some improvements are needed to make the elaboration of the signal coming from sensors more straightforward, automatic and trustworthy. This means that an efficient OMA approach must take into account at least the following steps:

- collecting and storing vibration data coming from sensors, under excitation sources which are assumed of white noise-type;
- applying one or more OMA methodologies for the identification of the selected dynamic parameters;
- removing environmental influences, such as temperature, humidity, etc., on the modal parameters;
- evaluating the evolution of such parameters over time and detecting any anomalies in the monitored structure.

Based on the above-mentioned considerations, some applications of the dynamic SHM methods on existing structures will be presented in this dissertation, in order

to highlight all the advantages of these approaches and underline their performances when applied to full-scale structures.

1.3 Organization of Dissertation

This dissertation presents a methodology developed for the continuous dynamic monitoring of civil engineering structures, in particular bridges. The main goal is showing how to automatically and effectively process and use data generated by a monitoring system, for understanding the performance characteristics of the monitored structure and detect any abnormal behaviour. The dissertation is organized as follows. Moreover, the logical relationship between chapters is illustrated in the Figure 1.4.

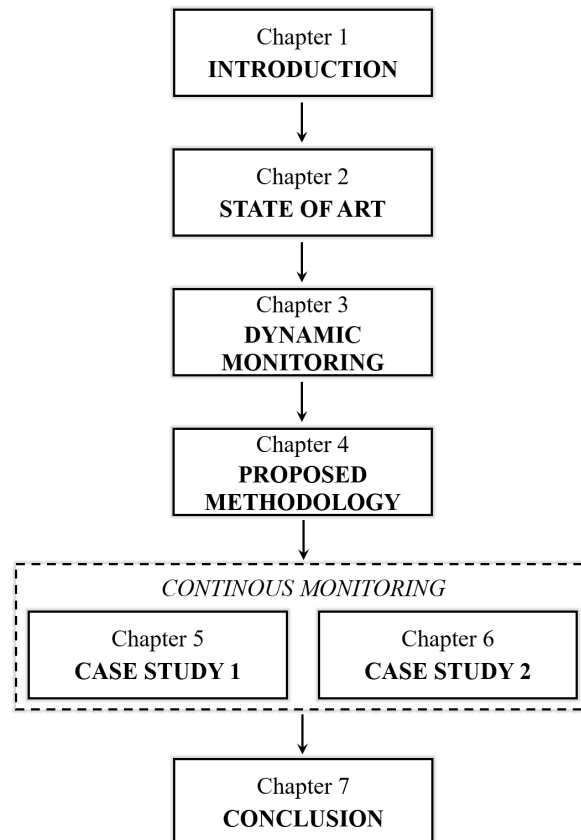


Figure 1.4: Organization of the dissertation

Chapter 1

It introduces the subject of this thesis, contextualizing the research field in which it develops. More in detail, the aging of structures issue is described, with a special focus on maintenance and inspection techniques currently used to evaluate the health of the majority of existing infrastructures. Structural Health Monitoring (SHM) process is presented as an alternative method for assessing the behaviour of a structure and detecting any change during its life. Special attention is paid to dynamic monitoring, which can be defined as the process of characterizing the behaviour of a structure through the study of vibrations induced by dynamic loads and/or ambient excitation on the system.

Chapter 2

It provides an overall description of the background of this work. In particular, previous research in the SHM area are underlined through an extensive review of the most impactful studies related to SHM methods and applications. An overview of vibration-based damage detection techniques is illustrated, followed by a detailed description of some of the most used frequency domain methods. Subsequently, particular attention has been paid to the literature related to long-term monitoring systems, able to continuously detect the evolution of damages over time. Finally, based on the literature review, the main objectives and contribution of this work have been highlighted.

Chapter 3

It defines the theoretical background behind some of the main used dynamic identification methods, as well as some of the most common pre-processing techniques for data coming from sensors installed on real structures. Afterwards, the application of these methodologies on a numerical case study is shown, in order to highlight advantages and drawbacks of each method.

Chapter 4

It describes and motivates the need for developing a new methodology for continuous and long-term monitoring of a network of structures, equipped with a large number of sensors. A multi-level damage detection methodology is presented, with the aim of highlighting the reliability, efficiency and robustness of the proposed approach. The first part relates to a data acquisition and storage procedure for efficiently collect data from sensors and discard those deemed to be lacking in information. Secondly, a strategy for elaborating a large amount of data in the shortest possible time is explained. Afterwards, the multi-level damage detection procedure, based on three different levels of alarm, is described. Special attention has been

paid to the interaction between different sites of computational capability, which allow the implementation of a reliable and computationally inexpensive monitoring framework for an early damage detection.

Chapter 5

It presents a complete description of the monitoring system installed on a highway composite box girder located in Italy. This case study has been used to demonstrate the reliability and robustness of the proposed methodology, described in Chapter 4, which allowed the identification of a real damage scenario occurred in the structure during the monitored period.

Chapter 6

It summarizes a meaningful case study of continuous monitoring system applied on a pre-stressed concrete highway bridge. This application shows the potentiality of the implemented methodology in identifying any anomalous condition in real operating bridges. More in detail, during the monitoring period, the structure has been subjected to strengthening works, which of course stiffened the structure, changing its intrinsic properties. Therefore, a very clear representation of the state of the structure before and after the restoration works has been provided by using the developed methodology, giving a very complete test of the implemented approach.

Chapter 7

It summarizes the main results of this dissertation, focusing on the most relevant outcomes obtained by applying the proposed methodology to real operating structures. Moreover, some future research topics are pointed out, in order to outline the plans for future developments in this area.

Chapter 2

State of Art

This chapter illustrates the key findings collected over the years from the literature, in order to provide a comprehensive state of the art related to SHM methods and applications. For this purpose, a extensive review of the most impactful studies has been conducted to highlight the main results obtained as well as to create a coherent overview on the most relevant aspects of the field. On the other hand, literature shortcomings are also underlined, with the aim of clearly define the overall purpose of the present research work.

More in detail, in a first section of this chapter the main steps of structural health monitoring have been reviewed with particular focus on highway bridge applications. Then, specific attention has been paid on vibration-based SHM methods, mainly used for the case studies described in this dissertation and being the research topic that has gained much interest from the scientific community in the last three decades. Static monitoring applications have also been analyzed, summarizing the current state-of-the-art related to the use of static measurements. Finally, particular requirements and constraints associated with the implementation of monitoring systems are analyzed, highlighting advantages and disadvantages of the available technologies and methods.

2.1 Structural Health Monitoring

Structural Health Monitoring (SHM) can be defined as the process of implementing a damage identification strategy for a mechanical or civil engineering structure, in order to determine the current state of system health [26].

Structural Health Monitoring starts to grow and develop since the 1980s, following some tragic bridge failures (Chester Bridge - Illinois, Autobahnbrücke Frankenthal Bridge - Frankenthal, Tacoma Bridge - USA etc...), that focused the attention on the vulnerability of civil engineering infrastructures and on the need of monitoring their health state over time. In 1985 Collacott [18] provides a large overview

of the main consequences of disasters affecting mechanical, aeronautical and civil structures. In particular, he concentrated on the awareness that the functional life of structures is limited in time and thus, it is essential to ensure their integrity over the years. The traditional way of identifying any structural damage or deficiency and therefore to guarantee the integrity of systems were and still are visual inspections. However, as mentioned in Chapter 1, visual inspections, as well as other experimental techniques, present several drawbacks, such as the need to know a priori the position of damages, the impossibility of inspecting the not accessible portions of the structure, the limited accuracy level of the inspection results and the very long times and high costs of each operation [50]. Moreover, traditional visual inspection-based methods allow to identify only damages which are visible from the outer surface of the structure; this means that all the structural deficiencies that do not cause external evidences, such as for example the breakage of precompression cables or early stage of corrosion in steel reinforcement bars, cannot be identified by visual inspections. For all these reasons, a more global inspection approach has come forward over the years, proposing a damage detection methodology that evaluates changes in some significant parameters of the structure, which are able to provide useful information about the health state of the monitored system. The development of structural health monitoring technology implicates the coexistence and integration of several fields of study including sensor electronics, signal processing and interpretation, structural knowledges, material science, etc...

The first research studies concerning the possibility of correlating a physical damage with the variation of some significant parameters focused on the dynamic properties of structures. Richardson [59] in 1980 reviews some results related to the young concept of structural health monitoring, applied mainly to nuclear power plants, rotating machinery and offshore platforms. He concentrated especially on the hypothesis that changes in the vibration modes of a structure indicate modifications in physical properties like mass, stiffness and damping. However, the author asserted that the effort of correlating structural failures to variations in dynamic properties of a system was still in its early stages at that time.

This topic has been a subject that has draw considerable attention by the scientific community in the '70s and '80s. An extensive literature is available in these years concerning the detection of damages using changes in dynamic properties of systems; in particular, several methods have been considered as effective for health monitoring. A detailed state of the art on structural health monitoring has been published by Doebling et al. [22] in 1996. In this research work, authors have summarized the most significant contributions found in literature by 1996, including some early papers published on the topic.

While changes in the dynamic properties induced by structural damages were investigated, other alternative forms of monitoring have been developed over the years. Special interest has been deserved for the so called static monitoring, in which the observed quantities evolve slowly in time (few months or few years). The

most common monitored parameters are displacements, tilts, deformations, cracks amplitude etc...They can be used to evaluate variations in the behaviour of the analyzed structure and/or in the material properties. A great number of methods and technologies are available for monitoring such quantities. However, more attention has been paid to the use of mechanical parameters as representative of the health state of a structure. Glisic and Inaudi [32] describes a structural monitoring system based on fibre-optic sensor technologies applied to a number of case studies. Fibre-optic sensors are used to measure strain, temperature, inclination, and load measurements with the aim of assessing the health condition of existing structures.

In 2006, DeWolf et al. [21] published an extensive report regarding a large-scale research program carried out by the Connecticut Department of Transportation and the University of Connecticut starting from 1994. In particular, four bridges of different structural type were instrumented with a long-term monitoring system, with the aim of better understand the behavior of bridges under operating conditions. Both strain and acceleration were monitored by using tiltmeters, strain gages and accelerometers. Results showed how both static and dynamic measurements provided useful information for characterizing each bridge and its behavior.

As stated before, a considerable amount of literature has been published over the past 30 years on structural health monitoring and damage identification topic. The field of study is very broad and comprises a large number of methods and applications; in this dissertation a more detailed analysis will be conducted only on methods that affect this research, neglecting those that are not directly applied. In light of this, the following paragraphs will present an analysis of the main procedures connected to dynamic and static structural monitoring, by using accelerometers and clinometers for bridge applications, respectively.

2.2 Dynamic Monitoring

In the last 30 years, SHM has gained the increased interest of the scientific community, especially with regards to vibration-based monitoring methods. Vibration-based monitoring methods can be define as all the "in situ non-destructive analysis of system characteristics – in the time, frequency or modal domains – for the purpose of detecting changes, which may indicate damage or degradation" [12]. The first applications of this approach has been registered for rotating machinery and only few years later it was also applied to civil engineering structures. The main concept behind the vibration-based monitoring method is that any damage that occurs in a structure causes a change in its physical parameters, such as stiffness, mass, or damping. Hence, detectable variation of dynamic properties of the system (natural frequencies, modal damping, and mode shapes) can be identified and evaluated in order to detect the damage. This means that if the structural response under a external random excitation is measured, modal properties can be

determined and evaluated in time. In fact, if the dynamic response of a system subjected to an external input is given by the following equation:

$$M\ddot{u} + C\dot{u} + Ku = F(t) \quad (2.1)$$

where M , C and K are respectively the mass, damping and stiffness matrices of the considered system and u is the displacement, is it possible to convert this equation from the time domain to frequency domain using the Fourier transform:

$$S(\omega) \cdot x(\omega) = F(\omega) \quad (2.2)$$

where:

$$S(\omega) = -\omega^2 M + i\omega C + K \quad (2.3)$$

is the system matrix, that depends only on frequency ω ; $x(\omega)$ and $F(\omega)$ are respectively the nodal degrees of freedom and nodal forces.

In light of this, any damage in a physical property of the structure will reflect in a change to the modal characteristics (natural frequencies, mode shapes, and modal damping values), according to the transformation illustrated in equation 2.2.

For the case studies illustrated in this dissertation, particular reference will be made to response-based methods, which depend only on data coming from sensors, that differ from model-based methods, which are based on a detailed numerical model of the structure [25].

Several methods have been developed for the identification of global damages in a structure. In particular, frequency domain methods and modal methods, which extract modal informations from frequency domain data, are the most used in literature because they are easier to be interpreted and than more attractive for potential practical applications. Alongside these two methods, time domain approaches also exist but are used less frequently. However, none of these methods (time, frequency and modal domain) is capable of solving all the damage detection problems exhaustively; therefore, the research field is still widely open.

Frequency and modal domain methods have been extensively applied when experimental modal analysis took its first steps in the world of damage detection. Then, when Operation Modal Analysis walked into the structural health monitoring field, they developed further, together with some time domain methods.

Some extensive review on vibration-based damage detection methods have been published over the years; reference can be made to [25], [12], [22], [63] for a more detailed state of the art on the topic. Hereinafter a summary of the main methods in the frequency domain is illustrated, according to what has been developed in this research work. In particular, the following methods are analyzed:

- Frequency-based methods;
- Mode shape-based methods;
- Curvature-based methods;
- Other methods.

2.2.1 Frequency-based methods

Frequency-based approach is one of the first method used for damage detection. It is based on the awareness that changes in physical properties of structures reflect in a shift of natural frequencies, which are inherent characteristics of a system. In particular, numerous studies have shown that natural frequencies decrease if a damage occurs. This method has several advantages being exploitable by using a very small number of sensors, which means low costs and reduced measurement times. On the other hand, frequencies can provide in most cases only informations about the overall health state of the structure and are unable to identify localized damages [61]. Moreover, in order to be able to appreciate a failure of reduced dimensions, very precise measurements are required; otherwise, no significant frequency shifts are registered [28]. However, there are examples where, after the removal of environmental effects, even very small frequency variations were appreciated, as in the case of the Z24 bridge [52].

The frequency domain method can be divided into two different approaches: a forward problem and an inverse problem.

The Forward Problem

The forward problem, as most engineering problems, aims at estimating the output of a known system subject to a given excitation force. In other words, the natural frequency variations are calculated for a given damage in a known structure. Damages are generally simulated through a mathematical model and the corresponding decrease in natural frequencies is compared with that obtained from in situ tests. This approach constitutes the theoretical foundation for the application of the subsequent inverse problem.

The Inverse Problem

The inverse problem is aimed at calculating the state of a structure knowing the system response to a given input. More specifically, if measurements in some points of the structure are available, damage location and size can be obtained through this method. The inverse problem has its roots in the late 1980s, when Adams et al. [3] introduced the concept of identifying damages in a structure by

measure natural frequencies in time. This method is actually the most commonly used, even if it retains all the limitations of a frequency-based approach.

2.2.2 Mode shape-based methods

Mode shape-based methods consist in extracting from the mode shapes of a structure useful information about possible damages affecting the structure itself. This method has several advantages when compared with frequency-based method. Firstly, it allows the identification of both global and local damages, since mode shapes are more sensitive to local variations than frequencies and thus they can be used to localize the failure. Moreover, the influence on mode shapes of environmental effects, such as temperature, is lower compared to frequencies. This means that closely spaced modes can be discerned and analyzed [29]. On the other hand, this method is certainly more expensive and time consuming with respect to the previous one, since a series of sensors is needed to be able to reconstruct the modes.

The introduction of this method led to the need of validating the experimental modal model that generates from measured data. For this purpose, different assurance criteria have been developed over the years [4]. All the proposed criteria are applicable for comparing theoretical vs measured data as well as measured vs measured data. Among all, MAC and COMAC criteria are the most frequently employed ones.

MAC Criteria

The Modal Assurance Criteria (MAC) [5] evaluates the correlation between two different mode shapes. In particular, the MAC value between the mode i from a dataset A and the mode j from a dataset B is obtained through the following equation:

$$MAC(\phi_{Ai}, \phi_{Bj}) = \frac{|\phi_{Ai}^T \phi_{Bj}|^2}{(\phi_{Ai}^T \phi_{Ai})(\phi_{Bj}^T \phi_{Bj})} \quad (2.4)$$

Equation 2.4 can assume values ranging from 0 to 1, where 1 indicates the strongest possible relationship between the two modes and 0 means the strongest possible disagreement. Therefore, the evaluation of MAC coefficient can be assumed as a good damage indicator. Indeed, if the MAC value calculated between modes in the dataset A and those of the dataset B decreases in time, it might be possible that a damage is evolving in the structure.

COMAC Criteria

The Co-ordinate Modal Assurance Criterion (COMAC) is an extension of the Modal Assurance Criterion and has been introduced by Lieven and Ewins [41] in 1988. Unlike the MAC, the COMAC compares different modes for the same location point, with the aim of identifying which measured mode shape is responsible for a low MAC value. It can be obtained by the following expression:

$$COMAC(i) = \frac{\left[\sum_{j=1}^N (\phi_{Ai})_j (\phi_{Bi})_j \right]^2}{\sum_{j=1}^N (\phi_{Ai})_j^2 \sum_{j=1}^N (\phi_{Bi})_j^2} \quad (2.5)$$

where i indicates one measurement location, N is the number of mode pairs that have been correlated and A and B are the two sets of mode shapes to be compared (A and B are obtained at different time moments and compared to detect anomalies). It takes values from 0 to 1, as for the MAC, where 0 indicates no correlation and 1 maximum correlation. In particular, if COMAC value is low for a single point of the structure, it possibly identifies a damage in that specific location.

Both MAC and COMAC can be used as useful tools for indentifying damages in a structure. However, some limitations must be underlined. Indeed, MAC values are less sensitive to localized damages since correlations between mode shapes are calculated by averaging data from all the measurement points; this means that if a single point shows a higher difference, it is hidden by the remaining points [2]. On the other hand, although COMAC is a good tool for identifying localized damages, it is unable to detect global failures that evolve slowly over time.

2.2.3 Curvature-based methods

Based on the aforementioned shortcomings of both frequency-based and mode shape-based methods, the scientific community has focused on researching methods that would be more sensitive to both localized and global damages. In 1991, Pandey, Biswas, and Samman [51] introduced the Mode Shape Curvature (MSC) method, which consists in calculating the second derivative of the displacement mode shapes. More in detail, the MSC values are obtained using a central difference approximation, as shown in equation 2.6.

$$\kappa_i = \frac{(u_{i+1} + u_{i-1} - 2u_i)}{L^2} \quad (2.6)$$

where u represent che displacement mode shape and L the distance between two consecutive measurement points.

This method results to be more sensitive to localized damages as well as global

ones. Nevertheless, this method has the drawback of needing at least one measurement point in the vicinity of the damage. This implies that, since the location of the damage is unknown, a large number of measurement points are necessary. Moreover, the derivative introduces a large of numerical noise in the final result and, without proper numerical strategies, results are almost useless.

2.2.4 Other methods

In addition to the methods illustrated above, other damage detection methods have been developed over the years. All these approaches will not be described in this dissertation; the most relevant ones are just mentioned below.

Among all the proposed methods, of particular interest are: Modal Flexibility Method, which uses variations in modal flexibility for damage detection; Modal Stiffness Error Method, that calculates an error matrix in function of the flexibility change in the structure and the initial stiffness matrix; Model Update Methods, whose purpose is to find damages by updating mass, stiffness and damping matrices to reproduce as closely as possible experimental data; Optimization Methods, that aim to solve damage detection problems as an optimization problem, maximizing or minimizing an objective function based on modal variables.

2.2.5 Long-term dynamic monitoring

All the above-mentioned methods have been widely used and applied over the years to test their effectiveness in identifying localized or global damages in civil infrastructures. It is thus available an extensive literature, which confirms that the use of these methods, applied individually or combined together, allows the identification of damages in civil engineering structures.

However, in recent years (since 2000 approximately) the scientific attention has increasingly focused on long-term and automatic monitoring systems. In fact, since damage detection techniques are able to detect the evolution of damages over time, interest has moved to the application of these methodologies to assess the health state of existing structures continuously. In particular, with the introduction of output-only modal identification approaches in place of the most traditional experimental modal analysis (ref. Chapter 1), the identification of the dynamic parameters can be performed without the need of exciting the structure with a controlled input force, by using only the response of the system subject to an unknown and random input. Thus, an effort as been made for monitoring structures, such as bridges, for long-term periods, using normal operating condition loads (traffic, wind, earthquake, etc.) as the main source of excitation.

One of the first and most relevant long-term applications of the last 20 years concerns the Z24 bridge, located in Switzerland, which has been monitored during

the year before demolition. In particular, Krämer, De Smet, and De Roeck [38] explained that this bridge was used as a test field for two main purposes: the first one was validating the damage detection procedures available for civil engineering structures while the second one was to assess the influence of environmental factors on bridge dynamics. The bridge was progressively damaged over a month, measuring the evolution of the damage with a series of sensors installed on the structure. Maeck, Peeters, and De Roeck [45] showed that natural frequencies along with modal displacements and their derivatives are good indicators of failures. In particular, modal parameters were obtained automatically from the response data through the stochastic subspace identification technique and the stabilisation diagrams, and their evolution in time was evaluated [39]. Modal curvature was also used as damage identification method, showing promising results especially for the lower modes [67]. Moreover, Peeters and De Roeck [52] investigated the influence of environmental parameters on the evolution of bridge dynamic characteristics in time. They discussed that temperature had a significant influence on the eigenfrequencies while other factors such as wind, rainfall and humidity showed a negligible effect.

The growing interest for long-term monitoring systems was addressed by Ko and Ni [37], which highlighted all the technical and technological challenges of installing a system that requires interdisciplinary skills such as sensors technology, communication, signal processing, system dynamics, data management, etc. More in detail, Ko and Ni [37] stated that progress has been made in the application of long-term monitoring systems; however, many aspects still remain open and thus they have to be further explored.

In 2006, Lynch et al. [44] evaluated the use of a network of wireless sensors for monitoring the Geumdang Bridge, Korea. This technology seemed to be cost-effective and allowed data processing directly at the wireless sensor, which is certainly a great advantage in terms of elaboration times. However, the application of the described technology has been limited to a total number of 14 sensors for a short-term utilization; in particular it has been adopted to record two sets of forced vibration tests. Thus, despite having a number of advantages, this application is not suitable for long-term monitoring of full scale structures. In fact, to accomplish a long-term usage, some improvements have to be introduced. Moreover, it adapts well only to structures with a reduced number of sensors; if not, the wireless bandwidth saturates and data processing can no longer be performed.

Another interesting example regarding the use of wireless sensors for civil engineering applications is presented by Zimmerman et al. [70]. As well as for the aforementioned research work [44], the competitive costs together with data processing capabilities provide undoubted advantages for wireless sensor systems with

respect to the traditional tethered systems. In particular, authors performed three different output-only methods on a number of processors embedded within a network of wireless sensors. Nevertheless, as pointed out before, the long-term applicability and the extension to a large number of sensors is still a challenge for this technology.

A long term monitoring application has been presented by Cigada et al. [17], in 2008. In order to evaluate the health state of a high capacity civil structure, such as the G. Meazza stadium in Milan, ambient vibration measurements have been performed over a year. Structure dynamic has been evaluated in terms of natural frequencies, modal shapes and damping factors by using OMA techniques. Since the amount of data to be analyzed was large, data processing were performed to all time windows which recorded significant vibrational levels.

Soyoz and Feng [64] illustrated a long-term monitoring system installed on a new concrete bridge located in Irvine, California. This bridge was instrumented by 13 wireless accelerometers about four years before it was opened to traffic. A total of 5 years have been monitored, trasmitting real-time data every time vibration levels exceeded a preset threshold. During the 5 years of monitoring, an high variation in natural frequencies was observed due to both the influence of moving vehicles and environmental effects (temperature and moisture). This study is of particular interest because it represents one of the first long-term monitoring attempts with automatic and real-time data processing.

An equally interesting example of long-term monitoring of bridge structures is shown by Magalhães, Cunha, and Caetano [46]. Authors describe a continuous monitoring system installed on a concrete arch bridge located in Porto, Portugal. Different methodologies were used to identify structural anomalies in real-time. Dynamic parameters were evaluated over 2 years, thanks to the use of automatic identification algorithms. However, damage detection was performed by comparing data from sensors to a numerical model; this represents a limitation since numerical models contain inherently some uncertainties which make the problem no longer well-defined.

Ubertini, Gentile, and Materazzi [65] showed, using experimental data from two Italian bridges, a fully automated identification method suitable for the continuous processing of data coming from long-term monitoring systems. In particular, the dynamic characteristics of the investigated structures have been studied through a cluster analysis, which proved to be a reliable tool for real-time automated structural monitoring.

Significant results have also been obtained by other authors in recent years, as

for example [11], [47], which have shown how the interest in long-term and almost automatic structural health monitoring systems is growing.

An equally significant effort has been made to apply machine learning algorithms for structural health monitoring. An extensive and in-depth work about the advantages deriving from the application of machine learning techniques has been published by Farrar and Worden [27] in 2012. Authors investigated the use of methods such as neural networks, genetic algorithms, supervised and unsupervised machine learning algorithms and support vector machines for detecting structural changes in civil engineering infrastructures. These techniques are very useful for automatic and blind detection of damages; indeed, they are a still open field of research.

2.3 Research Objectives and Main Contribution

Paragraphs 2.1 and 2.2 illustrated the key findings available in the scientific literature related to structural health monitoring and, more particularly, to dynamic monitoring methods and applications. Over the years, numerous studies have been carried out on the techniques that can be used to recognize damages in civil engineering systems, analyzing all the parameters which are most sensitive for identifying variations in the intrinsic dynamic characteristics of a system. Indeed, a large number of damage identification algorithms have been developed, from the simplest to the most sophisticated, capable of identifying even very small variations in the dynamic behavior of a structure. However, in most cases, these techniques have been tested and applied to numerical case studies or, at best, to real small structures with a limited number of sensors.

In recent years, an effort has been made towards continuous monitoring systems, which try to apply the developed damage detection methodologies to assess the health state of existing structures in real-time. Nevertheless, literature is currently lacking in real applications of widespread monitoring systems, with a large number of sensors, continuously active under normal operating conditions for long periods of time (see paragraph 2.2.5). Specifically, there are no examples of monitoring systems capable of generating, in case of anomalies, automatic alarms, which would turn in management actions on the structure. The crucial point lies precisely in the comparison between what has been developed over the years from a theoretical point of view and its applicability in the real world, where false alarms are not acceptable, in the same way that the occurrence of damages cannot be overlooked. Indeed, very few works describe real data, regularly collected along several years by reliable continuous dynamic monitoring systems installed on bridge structures. Above all, no methodology has been developed to cope with the most critical aspects related to the need of monitoring a large number of structures, equipped with many

sensors, and providing at the same time a monitoring service for reporting in real-time any anomalies in an automatic but reliable way.

Based on all these considerations, the major contribution of this work is to propose a methodology that can be effectively used for the continuous and automatic monitoring of a large number of structures instrumented with many sensors, overcoming many of the issues that inevitably arise in the application and management of real monitoring systems. More in detail, one of the main contributions is to fill up the large difference existing between making academic research based on numerical simulations or limited experimental analysis, and the real application of widespread systems which generate large databases collected in real structures continuously.

Therefore, taking into account the needs and shortcomings highlighted in this chapter, it is possible to summarize the main objectives and major contributions of this dissertation as follows:

1. development, implementation and validation of a new methodology for continuous and long-term monitoring of a network of structures, equipped with a large number of sensors, which allows to efficiently obtain reliable system health indicators, used for carrying out a preventive diagnostics of any progressive damage on structural elements;
2. conception and development of all the routines and algorithms needed for defining a multi-level distributed data analysis framework, able to automatically extract useful information from data continuously collected by dynamic systems, in order to create a smart, lasting and efficient monitoring architecture, based on Internet of Things (IoT) tools. In particular, sensor nodes, IoT gateways and a Data Center, also known as IoT Cloud, have been provided with Edge of Things (EoT) technology, in order to efficiently manage the large number of connected devices by using intelligent algorithms and architectures that lead to a more interoperable system. More in detail, the IoT Gateway allow IoT communication, that is device-to-device communications or device-to-cloud communications while the IoT cloud include the infrastructure needed for processing and storing real-time data;
3. Application of the proposed methodology to a significant number of structures (about 20 bridges), with different geometry, static scheme and intrinsic characteristics;
4. Identification of real damage scenarios, which have been recorded by the monitoring system, for two significant case studies. Notably, the developed monitoring system has been conceived and installed on the selected case studies, which have been monitored for more than 2 years and are still under real-time control. All the features of the dynamic monitoring system have been applied, showing the ability of the proposed methodology to provide reliable

and robust real-time information about the health status of the monitored structures, demonstrating the usefulness of vibration-based health monitoring systems, which make it possible to preventively detect real damage occurrence.

The objectives and contributions described above are detailed in the following chapters. In particular, it is important to underline that the motivations that led to the development of the methodology described in this work are to be found in the need of having a procedure that solves many of the issues that arise when applying theoretical studies to a practical case.

Chapter 3

Dynamic Monitoring

3.1 Chapter Introduction

This chapter illustrates the theoretical background behind some of the main OMA methods, used for the dynamic identification of civil engineering structures. Subsequently, the application of the described methodologies on a numerical case study is shown, in order to highlight advantages/disadvantages of each method. Finally, one of these OMA methods is selected for automatically detecting any structural damage, through a real-time, efficient and robust monitoring system to be applied to full-scale bridge structures under operating conditions (chapter 4).

As mentioned in chapter 1, output-only modal analysis has attracted much attention from the engineering scientific community in the last few decades, given the difficulty and high cost of exciting artificially (using for example hammers or shakers) large civil infrastructures and perform the well known Experimental Modal Analysis (EMA). Instead, Operational Modal Analysis (OMA) gives the possibility of estimating the modal characteristics of a structure without knowing and/or controlling the vibration input. In particular, the excitation source is a zero mean gaussian white noise, which represents the variety of ambient forces, assumed to be random, acting on the structure under its real boundary and load conditions. Through this analysis technique, it is possible to obtain the modal parameters describing the dynamic behaviour of the structure, such as mode shapes, natural frequencies and damping ratios. Considering that the ambient response analysis provides a non-deterministic knowledge of the input signal, but on the contrary is based on random processes, it is often identified as "stochastic system identification" technique. Inasmuch as this process is of random type, that is, it is the representation of quantities that varies randomly over time and with certain characteristics, some assumptions are needed.

First of all, it is assumed that all OMA methods retain linearity, which means that the dynamic response of a system can be obtain as a given combination of all the inputs acting on it. This assumption is most of the time quite reasonable,

even if there are cases of concentrated or widespread non-linearity for which specific analysis are required.

Secondly, the hypothesis of stationarity is also essential in order to consider the probability distribution of the stochastic process constant over time. This implies that any variation of the dynamic parameters characterizing the structure can be assumed as an indicator of a change in the system and therefore of a potential damage.

Finally, as the input is considered to be a white noise signal, it is assumed that the output contains full information about all the modes of the structure. This assumption does not actually correspond to the real operating conditions in which dynamic monitoring is performed. In fact, full-scale structures are excited by environmental factors, such as wind, traffic, etc., which themselves have a non-constant spectrum. This leads to the awareness that, although the assumption of having a white noise input has been made, some modes will be more excited than others according to the random forces acting on the system.

In all the applications presented in this chapter, the aforementioned assumption are considered holded.

3.2 Signal Processing

Signal processing plays a key role in extracting useful and correct information from data recorded by a network of sensors. Indeed, processing vibration signals in an appropriate way is essential for obtaining the most accurate representation of the real behavior of the structure. In particular, signal processing refers to all the numerical and technical operations needed for translating the real analog signal, corresponding to the dynamic response of the structure over time, to data suitable for subsequent analysis, such as modal identification processes.

Signal processing is particularly tricky when passing from time to the frequency domain. Indeed, vibration signals are defined as mathematical functions of time. However, they are commonly studied through mathematical models in which frequency is considered the reference variable. This conversion (time to frequency) involves a series of inevitable approximations in the transition from a digital signal to a frequency spectrum, which must be taken into account for obtaining a result without undetermined errors.

The effects of a poor signal processing can generate errors, such as *aliasing*, *leakage* and *quantization error*, which can affect the results of subsequent analyzes. For this reason it is crucial to mitigate, by the use of mathematical procedures, such errors.

The following paragraphs illustrate the main procedures used for avoiding an erroneous processing of data recorded by sensors.

3.2.1 Sampling frequency

Sampling can be defined as the reduction of a continuous-time signal to a discrete-time signal. Real signals are obviously continuous, i.e. analog, so it is necessary to convert them from analog to digital using an analog-to-digital converter (ADC), which punctually samples real continuous functions at regular intervals of time. This means that the sampling operation is performed by measuring the continuous function every T seconds, which represents the sampling interval. Thus, a sample can be defined as the value corresponding to a specific point in time. As a consequence, the sampling frequency is the number of samples per second:

$$f_s = \frac{1}{T} \quad (3.1)$$

The sampled digital signal can in turn be converted back to the continuous signal by interpolation algorithms. However, if the sampling frequency f_s has not been chosen carefully, errors in the signal processing can be produced.

Aliasing

Aliasing, as its name suggests, is the assumption of a "false identity" by a signal when sampled. It is a typical effect generated from an incorrect sampling rate which makes different signals indistinguishable when sampled. This implies that the reconstructed sampled signal is different from the original continuous one. Figure 3.1 shows an example of aliasing:

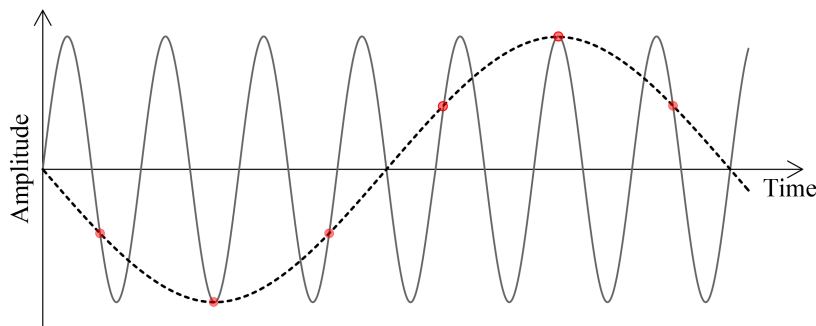


Figure 3.1: Aliased signal due to Undersampling

The main measure taken to prevent aliasing is to sample more than twice the highest frequency (Nyquist–Shannon sampling theorem), which avoid the construction of a distorted signal.

Moreover, since the interference of erroneous frequencies (aliasing) can occur even when the very wide band random signals are not correctly filtered and thus the

influence of very high frequencies compromises the sampling, an analog anti-aliasing filter (AAF) is necessary to prevent from aliasing. In particular, a low-pass filter is used to remove all frequencies above the Nyquist frequency prior to sampling.

Quantization error

Since the real analog signal is converted into a discrete digital signal, this discretization also applies in amplitude. This means that continuous input values are reduced to a smaller discrete dataset through a fixed number of digital levels, known as quantization levels. This process introduces a difference (round-off error) between the original values and the quantized ones, called quantization error.

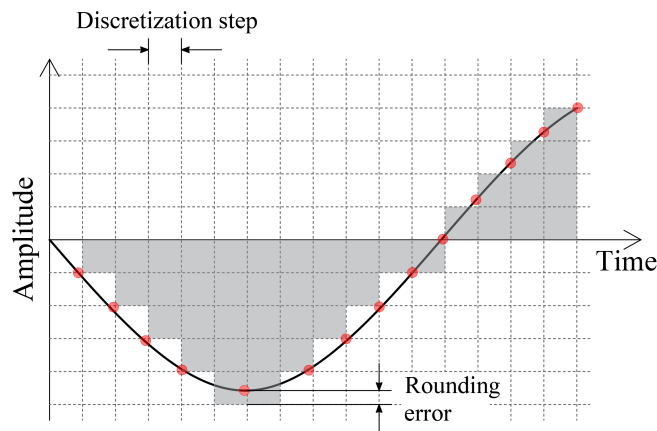


Figure 3.2: Quantization error

The higher the quantization error, the smaller the number of quantization levels, which depends on the number of bits (an n – bit converter has 2^n quantization levels). This means that an higher resolution is needed to prevent from this distortion. In particular, the relationship between resolution (in bits) and quantization noise can be expressed as:

$$S/N = -20 * \log \frac{1}{2^n} \quad (3.2)$$

where n is the resolution of the A/D converter in bits.

3.2.2 Spectral leakage

Spectral Leakage is an effect that takes place due finite windowing of the data. It is caused by the truncation of a signal to a finite length, which is not an integer multiple of the period of each and every signal component. As a consequence, in addition to the real frequency components of the signal, additional frequencies

starts appearing in the spectrum. This phenomenon of "migration" of the energy associated with the true frequencies to other frequencies is one of the most serious problems in signal processing.

To mitigate this distortion, the signal is usually pre-multiplied by a function, known as a *window function*. The objective of this operation is to obtain a gradual decay of the amplitude of the signal towards the ends of the sampling interval, so as to be more similar to a true periodic signal. Indeed, a window function is defined to be zero-valued outside of some chosen interval and symmetric around the middle of the interval.

A number of window function has been introduced over the year by the literature; however, the most widespread and effective one is the sinusoidal Hanning window, introduced by Julius von Hann and defined as:

$$\omega(n) = 0.5 - 0.5\cos\left(\frac{2\pi n}{M-1}\right) \quad (3.3)$$

where n is between 0 and $(M-1)$.

3.3 Dynamic models

In this section, some theoretical concepts concerning the dynamic models of structural systems are addressed. In particular, in order to describe the dynamic behavior of a structure, be it in the civil, aerospace or mechanical engineering field, there is a need for a mathematical model able to reproduce the relationship existing between the applied input forces and the response of the structure in terms of displacements, velocities and accelerations. In this regard, it should be emphasized that a model always represents an idealization of reality and therefore some simplifications must be made in any model. Moreover, different models can be adopted to describe the same behavior, which in this case is a time-invariant vibrating behavior. In this paragraph, three different models that can be used to describe the dynamic response of a system are illustrated. In particular, starting from the equations of motion for the Spatial Models (nodal representation), Modal Models (modal representation) and State-Space Models are described. An extensive literature is available on the subject ([15], [24],etc..) and therefore only essential concepts are illustrated in this section.

3.3.1 Spatial Model

The dynamic behavior of a physical system is traditionally described by the differential equation of motion, in terms of displacement, velocity and acceleration as a function of time. For a Multi Degree Of Freedom (MDOF) system, which is the case of real systems, the equation of motion is:

$$[M] \ddot{u}(t) + [C] \dot{u}(t) + [K] u(t) = f(t) \quad (3.4)$$

where M is the mass matrix, C is the damping matrix, K is the stiffness matrix, the vector $u(t)$ contains the displacements and $f(t)$ defines the input forces.

The second order linear differential equation 3.4 represents the Spatial Model in structural dynamics, in which forces and displacements are expressed with respect to the physical coordinates of the system. This equation, which in general refers to damped MDOF systems, has an exponential solution obtained solving an eigenvalues problem whose eigenvectors are complex (meaning that the different solutions are not in phase).

However, the equation 3.4 constitutes a system of n equations containing n variables. In general the n equations are coupled, which means that each equation includes different components of the displacement vector $u(t)$, corresponding to various DOFs. In order to overcome this drawback and make the solution of this equation simpler, the orthogonality properties of natural vibration modes can be used to decouple the equations of motion of a linear viscous system with N degrees of freedom, as reported in the following paragraph.

3.3.2 Modal Model

As mentioned in the previous paragraph, the solution of the equation 3.4 can be decomposed through the Modal Model formulation. Indeed, modal analysis allows decoupling the various equations, so that each of them represents a system with a single degree of freedom. This means that a MDOF system can be analyzed as a combination of multiple SDOF systems, corresponding to the different natural vibration modes of the structure. Each vibration mode is uniquely characterized by a single natural frequency value and shape.

The described transformation can be obtained by imposing that:

$$u(t) = \Phi q(t) \quad \dot{u}(t) = \Phi \dot{q}(t) \quad \ddot{u}(t) = \Phi \ddot{q}(t) \quad (3.5)$$

in which the displacement vector $u(t)$ is converted into a new vector $q(t)$ of size $n \times 1$, whose components refer to the modal (called normal or principal) coordinates and no longer the spatial ones. Φ is the modal matrix with size $n \times n$, containing in the columns all the n modes of the system. With reference to 3.5, the equation 3.4 can be thus rewritten in the form:

$$[M] \Phi \ddot{q}(t) + [C] \Phi \dot{q}(t) + [K] \Phi q(t) = f(t) \quad (3.6)$$

and, by multiplying all the terms of 3.7 for Φ^T on the left, the following expression can be obtained:

$$\Phi^T [M] \Phi \ddot{q}(t) + \Phi^T [C] \Phi \dot{q}(t) + \Phi^T [K] \Phi q(t) = \Phi^T f(t) \quad (3.7)$$

in which the modal mass, damping and stiffness matrices are diagonal for the orthogonality properties of the modes with respect to the mass and stiffness matrices.

$$\hat{M} = \Phi^T [M] \Phi = \begin{bmatrix} \ddots & & \\ & M_n & \\ & & \ddots \end{bmatrix} \quad (3.8)$$

$$\hat{C} = \Phi^T [C] \Phi = \begin{bmatrix} \ddots & & \\ & C_n & \\ & & \ddots \end{bmatrix} \quad (3.9)$$

$$\hat{K} = \Phi^T [K] \Phi = \begin{bmatrix} \ddots & & \\ & K_n & \\ & & \ddots \end{bmatrix} \quad (3.10)$$

that is:

$$\hat{M} \ddot{q}(t) + \hat{C} \dot{q}(t) + \hat{K} q(t) = \hat{F}(t) \quad (3.11)$$

Moreover, by dividing all the terms for the modal mass \hat{M} , the equation for a single mode i becomes equal to:

$$\ddot{q}_i(t) + 2\xi_i \omega_i \dot{q}_i(t) + \omega_i^2 q_i(t) = \frac{\hat{F}_i(t)}{\hat{M}_i} \quad i = 1, \dots, n \quad (3.12)$$

considering the well known following relationships:

$$\omega_i^2 = \frac{\hat{K}_i}{\hat{M}_i} \quad \xi_i = \frac{\hat{C}_i}{2\hat{M}_i \omega_i} \quad (3.13)$$

where ω_i is the modal frequency associated to the i -th mode and ξ_i represents the modal damping ratio.

As shown, the modal model allows transforming a MDOF system, including n coupled differential equations defined in terms of geometric coordinates, into n decoupled SDOF differential equations, defined in terms of modal coordinates.

3.3.3 State-Space Model

An analogous and equally valid method to solve the dynamic problem is represented by the so-called state-space formulation. According to this method, the second order differential equation problem can be transformed into a first order one, by using some mathematical trick. In particular, the displacement vector $u(t)$ can be converted into a state vector, so defined:

$$z(t) = \begin{Bmatrix} u(t) \\ \dot{u}(t) \end{Bmatrix} \quad (3.14)$$

With reference to 3.4, all the terms can be divided by the mass matrix M , thus obtaining:

$$\ddot{u}(t) + [M]^{-1}[C]\dot{u}(t) + [M]^{-1}[K]u(t) = [M]^{-1}f(t) \quad (3.15)$$

which, considering the assumption made in equations ?? and 3.15, leads to:

$$\dot{z}(t) = \begin{bmatrix} 0 & I \\ -M^{-1}K & -M^{-1}C \end{bmatrix} z(t) + \begin{bmatrix} 0 \\ M^{-1} \end{bmatrix} f(t) \quad (3.16)$$

From this equation it is possible to define the two following matrices:

$$A = \begin{bmatrix} 0 & I \\ -M^{-1}K & -M^{-1}C \end{bmatrix} \quad B = \begin{bmatrix} 0 \\ M^{-1} \end{bmatrix} \quad (3.17)$$

where A is defined as the state matrix, containing all the information about the dynamics of the system and B is known as the input matrix.

On the other hand, the observation equation can be written as:

$$u_i(t) = [C_a]\ddot{u}(t) + [C_v]\dot{u}(t) + [C_d]u(t) \quad (3.18)$$

where $u_i(t)$ is the vector containing the outputs from sensors and C_a , C_v , C_d are matrices that have all the elements equal to zero except in correspondence of the i -th degree of freedom, where the outputs are measured. In other words, these

matrices are used to identify which degree of freedom is recorded during the test phase. Now, it is possible to substitute $\ddot{u}(t)$ from equation 3.15 in equation 3.18, obtaining the following matrices:

$$C = [C_d - C_a M^{-1} K \quad C_v - C_a M^{-1} C] \quad D = [C_a M^{-1}] \quad (3.19)$$

where C is the output matrix and D is the direct transmission matrix, as it directly correlates the input given to the system to the measured outputs.

The equation of motion 3.4 can thus be transformed into the so-called state-space model, which is obtained by combining the state equation with the observation equation, as reported in the following expression:

$$\begin{cases} \dot{z}(t) = [A]z(t) + [B]f(t) \\ y(t) = [C]z(t) + [D]f(t) \end{cases} \quad (3.20)$$

where $z(t)$ represents the state vector containing the real displacement and velocity vectors of the dynamic system, as defined in equation 3.20, $f(t)$ is the excitation force and $y(t)$ is the output vector as measured.

Using this approach, the dynamic system is thus transformed into a $2N$ differential equations of the first order. In particular, the state equation describes the state process which depends only on the dynamic characteristics of the system ($[A]z(t)$) as well as on the input force ($[B]f(t)$). The observation equation represents the transformation of the hidden state $z(t)$ into an output signal, that is further corrupted by a noise process ($[D]f(t)$).

The state-space model described above refers to a continuous-time model. However, in real dynamic tests, the measurements of a dynamic system under the excitation of an input force are discrete in time. As a consequence, a transformation from a continuous-time model to a discrete-time model is needed to adequately describe experimental data. The relationship between continuous and discrete time system matrices is [30]:

$$\begin{aligned} [A_d] &= e^{[A_c]\Delta t} \\ [B_d] &= ([A] - [I])[A_c]^{-1}[B_c] \\ [C_d] &= [C_c] \\ [D_d] &= [D_c] \end{aligned} \quad (3.21)$$

where the subscript C indicates the continuous-time and the subscript D indicates the discrete one.

It is notable that the State-Space Model describes the state of a system under a particular realization; this means that there are infinite equivalent state-space representations for the same dynamic system subjected to different test conditions.

3.4 Theoretical background of OMA identification methods

As mentioned in paragraphs 1.2 and 3.1, Operational Modal Analysis (OMA) is a complementary technique for the identification of the modal properties of a structure using vibration data measured on site. Compared with traditional methods, OMA is based on measuring the response of the test structure only, being the input force unknown. OMA techniques allow the monitoring of civil, mechanical or aerospace structures knowing only the response of the system to a random dynamic input. In fact, all these structures (especially civil engineering ones) are difficult to be excited by a controlled external forcing, due to both their boundary conditions and their considerable size. With a view to monitor continuously the behavior of a structure, readings from sensors can be collected and processed using OMA methods without compromising the normal traffic operations, avoiding interferences or interruptions. Moreover, for all the reasons given, the cost of the OMA techniques is considerably lower than the EMA ones.

In this paragraph, a brief description of the most common OMA identification methods is presented. In particular, an overview of the available OMA algorithms is first delineated, followed by a detailed description of some of the most used and representative identification techniques that have been taken into account in the present research work.

3.4.1 Overview of OMA methods

Output-only system identification methods are based on the possibility of describing the dynamic behavior of a structure either through a set of differential equations in time domain, or through a set of algebraic equations in the frequency domain. Thus, all the techniques used for the identification of modal parameters of dynamic systems can be grouped into two main categories: time domain and frequency domain.

Time domain methods are based on the analysis of the time histories from sensors while frequency domain methods use the spectral density function to process data. All these methodologies can in turn be divided into parametric and non-parametric methods. The parametric methods estimate the modal characteristics of a dynamic system from a parametric model, extrapolated from the processed signal through a fitting procedure. The non-parametric models instead derive the

modal parameters directly from data, without the need to generate a descriptive model of the structure.

3.4.2 Frequency Domain Methods

Peak-Picking (PP)

The simplest and most immediate non-parametric method for the modal parameter identification, in frequency domain, is the so-called Peak Picking (PP). It consists in evaluating the natural frequencies from the simple observation of the peaks in the graph of the auto-spectra of the measured outputs, the vibrational modes from the ratio between peaks at various points of the structure and the damping ratios from the "width" of the peaks [23].

The peak-picking method is based on the assumption that close to a peak, that is around a resonance, the system behaves as a SDOF system, considering that just one mode is dominant and the contribution of other vibration modes is negligible.

According to this method, the resonant frequencies are thus obtained, for the i -th frequency, as:

$$\omega_i = \omega_{peak} \quad (3.22)$$

while, the relative damping is calculated as:

$$\zeta_i = \frac{\omega_2 - \omega_1}{2\omega_i} \quad (3.23)$$

where ω_1 and ω_2 , called half-power frequency points, are two frequency points (with the assumption that $\omega_2 > \omega_1$) on either side of the identified frequency ω_i for which:

$$|X(\omega_1)| = |X(\omega_2)| = \frac{|X(\omega_i)|}{\sqrt{2}} \quad (3.24)$$

Moreover, for the i -th resonance, the following equation can be written for a SDOF system:

$$H(\omega) = \frac{A_i}{\omega_i^2 - \omega^2 + 2i\zeta_i\omega\omega_i} \quad (3.25)$$

where A_i is the modal constant, related to the mode shape. Hence, by combining the equation 3.22 with the equation 3.25:

$$Q = |H(\omega_i)| = \frac{A_i}{2\zeta_i\omega_i^2} \quad (3.26)$$

So, the modal constant A_i can be obtained as:

$$A_i = 2Q\zeta_i\omega_i^2 \quad (3.27)$$

This method has the advantage of providing an acceptable approximation of modal parameters, if the modes are clearly separated, in a simple and quick way. It can be advantageously used for a first check of the quality of data collected by sensors as well as for a first estimation of the dynamic properties of the system. However, the method presents some limitations, mainly due to the low level of accuracy as well as the impossibility of identifying close modes.

Frequency Domain Decomposition (FDD)

One of the most advanced non-parametric frequency domain identification methods is the Frequency Domain Decomposition (FDD) method. This methodology has been firstly proposed by Brincker, Zhang, and Andersen [10] in 2000 and is based on the assertion that the eigenvectors, which represent the vibration modes of the system, constitute a base, being linearly independent, and therefore any movement of the system can be represented by their linear combination. It is therefore possible to separate the components of the different vibration modes. This property can be applied to the spectral density function (PSD), through a Singular Value Decomposition (SVD) of the spectral matrix into a set of auto spectral density functions, corresponding to SDOF systems.

It is possible to obtain the relationship between input $x(t)$ and output $y(t)$ for a general MDOF system, and thus the PSD matrix, by taking the Fourier transform:

$$[G_{yy}(\omega)] = [\Phi][G_{xx}(\omega)][\Phi]^H \quad (3.28)$$

where $G_{yy}(\omega)$ is the power spectral density (PSD) matrix of the output, $G_{xx}(\omega)$ is the input PSD matrix and Φ is the modal matrix, defined according to 3.5. By applying the well known Singular Values Decomposition (SVD) to the power spectral density matrix at a specific frequency, the following expression can be obtained:

$$[G_{yy}(\omega)] = [U][\Sigma][V]^H \quad (3.29)$$

where $[\Sigma]$ is the singular value matrix and $[U]$ and $[V]$ are the unitary matrices holding the left and right singular vectors. The $[\Sigma]$ matrix is a diagonal matrix, having the following form:

$$[\Sigma] = \begin{bmatrix} s_1 & 0 & 0 & \cdot & \cdot & 0 \\ 0 & s_2 & 0 & \cdot & \cdot & 0 \\ 0 & \cdot & s_3 & \cdot & \cdot & \cdot \\ \cdot & \cdot & \cdot & \cdot & \cdot & \cdot \\ \cdot & \cdot & \cdot & \cdot & s_r & 0 \\ 0 & \cdot & \cdot & 0 & 0 & 0 \end{bmatrix} \quad (3.30)$$

The elements s_1, \dots, s_r in the matrix 3.30 are the singular values whose corresponding singular vectors are contained in the matrices U and V . The number of non-zero values in the matrix $[\Sigma]$, indicated by r , corresponds to the rank of the PSD matrix $[G_{yy}(\omega)]$ at a specific frequency. This means that a one-to-one relationship can be recognized between singular vectors and mode shapes. In fact, for a fixed frequency, the rank of the PSD matrix and therefore the number of singular values, coincides with the modes that are involved in that specific frequency. This implies being able to identify very close or even coincident modes.

Each line in the FDD plot represents a singular value for a single degree of freedom (SDOF) system. If the modes of the structure are well separated, only the first singular value will present the peaks corresponding to all the resonance frequencies of the structure, while all the other singular values will show negligible values for all the frequencies. On the contrary, if the structure has close or coincident modes, frequency peaks will be evident in the singular values following the first one. In other words, the first singular value of each frequency contains the information regarding all the dominant modes, while the following singular values could represent modes that are close to the dominant ones or the intensity of the noise.

Moreover, it is possible to estimate the mode shapes of the structure by looking at the singular vectors associated with the frequencies of the identified peaks.

This method has several advantages, including the ability of identifying very close or even coincident modes, which would be almost impossible with the Peak-Picking method. Moreover, it is computationally simple and fast to execute.

Different variants of this method are present in literature, as for example the EFDD (Enhanced Frequency Domain Decomposition) method [31] or the Frequency-Spatial Domain Decomposition (FSDD) method [69].

Polyreference Least-squares Complex Frequency-Domain Method (Poly-MAX)

The frequency domain methods illustrated in the previous paragraphs (PP and FDD) belong to the category of the so-called nonparametric methods, meaning that

the eigenfrequencies are obtained without using a model for fitting data. Along with these methodologies, methods in which a parametric model is estimated from data are also extensively used, falling within the so-called parametric OMA methods. The Polyreference Least-squares Complex Frequency-Domain Method (PolyMAX) [53] is one of the most used parametric method in modal analysis applications. It starts from the least-squares approach and uses multiple-input-multiple-output FRF as primary data.

An extensive literature is available for the analytical description of the method [53], [57]. In this paragraph, a summary of the main points underlying the PolyMAX method is reported.

PolyMAX method starts by identifying the FRF matrix using the right matrix-fraction (RMFD) model:

$$[H(\omega)] = [B(\omega)][A(\omega)]^{-1} \quad (3.31)$$

where $H(\omega)$ is the FRFs matrix in which the FRFs between inputs and outputs are included, $B(\omega)$ is the numerator matrix polynomial while $A(\omega)$ is the denominator matrix polynomial. With reference to equation 3.31, one single row of the RMFD model is obtained as:

$$\forall k = 1, 2, \dots, l : \langle H_k(\omega) \rangle = \langle B_k(\omega) \rangle [A(\omega)]^{-1} \quad (3.32)$$

where:

$$\begin{aligned} \langle B_k(\omega) \rangle &= \sum_{r=0}^p \Omega_r(\omega) \langle \beta_{kr} \rangle \\ [A(\omega)] &= \sum_{r=0}^p \Omega_r(\omega) [\alpha_r] \end{aligned} \quad (3.33)$$

in which $\Omega_r(\omega)$ represents the polynomial basis functions while β_{kr} and α_r are the unknown parameters, collected in a single matrix θ , as shown below:

$$\begin{aligned}
 \beta_k &= \begin{pmatrix} \beta_{k0} \\ \beta_{k1} \\ \dots \\ \beta_{kp} \end{pmatrix} \in \mathbb{R}^{(p+1) \times m} (\forall k = 1, 2, \dots, l) \\
 \alpha &= \begin{pmatrix} \alpha_0 \\ \alpha_1 \\ \dots \\ \alpha_p \end{pmatrix} \in \mathbb{R}^{m(p+1) \times m} \\
 \theta &= \begin{pmatrix} \beta_0 \\ \beta_1 \\ \dots \\ \beta_l \\ \alpha \end{pmatrix} \in \mathbb{R}^{(l+m)(p+1) \times m}
 \end{aligned} \tag{3.34}$$

The objective of this method is to estimate these unknown coefficients by using experimental data. In particular, an error minimization process is used, considering the non-linear least-squares (NLS) equation errors described by the following equation:

$$\epsilon_k^{NLS}(\omega_n, \theta) = \omega_k(\omega_n)(H_k(\omega_n, \theta) - \hat{H}_k(\omega_n)) \tag{3.35}$$

which can be written as:

$$\epsilon_k^{NLS}(\omega_n, \theta) = \omega_k(\omega_n)(B_k(\omega_n, \beta_k)A^{-1}(\omega_n, \alpha) - \hat{H}_k(\omega_n)) \tag{3.36}$$

where $\omega_k(\omega_n)$ is the weighting function, used to evaluate the differences between all the collected outputs. The minimization problem is realized through the following cost function:

$$l^{NLS}(\theta) = \sum_{k=1}^l \sum_{n=1}^{N_f} \text{tr} \left\{ (\epsilon_k^{NLS}(\omega_n, \theta))^H \epsilon_k^{NLS}(\omega_n, \theta) \right\} \tag{3.37}$$

this minimization equation can be written in the form of:

$$[J][\theta] = [0] \tag{3.38}$$

where $[J]$ is the Jacobian matrix defined as follows:

$$[J] = \begin{bmatrix} [\Gamma_1] & [0] & \dots & [0] & [\Upsilon_1] \\ [0] & [\Gamma_2] & \dots & [0] & [\Upsilon_2] \\ \vdots & \vdots & \ddots & \vdots & \vdots \\ [0] & [0] & \dots & [\Gamma_l] & \Upsilon_l \end{bmatrix} \quad (3.39)$$

where the matrices $[\Gamma_l]$ and $[\Upsilon_l]$ are obtained as:

$$[\Gamma] = \begin{bmatrix} [1 & z_1 & \dots & z_1^m] \\ [1 & z_1 & \dots & z_1^m] \\ \dots & \dots & \dots & \dots \\ [1 & z_{N_f} & \dots & z_{N_f}^m] \end{bmatrix} \quad (3.40)$$

$$[\Upsilon] = \begin{bmatrix} -[1 & z_1 & \dots & z_1^m] \otimes [\hat{H}_k(\omega_1)] \\ -[1 & z_2 & \dots & z_2^m] \otimes [\hat{H}_k(\omega_2)] \\ \dots & \dots & \dots & \dots \\ -[1 & z_{N_f} & \dots & z_{N_f}^m] \otimes [\hat{H}_k(\omega_{N_f})] \end{bmatrix} \quad (3.41)$$

where the symbol \otimes indicates the Kronecker product. Under this transformation, the cost function can be expressed by:

$$l^{LS}(\theta) = tr([\theta]^H [J]^H [J] [\theta]) \quad (3.42)$$

where, by reducing the dimension of matrix equation:

$$[J]^H [J] [\theta] = \begin{bmatrix} [R_1] & \dots & [0] & [S_1] \\ \vdots & \ddots & \vdots & \vdots \\ [0] & \dots & [R_l] & [S_l] \\ [S_1]^H & \dots & [S_l]^H & \sum_{k=1}^l [T_k] \end{bmatrix} \begin{bmatrix} [\beta_1] \\ \vdots \\ [\beta_l] \\ [\alpha] \end{bmatrix} = [0] \quad (3.43)$$

with:

$$\begin{aligned} [R_k] &= [\Gamma_k]^H [\Gamma_k] \\ [S_k] &= [\Gamma_k]^H [\Upsilon_k] \\ [T_k] &= [\Upsilon_k]^H [\Upsilon_k] \end{aligned} \quad (3.44)$$

so, in order to minimize the cost function 3.42, its derivatives calculated with respect to θ are put equal to zero:

$$\frac{\partial l^{LS}(\theta)}{\partial \beta_k} = 2(R_k \beta_k + S_k \alpha) = 0, \forall k = 1, \dots, l \quad (3.45)$$

$$\frac{\partial l^{LS}(\theta)}{\partial \alpha} = 2 \sum_{k=1}^l (S_k^T \beta_k + T_k \alpha) = 0 \quad (3.46)$$

Since the poles and modal participation factors are contained in the coefficient α , it is possible to reduce the dimension of the problem by neglecting the β_k coefficient, considering the following equation obtained from the 3.45:

$$[\beta_k] = -[R_k]^{-1} [S_k] [\alpha] \quad (3.47)$$

as a consequence, the so-called reduced normal equations are obtained:

$$\sum_{k=1}^l ([T_k] - [S_k]^H [R_k]^{-1} [S_k]) [\alpha] = [M] [\alpha] = [0] \quad (3.48)$$

From equation 3.48 it is possible to obtain the $[\alpha]$ coefficients, imposing some necessary constraint in order to avoid the solution $[\alpha] = 0$. Once $[\alpha]$ coefficients have been calculated, $[\beta_k]$ coefficients can also be determined through equation 3.47.

3.4.3 Time Domain Methods

Ibrahim Time Domain (ITD)

One of the first OMA identification methods is the Ibrahim time domain (ITD) technique, which was introduced for the first time in 1987 by Mikulcik and Ibrahim [49]. This methodology belongs to the Time Domain methods, namely those procedures in which measured time signals are used directly. More specifically, the ITD approach falls within the class of OMA methods identified as NExT (Natural Excitation Technique). These techniques, starting from the methods developed for the traditional input–output applications, are based on the possibility of expressing the correlation function of a structural response under a unknown ambient excitation as sum of decaying sinusoids. The modal information of the structure can therefore be deduced from the modal properties of these sinusoids. In particular, the Time Response Function (TRF) has to be obtained as first step and then the identification of the structural dynamic properties can be performed through the common TD methods.

ITD method starts from the free response of a structure subjected to random input forces. As known, any response can be decomposed as a linear combination of modes, as follows:

$$\mathbf{y}(t) = \mathbf{y}(n\Delta t) = \psi_1 e^{\lambda_1 n \Delta t} + \psi_2 e^{\lambda_2 n \Delta t} + \dots = \psi_1 \alpha_1^n + \psi_2 \alpha_2^n + \dots \quad (3.49)$$

It is thus possible to arrange the measured free vibration response in a matrix:

$$\mathbf{Y} = \begin{bmatrix} y(0) & y(1) & \dots & y(n-1) \\ y(1) & y(2) & \dots & y(n) \\ \vdots & \vdots & \vdots & \vdots \\ y(n-1) & y(n) & \dots & y(2n-2) \end{bmatrix} \quad (3.50)$$

This matrix is commonly known as a block Hankel matrix, considering that the sampled dynamic response vectors (the blocks) are constant along the anti diagonals. The described matrix, comparing equations 3.49 and 3.50, can be rewritten in the form:

$$\mathbf{Y} = \begin{bmatrix} \psi_1 & \psi_2 & \dots \end{bmatrix} \begin{bmatrix} \alpha_1^0 & \alpha_1^1 & \dots \\ \alpha_2^0 & \alpha_2^1 & \dots \\ \vdots & \ddots & \ddots \end{bmatrix} = \psi \Lambda \quad (3.51)$$

where $[\Psi]$ is the matrix of modes shapes while $[\Lambda]$ contains information about the system poles. The Henkel matrix could be divided in two parts by time-shifting the blocks in the matrix, thus obtaining:

$$[Y_{1|n}] = [\Psi_1][\Lambda] \quad (3.52)$$

The system matrix $[A]$ is able to relate the two modal matrices as follows:

$$[\Psi_1] = [A][\Psi] \quad (3.53)$$

Therefore, considering equations 3.52 and 3.53, is it possible to rewrite the second Henkel matrix as:

$$[Y_{1|n}] = [A][\Psi][\Lambda] \quad (3.54)$$

this means that, by substituting equation 3.50 in equation 3.56, the following expression can be obtained:

$$[Y_{1|n}] = [A][Y_{0|n-1}] \quad (3.55)$$

The eigenvectors and eigenvalues can therefore be obtained by solving the eigenvalue problem of the matrix $[A]$:

$$[A] = [Y_{1|n}][Y_{0|n-1}]^T \quad (3.56)$$

The solution of the eigenvalue problem allows obtaining the eigenvalues, which represent the system poles, and the corresponding eigenvectors, that are an estimation of the mode shapes of the system.

Covariance-driven Stochastic Subspace Identification Method (Cov-SSI)

One of the most common and powerful methods in the Time Domain is the Covariance-Driven Stochastic Subspace Identification (Cov-SSI) method. This methodology is based on the stochastic realization problem, according to which a stochastic state-space model can be estimated from vibration measurements [33]. The Cov-SSI methodology fall within the so called parametric methods.

Starting from the random measured accelerations, identified as $[Y]$, the correlation matrices can be calculated as follows:

$$[R_i] = \frac{[Y_{1|N-i}][Y_{i|N}]^T}{N - i} \quad (3.57)$$

where N is the number of samples, $[Y_{1|N-i}]$ and $[Y_{i|N}]$ are obtained from the $[Y]$ matrix by eliminating the last i samples and the first i samples respectively. The following Toeplitz matrix $[T_{1|i}]$ can be constructed with the calculated sub-matrices, representing the correlation between all the measurement channels:

$$[T_{1|i}] = \begin{bmatrix} R_i & R_{i-1} & \dots & R_1 \\ R_{i+1} & R_i & \ddots & R_2 \\ \vdots & \vdots & \ddots & \vdots \\ R_{2i-1} & R_{2i-2} & \dots & R_i \end{bmatrix} \quad (3.58)$$

The correlation matrices R are square matrices of $l \times l$ dimensions; this means that the Toeplitz matrix has dimensions $li \times li$.

In order to obtain an estimation of the state-space model, which is able to describe the dynamics of the monitored system, it is crucial to ensure that all the

relevant system states are both controlled (excited) and observed. To determine if a system is or not controllable and observable, some conditions have to be fulfilled. In particular, with reference to the so-called controllability and observability matrices, it is necessary to verify that the rank of these matrices is equal to the order of the considered system. This means that a system of order k can be considered observable and controllable only if the rank of both observability and controllability matrices is exactly equal to k . All this translates into the need to have a number of rows in the Toeplitz matrix, indicated with l_i , greater than or equal to the order of the system (n) to be identified:

$$l_i \geq n \quad (3.59)$$

According to equation 3.59, a proper i value can be selected, once the order of the system has been estimated. The Toeplitz matrix can thus be rewritten as a function of the corresponding observability and controllability matrices:

$$[T_{1|i}] = [O_i][\Gamma_i] \quad (3.60)$$

where $[O_i]$ is the observability matrix, defined as:

$$[O_i] = \begin{bmatrix} [C] \\ [C][A] \\ \vdots \\ [C][A]^{i-1} \end{bmatrix} \quad (3.61)$$

while $[\Gamma_i]$ is the controllability matrix, defined as:

$$[\Gamma_i] = \begin{bmatrix} [A]^{i-1}[G] & \dots & [A][G] & [G] \end{bmatrix} \quad (3.62)$$

In equations 3.61 and 3.62, matrices $[A]$ and $[C]$ are the state matrix and the output matrix respectively, according to the state-space model described in detail in section 3.3.3. It is important to emphasize that $[O_i]$ and $[\Gamma_i]$ have dimensions $l_i \times n$ and $n \times l_i$, which leads to a rank of the block Toeplitz matrix equal to n .

Singular Value Decomposition (ref. section 3.4.2) has been applied to the Toeplitz matrix, as follows:

$$[T_{1|i}] = [U][\Sigma][V]^T \quad (3.63)$$

After computing the SVD of the Toeplitz matrix, it has to be truncated to the model order n , thus obtaining:

$$[T_{1|i}] = [O_i][\Gamma_i] = [U_1][\Sigma_1][V_1]^T \quad (3.64)$$

starting from equation 3.64, it is possible to obtain $[O_i]$ and $[\Gamma_i]$, by splitting the SVD in two parts:

$$[O_i] = [U_1][\Gamma_1]^{1/2}[T] \quad (3.65)$$

$$[\Gamma_i] = [T]^{-1}[\Gamma_1]^{1/2}[V_1]^T \quad (3.66)$$

It is then possible to obtain the state matrix A as follows:

$$[A] = [O_i^{up}]^+ [O_i^{down}] \quad (3.67)$$

where $[O_i^{up}]$ and $[O_i^{down}]$ are formed starting from matrix $[O_i]$ and removing the last or the first l rows respectively. The output matrix $[C]$, containing the information about the mode shapes, is also obtained from $[O_i]$ selecting the first l rows:

$$[C] = [O_i]_{1:l} \quad (3.68)$$

so, the eigenvalues and corresponding eigenvectors can be obtained from eigenvalue decomposition of the state matrix $[A]$.

3.5 Numerical case study

The purpose of this paragraph is to compare some of the main OMA identification methods described above, in order to identify the most suitable one to be applied for the automatic real-time monitoring case studies presented in this dissertation. In particular, 4 methods have been selected: PP, FDD, Cov-SSI and PolyMAX. The following numerical tests are intended to evaluate the effectiveness of each of these methods in different operating conditions, considering the uncertainty due to some factors such as noise levels, data synchronization, number of reading points etc...The numerical model assumes the use of time-based discrete sensors, replicating those applied on full-scale structures for damage detection and health state assessment.

3.5.1 Numerical FEM Model

A numerical 3D finite element (FE) model of a typical highway bridge was developed using FEM software SAP2000 [62].

Description of the structure

In order to assess the performances of the different OMA methodologies, the acceleration response data sets from a finite element model of a simply-supported bridge were used. One of the main advantages of using a numerical model for this purpose is that the modal properties of the analyzed system are known a priori and thus it is possible to evaluate the accuracy of the dynamic characteristics identified using one or more OMA methods.

The structure modeled using the finite element code is a pre-stressed simply-supported concrete girder bridge. The choice of this structure is motivated by the fact that, due to its geometric and design features, it can be considered as representative of many highway infrastructures designed around the 1960s and '70s.

The structure is composed by eight simply-supported pre-stressed concrete spans. The spans are 21.4 m long and are supported by seven concrete columns and two concrete abutments. The cross-section is a pre-stressed reinforced concrete girder in which nine longitudinal beams and four transversal beams are the primary support for the deck, a reinforced concrete slab. The beams cross-section has a constant height in the longitudinal direction of about 1.2 m. The bridge develops slightly in curve; the roadway has a width of 9.8 m, while the total size of the decks in the transverse direction is 11 m. Figure 3.3 and Figure 3.4 show a plan view, elevation and cross-sections of the described structure.

The different elements of bridge spans (including beams, slabs, and diaphragms) were modelled as elastic one-dimensional frame elements; each element has been assigned the mechanical characteristics of the corresponding reinforced concrete section. Bridge bearings were modeled as spring elements connecting the superstructure with the piers. In particular, in order to account for the difference between longitudinal and transversal restrained action, each span has been constrained by an alignment of fixed longitudinal supports (FL) to which one fixed transversal joint (FT) has been added, in order to prevent translational lability. The material characteristics used for the FE model have been extracted from design drawings.

The complete FE model of the bridge has a total number of 4413 elements and 2460 nodes. Figure 3.5 shows a 3D view of the FE model.

In the following section, in order to simplify the result reading, only one of the simply-supported bridge spans is considered. Being simply-supported spans, similar considerations apply to the remaining spans.

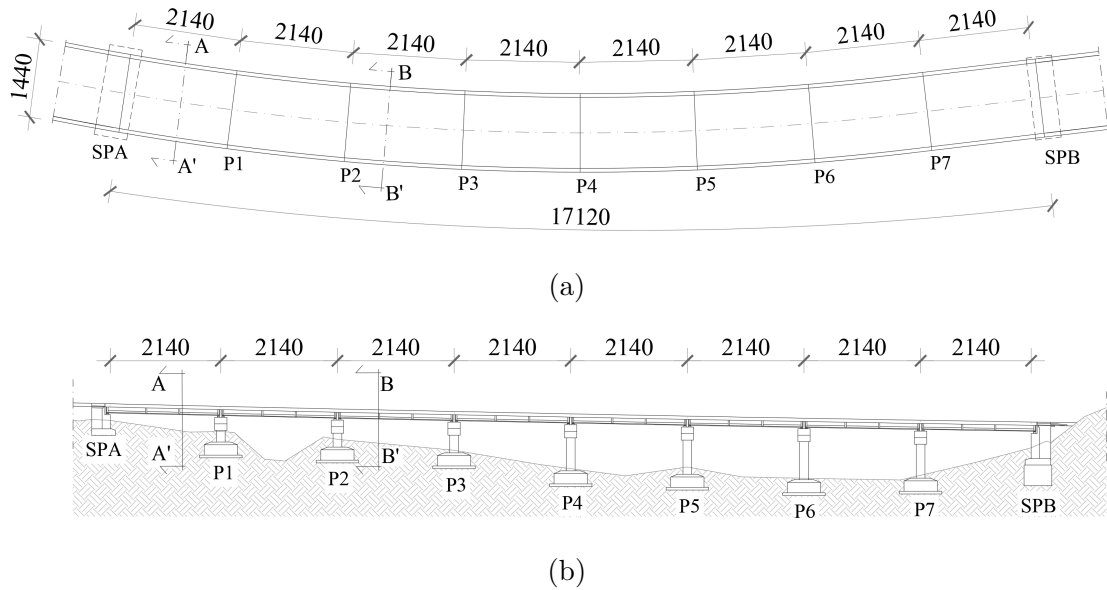


Figure 3.3: (a) Plan view and (b) elevation of the analyzed bridge

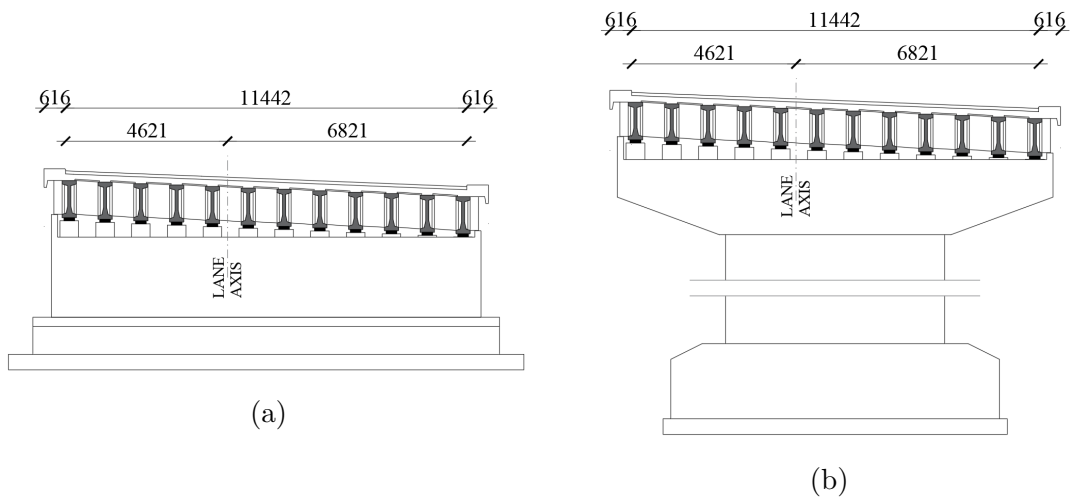


Figure 3.4: Cross-sections of the bridge: (a) A-A' section (b) B-B' section

Description of the dynamic model

In order to test the effectiveness of the selected methods (mentioned above) for identifying the resonance frequencies of the highway bridge chosen as reference, an artificial input force has been used to excite the analyzed system. The most common dynamic loads on bridges come from traffic and wind, which are assumed to be continuous and random inputs. Thus, a white noise signal, named e_i , has been generated with the following characteristics:

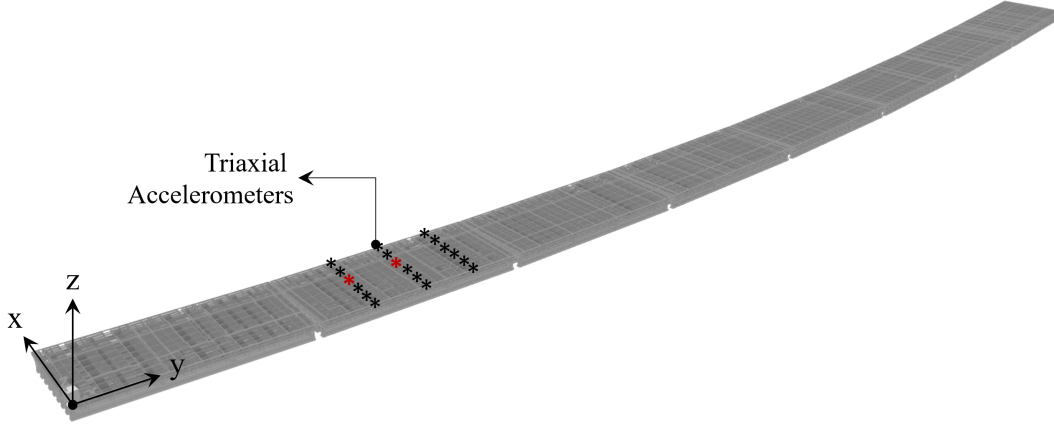


Figure 3.5: 3D view of the FE model of the analyzed bridge

$$E[e_i] = 0 \quad (3.69)$$

$$E[e_i e_j] = \lambda \delta_{ij} \quad (3.70)$$

where λ is the covariance and δ_{ij} represents the Kronecker symbols which is 1 if $i=j$ and 0 otherwise.

Artificial input data were generated at a sampling frequency of 300 Hz during 600 s (10 minutes). The following figure shows the input signal in the three measurement directions x, y, z for the first 100 seconds.

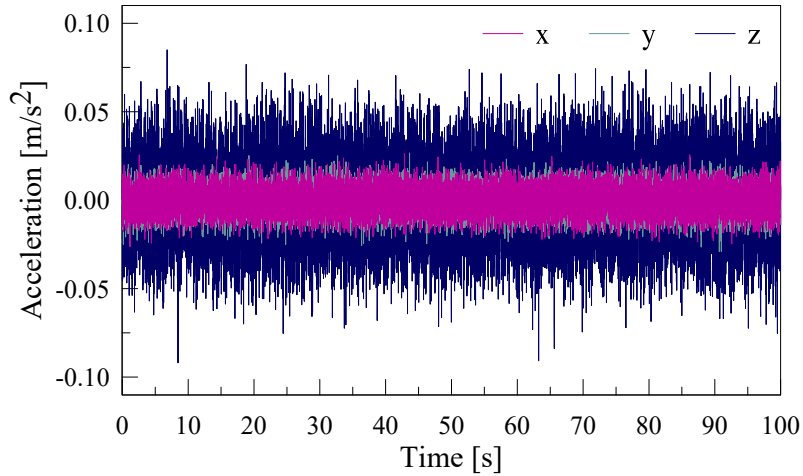


Figure 3.6: White noise signal used as input for the numerical model

System dynamics has been simulated through a state-space model in MATLAB/Simulink. State-space formulation is a really useful method for modeling dynamic systems in time domain (ref. Paragraph 3.4). In particular, state-space models can be easily implemented by using a Simulink block diagram, which allows solving step by step state equations in order to obtain a discrete output representing the response of the system to a given input. Figure 3.7 shows the block diagram used to simulate the system dynamics.

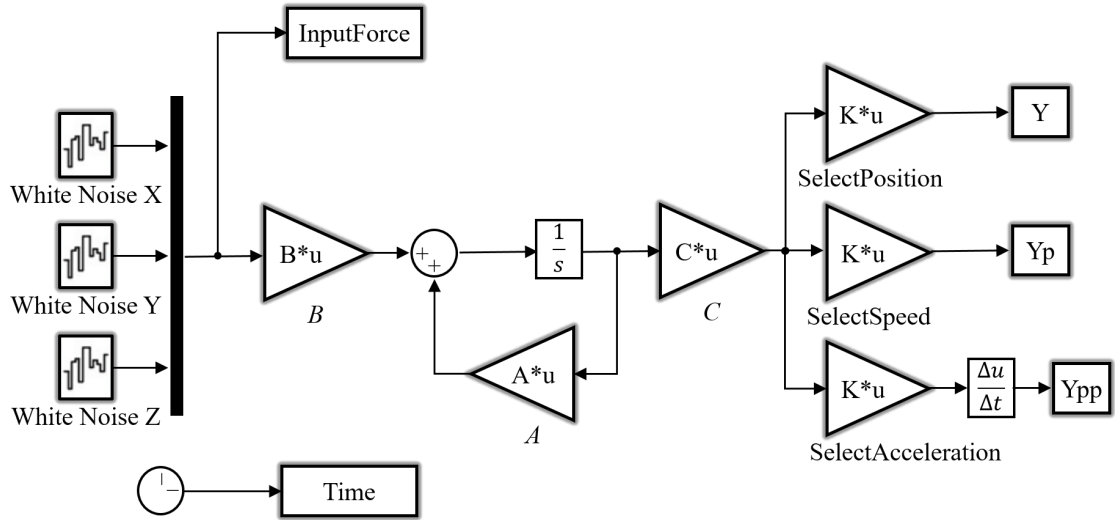


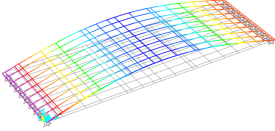
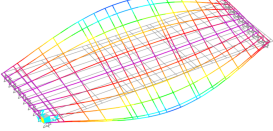
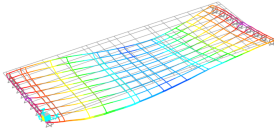
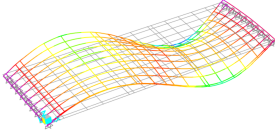
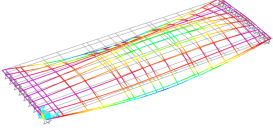
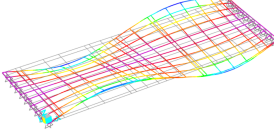
Figure 3.7: Simulink block diagram used for simulating the system dynamics

With reference to equation 3.20, A , B and C are the discrete state-space matrices describing the physical system subjected to a white noise input. In order to simulate the real operating conditions of a civil engineering infrastructure that is monitored through the use of a series of acceleration sensors, noise has been added to the output signal. More in detail, a random peak-to-peak noise of 3 mV has been considered for each channel. Moreover, the sensitivity of a MEMS accelerometer of 250 mV/g with a 5g full scale has been taken into account. A signal-to-noise ratio (SNR) of about 9 dB as been calculated as the logarithm of the ratio of the main and noise signals. In order to replicate the standard behavior of accelerometers used for structural health monitoring, output data have then been obtained for all the considered sensors nodes in the 3 measurement directions x , y , z . These signals have been properly undersampled at a frequency of 100 Hz and a Butterworth anti-aliasing filter has been also applied before the sampler, with the aim of reproducing the discrete accelerometer sampling. With reference to Figure 3.5, the output signals of two accelerometers, located respectively in the middle of the span and near the left support, are considered.

3.5.2 Results discussion

The aforementioned methodologies have been applied to output signals with the aim at selecting the method able to identify more precisely the resonance frequencies of the structure. In particular, in view of a full-scale application, the main purpose is to identify natural frequencies automatically over time; this means that it is necessary to choose a OMA procedure that is as reliable and robust as possible. The first 6 resonance frequencies have been considered for the methods evaluation. Frequency values and the corresponding mode shapes are listed in Table 3.1

Table 3.1: Natural Frequencies from FEM model

Mode 1 $f_1=5.434$ Hz	Mode 2 $f_2=6.648$ Hz	Mode 3 $f_3=15.413$ Hz
		
Mode 4 $f_4=19.570$ Hz	Mode 5 $f_5=20.293$ Hz	Mode 6 $f_6=21.161$ Hz
		

Identified frequency values are thus compared with those extracted from the FEM model. The mean percentage error (MPE) is computed as the average of percentage errors (on the 6 considered frequencies) in order to estimate how much the indentified values differ from the actual values. The mean percentage error is obtained using the following expression:

$$MPE = \frac{100\%}{n} \sum_{i=1}^n \frac{f_{real} - f_{id}}{f_{real}} \quad (3.71)$$

where f_{real} is the actual value of the natural frequency, f_{id} is the identified frequency by the OMA method and n is the numer of considered frequencies.

Peak-Picking (PP)

From the acceleration signal time-histories, power spectral densities (PSDs) are calculated for each sensor by using Welch's modified periodogram method [68].

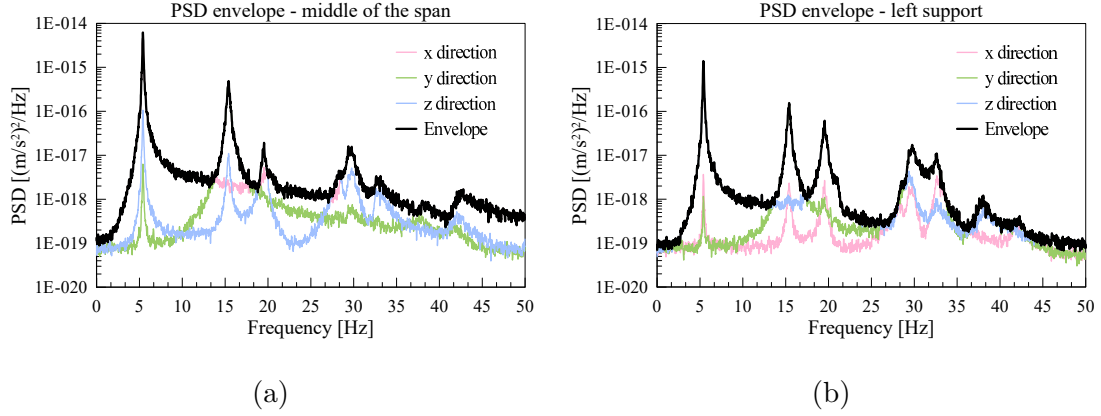


Figure 3.8: Spectral envelope between the three measurement directions x, y and z: (a) Sensor located in the middle of the span; (b) Sensor located at left support

In more detail, 30 s data blocks were considered, corresponding to a frequency spacing of 0.03Hz. Estimation of PSD by Welch’s method has been performed by using a no-overlap Hanning window, considering its good frequency resolution and reduced spectral leakage. Figure 3.8 shows a resulting characteristic spectrogram concerning the response in the three measurement directions x, y and z of the considered accelerometers, with the computed spectral envelope.

From PSDs, natural frequencies were obtained through automated peak-picking algorithm. The algorithm has been developed to identify peaks in signal spectrum without knowing a priori their number, shape or location. The main idea consists in selecting prevailing local maxima in the PSD curve and discarding a certain number of frequencies according to the following criteria:

- Consider only local maxima with amplitude above a threshold calculated in function of the median of the spectrum;
- Remove all local maxima approaching another higher local maxima and mark it as a peak. Local maxima are indeed ordered by height and, by starting from the highest, all the maxima close to it (a specific frequency range is defined) are discarded;
- For the selected peaks, the amplitude-prominence ratio is calculated and all peaks under a predefined threshold are discarded.

The identification of the natural frequencies through the PP procedure is shown in Figure 3.10 (a).

The identified frequency values are listed in Table 3.2.

As shown in the table 3.2, only three (modes 1, 3, 4) of the six considered natural frequencies were correctly identified, while the remaining three (modes 2,

Table 3.2: Natural Frequencies - PP results

Mode	f_{real} [Hz]	f_{id} [Hz]	Error [%]
1	5.434	5.401	0.61 %
2	6.648	-	100 %
3	15.413	15.402	0.07 %
4	19.570	19.536	0.17 %
5	20.293	-	100 %
6	21.161	-	100 %

5, 6) were not identified by the PP method. The identified frequencies show an identification error in the order of a few hundredths of Hz (0.03Hz, 0.01 Hz, 0.05 Hz respectively), which is comparable to the expected variation in the event of damage occurring.

MPE value has also been obtained for the PP method, that is:

$$MPE = 50\% \quad (3.72)$$

As can be deduced from the the above, the PP method provides acceptable estimates of resonance frequencies if vibration modes are well separated. However, if close modes are present (as in this case), this procedure is not able to properly distinguish them, leading to incorrect and incomplete dynamic identification. Moreover, in the case of low excitation or higher noise levels, the identification of peaks would be affected by an increasing error value. Therefore this methodology, although has the advantages of being quite simple and time effective (it does not require long processing times), results to be not reliable for continuous and automatic monitoring systems.

Frequency Domain Decomposition (FDD)

As underlined in section 3.4.2, FDD is a non-parametric OMA method, which is based on the evaluation of the spectral matrix and the consecutive application of the Singular Value Decomposition (SVD) procedure at each frequency line. This methodology, contrary to the PP approach, is able to identify close modes, thus obtaining better results. In fact, the decomposition into SDOF systems allows to separate modes with very close frequencies.

FDD technique has been applied to output time-series, by considering data windows of 30s, without overlapping. Singular Values (SV) have been extracted using

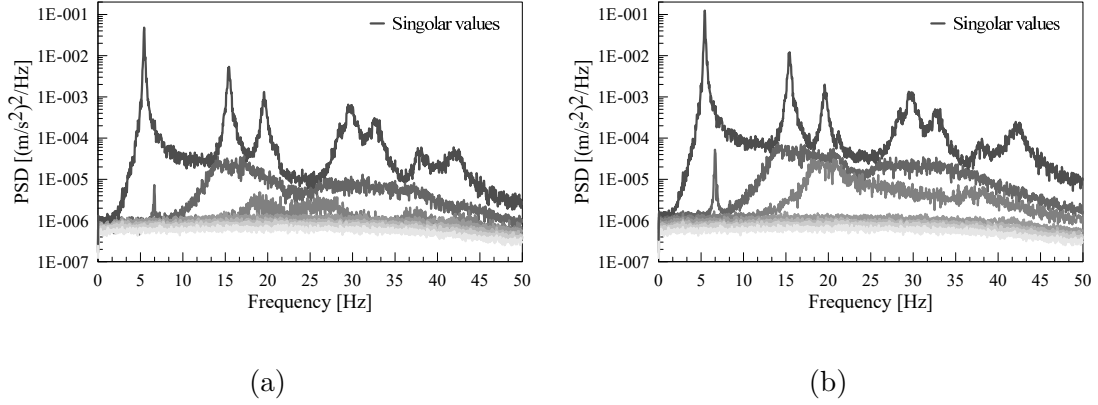


Figure 3.9: SVD diagram: (a) Sensor located at left support; (b) Both sensors (left support and middle of the span)

SVD of the power spectral density. In Figure 3.9, SVD diagrams obtained considering one accelerometer (installed on the left support) and both accelerometers (left support and middle of the span) are illustrated.

As shown in Figure 3.9, the bridge has two close modes (1st frequency 5.434 Hz and 2nd frequency 6.648 Hz) which are well identified by two different singular values. It is noteworthy that in the case of SVD calculated using time series from both accelerometers (Figure 3.9 (b)) the peaks are more easily identifiable (especially looking at the II singular value) than in the case of a single accelerometer (Figure 3.9 (a)).

From SVD diagrams, frequencies were subsequently extracted through the peak-picking algorithm described above, applied to singular values curves. Table 3.3 listed the identified frequencies, with the corresponding error with respect to actual values and the Singular Values (SV) for the identified modes.

Table 3.3: Natural Frequencies - FDD results

Mode	f_{real} [Hz]	f_{id} [Hz]	Error [%]	SV
1	5.434	5.435	0.02%	I
2	6.648	6.636	0.18%	II
3	15.413	15.44	0.18%	I
4	19.570	19.56	0.05%	I
5	20.293	20.81	2.55%	I
6	21.161	21.21	0.23%	I

It is shown in Table 3.3 that both first two frequencies, which are pretty close

to each other, have been detected using FDD method. Moreover, with reference to Figure 3.10 (a) and (b), it is possible to observe that, although both methods (PP and FDD) use peak-picking approach to detected frequencies, FDD method presents smoother and more explicit curve with respect to PSD, so that peaks are more easily identified.

MPE value has also been obtained for the FDD method, that is:

$$MPE = 1\% \quad (3.73)$$

As deduced from the MPE value, FDD method proved to be more accurate than the previous one (PP). This approach is used usually as a multi-channel method, which means that the responses of all the sensors installed on the bridge are taken as input of the FDD. Using multiple measurements leads to a more correct and complete frequency identification. Moreover, as underlined before, close modes can be easily distinguished by decomposing the spectral density matrix into a set of single degree of freedom systems.

However, the identification of some frequencies (modes 5, 6) is not very accurate, with errors in the order of tenths of Hz (0.5 Hz and 0.05Hz respectively), which are unacceptable in a damage identification process.

Covariance-driven Stochastic Subspace Identification Method (Cov-SSI)

Cov-SSI method, whose analytical description is given in section 3.4.3, utilizes the covariance functions, estimated from raw measurements, for the modal parameter identification. A block Hankel matrix of covariance functions has been used to develop SSI-Cov algorithm. Stabilization diagrams were adopted to distinguish physical modes from spurious modes, in order to correctly estimate the modal parameters of the bridge. In fact, physical modes should appear with consistent modal properties (e.g. frequencies) at various model orders while spurious ones should show a non-constant behavior. Physical modes are separated from spurious mathematical ones by identifying alignments of stable poles, since the spurious ones tend to be more scattered and typically do not stabilize. More in detail, the following stability requirements have to be fulfilled for stability condition:

$$\left(\frac{|f(n) - f(n+1)|}{f(n)} \right) < 0.01 \quad (3.74)$$

$$\left(\frac{|\xi(n) - \xi(n+1)|}{\xi(n)} \right) < 0.05 \quad (3.75)$$

Once identified, noise modes are discarded and only real modes are considered. Figure 3.10 (c) illustrates the stabilization charts obtained from the processed time histories plotted together with the PSD curve.

From Figure 3.10 (c) it is possible to note that stable and noise modes have been successfully recognized in the frequency range of 0-50 Hz. Moreover, the identified resonant frequencies show a good agreement with the peak frequencies from PSD. As for the previous methods, identified frequencies are listed in Table 3.4, with the corresponding error with respect to actual values.

Table 3.4: Natural Frequencies - Cov-SSI results

Mode	f_{real} [Hz]	f_{id} [Hz]	Error [%]
1	5.434	5.431	0.07%
2	6.648	6.648	0.00%
3	15.413	15.411	0.01%
4	19.570	19.568	0.02%
5	20.293	20.261	0.16%
6	21.161	21.127	0.16%

As can be seen, all the considered resonance frequencies have been detected with quite good precision. MPE value, that is:

$$MPE = 0.07\% \quad (3.76)$$

is in fact lower than the two previous methods. This methodology, which has proved to provide consistent and sufficiently accurate results, is recognized by the literature [19] as one of the most reliable OMA methods, due to its relatively short computational time, the accuracy of results, even in the case of very close modes, and the possibility of making the identification automatic, given its quite simple theoretical formulation. However, some considerations must be made on setting the input parameters. The following section will clarify such a point.

Polyreference Least-squares Complex Frequency-Domain Method (PolyMAX)

A very common parametric method working in the frequency domain is the Polyreference Least-squares Complex Frequency domain method, known with the name of PolyMAX, as described in section 3.4.2.

Stabilization diagrams, obtained by cyclically repeating the PolyMax procedure for increasing model order, were used for separating the physical system poles from

mathematical ones, as described for Cov-SSI method. Figure 3.10 (d) illustrates the stabilization charts obtained from the processed time histories plotted together with the PSD curve.

From Figure 3.10 (d) it is possible to note that stable and noise modes have been successfully recognized in the frequency range of 0-50 Hz. The identified resonant frequencies show a good agreements with the peak frequencies from PSD. As for the previous methods, identified frequencies are listed in Table 3.5, with the corresponding error with respect to actual values.

Table 3.5: Natural Frequencies - PolyMAX results

Mode	f_{real} [Hz]	f_{id} [Hz]	Error [%]
1	5.434	5.444	0.20%
2	6.648	6.650	0.02%
3	15.413	15.424	0.08%
4	19.570	19.574	0.02%
5	20.293	20.284	0.04%
6	21.161	21.148	0.06%

As can be seen, all the considered resonance frequencies have been detected with quite good precision. MPE value is:

$$MPE = 0.07\% \quad (3.77)$$

which is the same value obtained from the Cov-SSI method.

Results show that this method allows to obtain very well ‘stabilized’ poles, with a very limited number of unstable poles. The stabilization charts are certainly clearer if compared to Cov-SSI results; however this method is a more time consuming process.

3.5.3 Final Considerations about OMA methods

In the previous paragraphs, results from the application of some of the more widely used OMA methods to a numerical case study have been illustrated. Far from being a comprehensive evaluation of all the different OMA techniques, the application of the aforementioned methodologies to a numerical case study provided an overview of the main advantages and disadvantages of each method, giving the opportunity to make some considerations aimed at choosing one of these methods to be applied for the automatic and continuous monitoring of a network of structures.

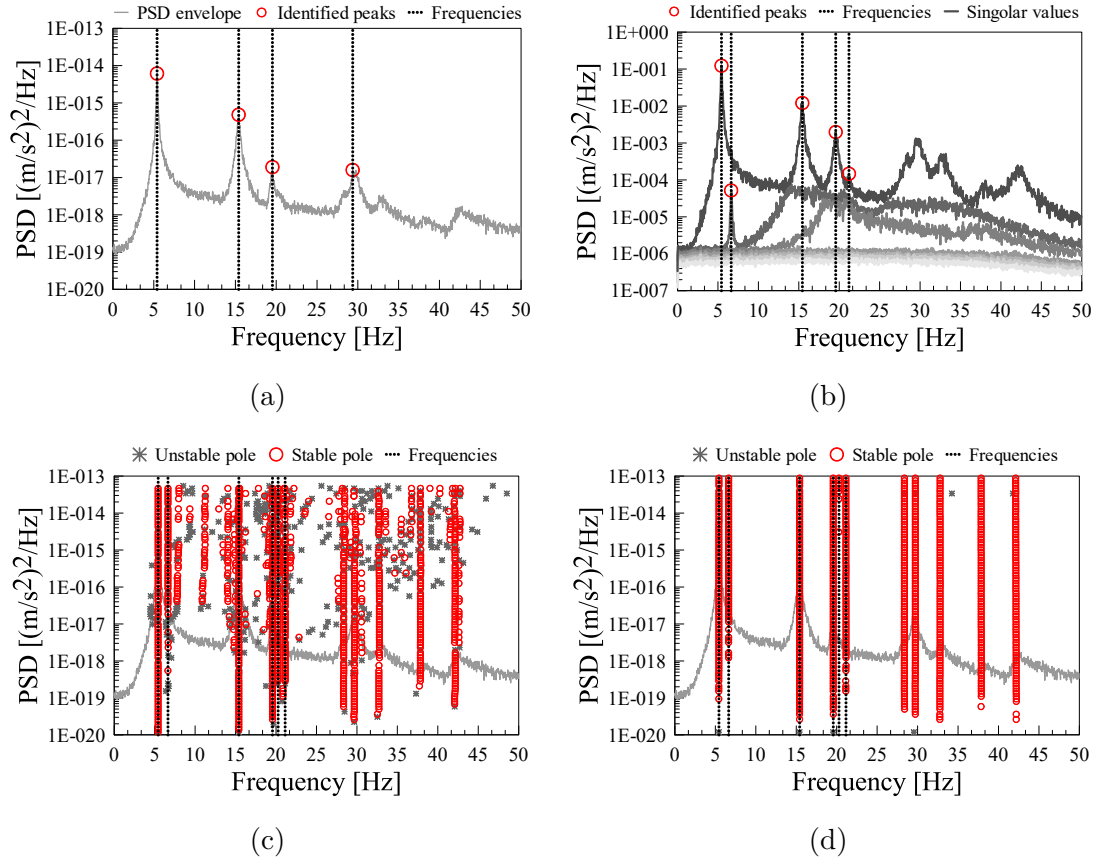


Figure 3.10: Comparison between different OMA identification methods: (a) Peak-Piking; (b) Frequency Domain Decomposition; (c) Covariance-driven Stochastic Subspace Identification Method; (d) PolyMAX

Based on the above, this paragraph summarizes the main comparative results of the previously illustrated OMA methods. The following observations underlie the selection of the OMA approach implemented into the real-time monitoring system, which has been installed on a significant number of structures currently under control.

Peak-Peaking is one of the first developed and widely applied method for modal identification problems of civil engineering structures. It is a very simple, fast and easy to implement method. However, despite its historical relevance, it shows obvious limitations compared to more robust and recently developed methods. First among them, this method is unable to separate and distinguish closely spaced modes, as observed for the presented case study. Moreover, the accuracy of this method is very limited and therefore it is not suitable for being used in a monitoring system with automatic alarm activation, because a large number of false alarms would be produced.

A more accurate method compared to Peak-Peaking is the FDD approach. This methodology is also quite fast and simple to implement and can be advantageously used for providing acceptable estimates of the modal parameters. Moreover, FDD is able to identify very close or even coincident modes, which would be almost impossible with the Peak-Piking method. However, although the accuracy of this method is quite good if compared with PP results, there are methods able to guarantee much higher levels of precision, such as Cov-SSI and PolyMAX methods.

PolyMAX is a parametric method used for identifying very closely spaced modes through a polynomial model. This method is able to provide very accurate estimates of modal parameters by making the selection of the system poles very effective, almost completely eliminating the presence of unstable poles. It performs also very well for the automation of the modal identification process, thanks to the very limited number of spurious poles. However, it is more complicate to implement and computational demanding with respect to others equally performing methods.

Cov-SSI belongs to the subspace methods and it is both less computational demanding with respect to PolyMax and and very accurate in estimating modal parameters. Indeed, since linear algebra is used to solve the identification problem, lower computational effort is needed for estimating the dynamic properties of the system. These advantages have made this method very popular and widely used for structural monitoring applications.

Based on these considerations, the Cov-SSI method was chosen for the continuous and automatic monitoring system installed on all the structures described in this dissertation.

Chapter 4

Proposed Methodology

4.1 Chapter Introduction

This chapter describes a new methodology for continuous and long-term monitoring of a network of structures, equipped with a large number of sensors. As mentioned in Chapter 3, dynamic monitoring has increasingly gained attention among the scientific community in the past two decades. Over the years, a large number of damage identification algorithms have been developed, from the simplest to the most sophisticated, capable of identifying even very small variations in the dynamic behavior of a structure. However, in most cases, these techniques have been tested and applied on small structures with a limited number of sensors. But, as is known, the number of civil engineering structures affected by aging and degradation worldwide is very large and tends to increase more and more over time. This means that being able to monitor as many structures as possible in the coming years is currently a priority. With this in mind, the proposed methodology aims to provide a framework for continuous and long-term monitoring of a large number of infrastructures, in an automatic and effective way.

4.2 Aim of the proposed Methodology

The main goal of the proposed methodology is to provide a complete data-driven method, able to automatically generate system health indicators without any specific analysis on the monitored structure. Indeed, the currently used monitoring systems are based on a system driven approach, which requires a strong knowledge of the structure under observation. However, in the case of a large number of monitored systems, it is impossible to analyze each structure individually. Furthermore, considering that structures could be instrumented with a dense array of sensors, real-time data processing could prove to be very expensive on a computational level and often useless (for example in the case of a non-excited structure).

It is important to emphasize that all the techniques currently used for structural health monitoring are aimed at detecting, localizing and quantifying damages, in order to predict the remaining life of a structure. However, with a view of instrumenting a large number of structures with long-term monitoring systems, it is difficult, if not impossible, to go beyond the damage detection. In fact, to estimate the location and extent of the damage, a very large number of sensors would be required, which is very arduous in a view of a network of structures for costs and amount of data generated to manage. Therefore, the challenging goal of a reliable long-term monitoring system is to notice an evolving damage in its initial stage, in order to trigger more detailed analysis.

For these reasons, a multilevel monitoring system has been developed, based on different levels of complexity to assess the health status of a structure. In particular, this methodology does not need any by-hand configuration and is able to automatically set proper threshold values with the aim of effectively detect any structural damage. In order to make the monitoring system, and therefore the damage identification algorithms, reliable, efficient and robust, modal parameters were combined with statistical analysis and machine learning approaches with the goal of detecting anomalous behaviour from acceleration time series continuously acquired by sensors while reducing the occurrence of false alarms. One of the main advantages of using different types of analysis lies in the possibility of having a global view of the health condition of the structure, observed from different perspectives. This means that a damage can be detected (but not localized or quantified) without measuring points close to the damaged zone. Moreover, the multilevel approach allows, on one hand, making the alert signals sufficiently robust and reliable while, on the other, avoiding high computational cost and time. Therefore, the monitoring methodology is crucial in this context.

Taking into account the aforementioned needs, the following main objectives have been achieved by the developed methodology:

1. development, implementation and testing of a data acquisition and storage procedure, in order to efficiently collect data from sensors by discarding those deemed to be lacking in information and therefore limiting the amount of data stored and analyzed. More in detail, this topic includes:
 - development of a Principal Component Analysis (PCA) procedure aimed at recognizing significant (and thus useful) dataset while discarding not sufficiently excited vibration data;
 - definition of a proper (minimum) time-window of continuous and synchronized acceleration data to be used for obtaining accurate modal parameter estimates;
 - implementation of a statistical procedure to identify observations that appear to be rare given the available data. The main goal is to identify

- exceptional (and instantaneous) events, such as earthquakes, landslides, explosions, in order to analyze in real-time the effect of these events on the monitored structure, by triggering further actions;
- conception and implementation of spatial logics between sensor nodes, in order to create a communication network that takes into account the measurement exchanged among neighbouring devices.
2. development and implementation of a strategy to efficiently elaborate a large amount of data in the shortest possible time fully exploiting the resources of the cloud platform;
 3. conception and development of a multilevel damage detection procedure, aimed at providing an early-stage alert of anomalous conditions that should trigger more detailed analysis or, if necessary, in situ inspections. In particular, the proposed methodology is based on different levels of alarm (three levels), fully exploiting the potentiality of the monitoring system, where the interaction between different sites of computational capability has been used to produce a reliable alert in case of damage. The main contributions of the proposed methodology are:
 - the definition and implementation in each sensor node of a first level of alarm, which is computationally inexpensive, to make a first selection of the possible anomalous conditions;
 - the definition and implementation of a second level of alarm, performed inside the IoT gateway, based on a machine learning model;
 - the definition and implementation of a third level of alarm, checked by the IoT cloud, based on OMA methods that requires more computational capacity, used for verifying whether the reported anomalous condition was actually a structural damage or not;
 - implementation of a new parametric methodology to perform the automatic tuning of the parameters used for OMA identification algorithms, in order to provide a tool that can independently and automatically set the best values to be use for each monitored structure;
 - evaluation of the influence of environmental factors on modal parameters and implementation of a procedure able of automatically remove this influence from data.
 4. application of the proposed methodology for the long-term real-time monitoring of a significant number of structures (about 15 bridges) currently in operation;

5. automatic and real-time identification of damages occurred on two of the currently monitored structures, demonstrating the robustness and reliability of the proposed methodology. The two aforementioned case studies, illustrated in detail in chapter 5 and chapter 6, are:
 - a box composite highway bridge, strengthened by both internal and external prestressing, where all the features of the proposed methodology were applied and permitted to prove the effectiveness, feasibility and reliability of the adopted techniques, being able to detect real damages occurred during the monitoring period;
 - a pre-stressed concrete bridge from the early 1965s, where real changes in structural stiffness were identified through a dynamic monitoring system in which the proposed methodology has been adopted;
6. effective management of Big Data generated continuously by a large number of sensors installed on a large number of structures, ensuring a high level of data quality and accessibility for the assessment of the health status of a system.

In the following paragraph, the proposed methodology is described in detail. Moreover, it has been successfully applied to more than 15 concrete highway bridges currently monitored (a large set of traffic-excited vibration data is available for each structure) and allowed to identify real stiffness changes occurred in the last 3 years on some of the monitored systems.

4.3 Monitoring system description

In this dissertation an innovative framework for long-term continuous monitoring systems is proposed. In particular, a multi-level distributed structure is adopted, in order to make the system lasting and more efficient. The proposed monitoring system is based on vibration measurement through the use of MEMS accelerometers and data acquisition systems able to measure the response of the studied structure under a unknown excitation. MEMS (Micro Electromechanical Systems) sensing techniques have been widely used since the 1990s, mainly due to their lower costs, greater miniaturization and the possibility of using them in a greater number of applications [14]. It has been shown [58] that MEMS sensors present overall good performances for the estimation of dynamic parameters.

Civil engineering structures, such as bridges, are instrumented with a network of cooperative tri-axial accelerometers, which are dispersedly installed on the structure to monitor its dynamic behavior over time.

Each tri-axial MEMS accelerometer provides data in the 3 orthogonal directions (x, y, z). Dealing with bridges, the x axis is the transversal direction of the deck,

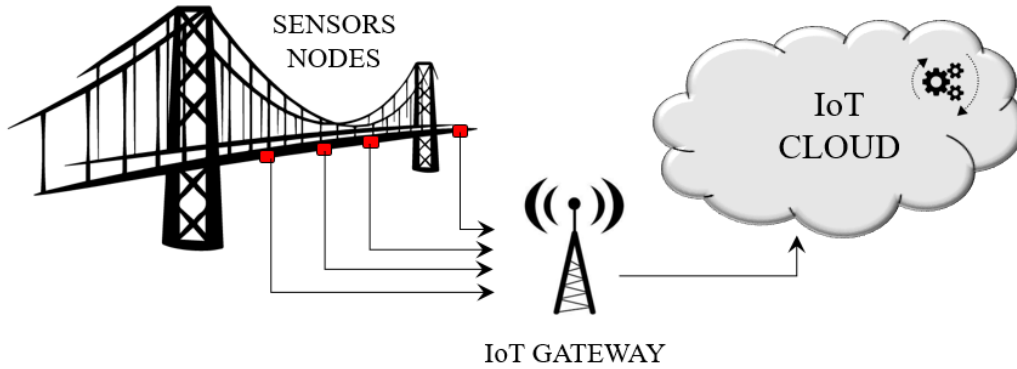


Figure 4.1: IoT Monitoring system overview

y axis is parallel to the longitudinal extension of the bridge and z axis points downwards so that it is aligned with gravity.

The main problem to be faced dealing with long term monitoring systems is the maximum data streaming rate, a real sticking point when working with accelerometers, as well as the maximum allowable sampling rate per channel. For these reasons, the system was properly designed in order to cope with the monitoring needs. In particular, the installed SHM system can be divided into three main parts: the sensor nodes, the IoT gateway and the Data Center, also known as IoT Cloud.

Sensor nodes can be defined as nodes in a sensor network that can perform some processing inside the node itself, collect information and communicate with other connected nodes in the network. Therefore, a sensor node is something different from traditional sensors adopted for SHM: in fact, in addition to the sensor, it also includes a microcontroller which is able to perform tasks like local sampling, data elaboration to compress information and the management of data that have to be transferred to the gateway through a wired or wireless connection. Moreover, a humidity and temperature sensor is included in the sensing device, in order to collect environmental data which must be taken into account when processing accelerometric data (especially temperature). The tri-axial accelerometers are characterized by a range of ± 2.5 g and a bandwidth of 50 Hz. To increase accuracy, acceleration data are sampled at the sensor level at 25.6 kHz, filtered down and down sampled to finally obtain a sampling rate of 100 Hz; this sampling frequency is the maximum allowable sampling rate per channel, due to the data streaming limitation through the network.

Once collected, acceleration data are encoded by the microcontroller into a CAN BUS driven network and sent to a local IoT gateway. The IoT gateway is able to collect data from the measurement nodes, do some preliminary preprocessing

and send a set of chosen information to the cloud. Pre-processing is especially aimed at filtering acceleration data, in order to detect unusual patterns that do not conform to the expected behavior (outliers), discard corrupted data and generate anomaly alert messages when needed. Moreover, the IoT gateway can calculate different parameters for a preliminary quick inspection, such as the average (AVG), maximum/ minimum (MIN/MAX) and root-mean-square(RMS) values on interval-by-interval basis. As it will be explained in the following paragraphs, the IoT gateway represents an interesting stage of the monitoring system, where a first step of the damage detection process can be carried out at a higher level than just on one sensor node; as at this level, more channels can be evaluated, accounting for the available cross sensor information.

Finally, the acceleration, temperature and humidity time series coming from measurement nodes are sent to the cloud monitoring infrastructure. Indeed, the monitoring system is connected to the internet via a 5 GHz point-to-point Wi-Fi link between two access points, located on the structure. An Ethernet cable connects the access points to the two IoT gateways.

Data are then available to be accessed, downloaded or processed on a IoT cloud environment. Considering that the amount of stored data is of noticeable dimensions, the main challenge when designing the system is to elaborate this huge amount of information in the shortest time by using cloud resources at best. Taking advantage of the high parallelism (up to 1000 simultaneous executions) available in the IoT cloud, data composed by time series of length T seconds can be subdivided into m slot of T_w seconds such that the algorithm can elaborate a slice of data with low time and memory consumption.

It is important to notice that the different components of the monitoring system (sensor nodes, IoT gateway, IoT cloud..) can be remotely accessed, so it is possible to change the system configuration and the control parameters if necessary during the monitoring period.

The main challenge is, then, exploiting all the potentiality of the monitoring system, avoiding waste of resources. Being aware of the capacity and limits of the different components, a strategy for early detection damages has been developed.

The following paragraph describes in detail the proposed methodology. In particular, the focus is primarily on the data acquisition and storage procedure, aimed at efficiently and automatically collect acceleration records from sensors while discarding unnecessary data. Subsequently, the multilevel procedure for damage detection is detailed, allowing real-time structural system identification through model-free techniques.

4.4 Acquisition and Storage Protocol

As aforementioned, the goal of the proposed methodology is mainly to provide a framework for continuous and long-term monitoring of a large number of structures. With reference to paragraph 4.3, in order to monitor as many structures as possible with an adequate number of acceleration sensors, low-cost systems based on MEMS sensing techniques are used, taking into account practical and economical SHM needs. As it can be easily imagined, a network of accelerometers installed on a network of structures generates a large amount of sensor data per second. This means that, if multiple structures are monitored for long time (years), the amount of data becomes enormous. Efficiently dealing with this Big Data in a resource-constrained system is then a challenge. Indeed, vast amounts of data require an infrastructure to store them, which often means investing in cloud solutions that are more expensive the more data are stored in them. Moreover, the more data you need to store, the more complex these problem will become. In parallel, the collected data must be processed and analyzed to generate information, which implies a large computational power consumption in relation to the amount of data to be processed.

For all these reasons, smart data acquisition and storage is therefore essential in order to limit the amount of data to be archived (and therefore the space needed to store them) and to be analyzed.

The proposed methodology is based on the idea that only data that can effectively be used to generate information on the health status of a structure must be acquired and stored. These data correspond to the moments in which the structure is sufficiently excited, i.e. when the acceleration values exceed a predetermined threshold. Dealing with bridge structures, the main excitation sources are traffic and wind. The proposed framework is based on a wake-up mechanism according to which, if the traffic rate (or wind) is sufficiently high, the sensor "wakes up", acquiring and storing the corresponding accelerometric readings while, if the traffic is low or absent, data are discarded.

More in detail, the developed smart data recording and storing procedure consists of the so called "active/passive" sensing status. In passive mode, sensor nodes collect vibration data continuously and can intelligently understand whether recorded data are significant or not. If meaningful data are recognized, active mode is activated and data are processed and stored. Unnecessary data are discarded, improving the performances of the network and simplifying data management.

The standard deviation (STD), which is a measure of the dispersion of the acceleration data relative to its mean, was chosen as the representative parameter of the vibration energy contained in the signal. The reason for this choice can be found in the nature of the expected input (mainly traffic or wind), which is perceived as an impulse by the accelerometers. This means that, if the structure is excited, the standard deviation increases (the variation of data around the mean would

increase due to the impulse recorded); on the contrary, if the excitation is poor or absent, the standard deviation tends to a very low constant value, which is the intrinsic noise of the instrument. Therefore, the measure of the energy contained in the vibration signals is carried out by evaluating the STD value during the preprocessing of data at node level. However, some considerations must be made regarding the acquisition and storage protocol:

- it is necessary to define a threshold value that is able to "wake-up" the system when an appropriate excitation level is detected;
- a fundamental aspect is then the definition of a proper (minimum) time-window of continuous and synchronized acceleration data to be used for obtaining accurate modal parameter estimates. In fact, if only meaningful data (above threshold) were stored, the risk exists of storing and analysing many time histories few seconds long (corresponding, for example, with the cars passing on a bridge), which would not allow an adequate modal identification process. For this reason, it is essential to evaluate a minimum number of samples (N_{min}) needed for an accurate identification of the dynamic parameters of the structure;
- once a minimum time-window to carry out a modal analysis has been identified, it is necessary to define a second threshold value to evaluate whether the data included in the window are significant or not. To better understand the topic, imagine that a minimum time-window of 10 minutes (corresponding to $6 * 10^4$ samples) of consecutive vibration data has been defined for an highway bridge. It could happen that the system is awakened by the passage of a vehicle (which would generate an STD value above the threshold) and that for the next 10 minutes no other vehicles cross the bridge. This would involve acquiring and storing 10 minutes of data that is actually meaningless. Therefore, in addition to the wake-up threshold, another threshold value, aimed at evaluating whether the data collected within the identified time-window are sufficiently excited or not, has been defined;
- it is also fundamental to consider that, for an effective identification of modal parameters, data collected by all the sensors installed on a single structure must be synchronized. This means that, even if the threshold check takes place on each sensor node, the data storing action must be triggered for all sensors together. This implies the definition of a minimum percentage of sensors, whose threshold exceeding is capable of triggering the data storage action;
- it is also essential to take into account sudden and exceptional events. The main idea is that, if an extreme event occurs generating vibrational levels

far outside the standard values recorded under normal operating conditions, storage and analysis logics of these data must follow a different protocol with respect to the normal acquisition procedures. Indeed, civil engineering infrastructures can experiment sudden and exceptional events, such as natural disasters like earthquakes and landslides, or human-induced hazards like explosions, traffic accidents etc...It is thus crucial on the one hand detecting such sudden events, in order to trigger further actions aimed at assessing the condition of the structure, and on the other make sure that the acceleration signals relating to the event are properly stored. For these reason, a specific threshold has been defined in order to cope with the aforementioned needs.

Based on these considerations, three different threshold values are defined:

- *Wake-up threshold (T_{WU}):* the wake-up threshold is calculated on the STD value obtained by dividing the available time series in segments of 1 second (100 samples), corresponding to the sampling frequency of the measuring instrument, 100 Hz. It indicates that the measured vibration data correspond to a significant (traffic induced) excitation level of the structure. This threshold is used to wake up the system and start storing (on the IoT Gateway) the defined minimum number of samples (N_{min});
- *Trigger threshold (T_T):* the trigger threshold is calculated on the defined minimum number of samples (N_{min}) and indicates whether the data packet consisting of N_{min} samples is significant or not. In case of meaningful data, samples are stored and analyzed;
- *Sudden event threshold (T_{SE}):* the sudden event threshold indicates that an abnormal vibration level has been reached, so data must be acquired and further actions must be activated.

A graphical representation of the implemented acquisition and storage procedure can be found in Figure 4.2.

As can be deduced from the flow chart, the implementation of the acquisition and storage protocol follows the following steps:

1. acceleration signals are continuously acquired at a sampling rate of 100 Hz by sensor nodes, in the 3 measurement directions x, y, z. The expected output a_i is given by:

$$a_i = \begin{bmatrix} x_i \\ y_i \\ z_i \end{bmatrix} \quad (4.1)$$

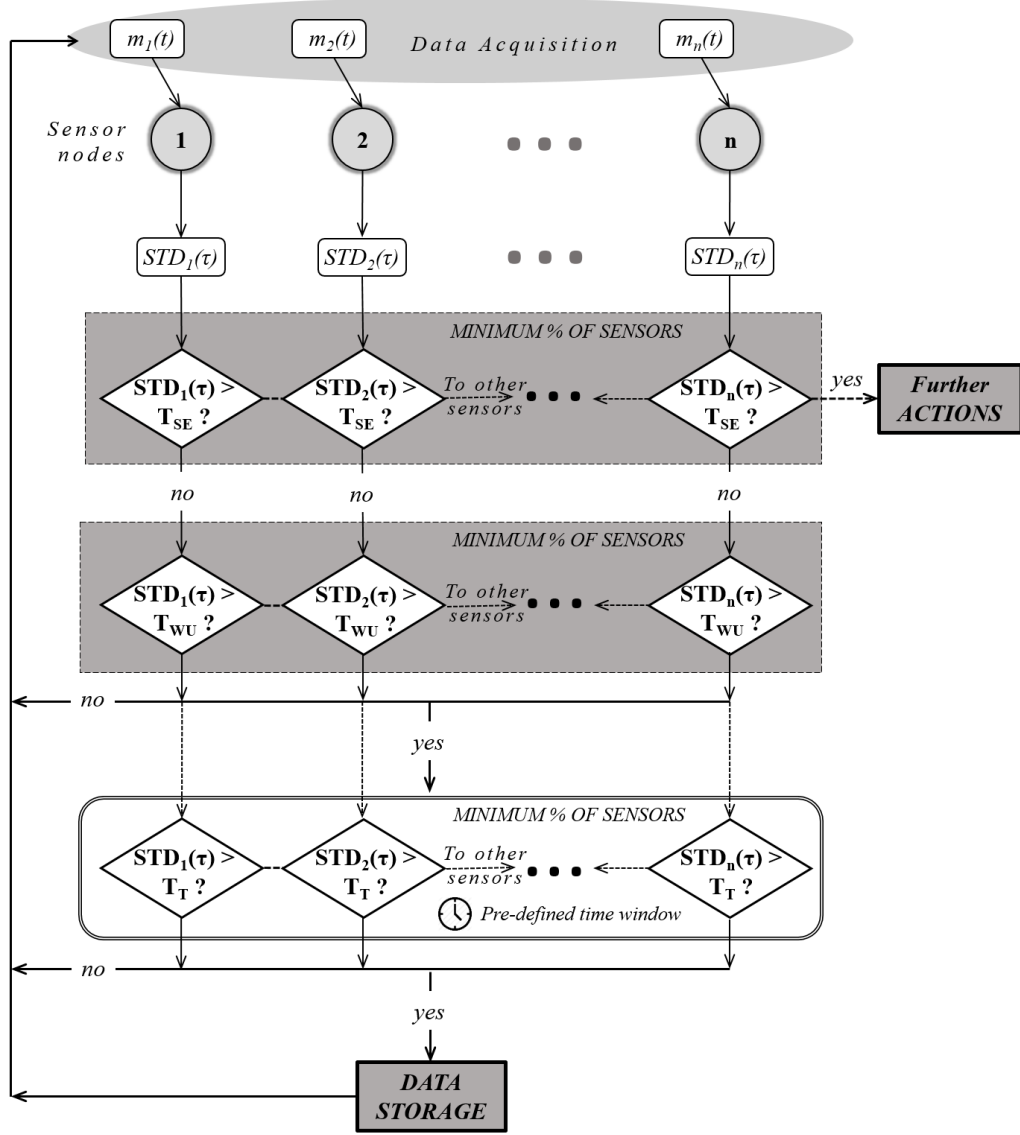


Figure 4.2: Acquisition and storage procedure

- in order to take into account the contribution of all axes, the modulus of a_i is determined as:

$$m_i = \sqrt{x_i^2 + y_i^2 + z_i^2} \quad (4.2)$$

- standard deviation value (STD) is calculated every 100 samples for each sensor node;

4. STD value is compared with the T_{SE} threshold for each sensor. The information regarding this check is exchanged among neighbouring sensor nodes in order to verify whether the minimum percentage of sensors exceeding the threshold has been reached or not;
5. if the minimum percentage of sensors exceeding the T_{SE} threshold has been reached, other actions are triggered (ref. Paragraph 4.4.3);
6. if the minimum percentage of sensors exceeding the T_{SE} threshold has not been reached, STD value is compared with the T_{WU} threshold for each sensor. The information regarding this check is exchanged among neighbouring sensor nodes in order to verify whether the minimum percentage of sensors exceeding the threshold has been reached or not;
7. if the minimum percentage of sensors exceeding the T_{WU} has not been reached, meaning that no significant energy is contained in the signal, data are discarded and the acquisition process continues without storing that time series;
8. if the minimum percentage of sensors exceeding the T_{WU} threshold has been reached, a clock is activated synchronously for all sensors and data starts to be stored in a local buffer until reaching the pre-defined number of sample N_{min} (corresponding to a pre-defined time-window);
9. standard deviation value (STD) is calculated for the N_{min} samples;
10. STD value is compared with the T_T threshold for each sensor. The information regarding this check is exchanged among neighbouring sensor nodes in order to verify whether the minimum percentage of sensors exceeding the threshold has been reached or not.
11. if the minimum percentage of sensors exceeding the T_T threshold has been reached, data (of all sensors) are sent to the IoT cloud and stored;
12. if the minimum percentage of sensors exceeding the T_{WU} has not been reached, meaning that no significant energy is contained in the signal, data are discarded and the acquisition process continues without storing that time series;

The minimum percentage of sensors exceeding the threshold has been set, for all the applications described in this dissertation, at 80% for all types of threshold. The idea behind this choice is that all the points of the structure are subjected to the same environmental conditions (traffic, wind or exceptional events); it follows that any event that generates an excitation on the structure must be recorded by most of sensors. The remaining 20% take into account any compromised (or malfunctioning) sensors in the system.

In the following paragraphs all the procedures used for defining and calculating the aforementioned threshold values and for identifying the minimum time-window necessary for an adequate modal identification process are illustrated.

4.4.1 Thresholds definition - Principal Component Analysis (PCA) approach

This paragraph describes the methodology applied to calculate the value of thresholds T_{WU} and T_T . In particular, the developed methodology allows to automatically set the most suitable threshold values for each sensor, in order to identify the excitation of the structure. To achieve this goal, a Principal Component Analysis (PCA)-based approach has been used.

Principal Component Analysis is a multivariate procedure whose main purpose *"is to reduce the dimensionality of a data set in which there are a large number of interrelated variables...by transforming them to a new set of variables, the principal components, which are uncorrelated and ordered so that the first few retain most of the variation present in all of the original variables"* [36]. PCA has been widely used in SHM for damage detection purposes, with the aim of extracting data features that allows to distinguish between the health status and the damaged one [26]. However, the use of PCA in long-term continuous monitoring systems has several limitations mainly due to its computational cost and data memory footprint, which makes it difficult to use for damage detection in applications where a network of structures is equipped with a large number of sensors.

Nevertheless, in this context, the use of PCA is proposed as a tool for identifying the most suitable thresholds to be used for the acquisition and storage needs. The main idea behind this approach is to use the reconstruction error as the key parameter for identifying the most appropriate threshold value. More in detail, an iterative algorithm has been implemented, using a very low initial threshold guess (close to zero) to generate a sequence of higher solutions until reaching the convergence criterion limits.

Before going into detail about the proposed approach, some basic assumptions have to be underlined:

1. threshold values are updated once a day up to the first month from the installation of the monitoring system and then, they remain unchanged until a possible subsequent update;
2. a one month training period is considered, in order to obtain a valid representation of the system dynamics. During the first month of monitoring, the training period increases day by day up to 30 days;
3. the threshold values must be periodically updated as the amount of data collected increases in time. In particular, threshold values are updated once

a month, if no anomaly is registered;

Principal Component Analysis (PCA)

PCA is a data simplification technique mainly used in multivariate statistics. It was first proposed in 1901 by Karl Pearson and then developed by Harold Hotelling in 1933. The method is aimed at reducing the number of variables that describe a set of data to a smaller number of latent variables, describing most of the available variance. This reduction process occurs through an orthogonal linear transformation that projects the original data into a new coordinate system, in which the first new variable (first principal component) with the greatest variance is projected on the first axis, the second new variable (second principal component), second by variance, on the second axis and so on (ref. Figure 4.3 for a two-dimensional features space).

Suppose that $[X] \in \mathbb{R}^{p \times N}$ is the dataset matrix of p random variables and N observations:

$$[X] = \begin{bmatrix} x_{11} & x_{12} & \dots & x_{1N} \\ x_{21} & x_{22} & \dots & x_{2N} \\ \vdots & \vdots & \ddots & \vdots \\ x_{p1} & x_{p2} & \dots & x_{pN} \end{bmatrix} \quad (4.3)$$

where the columns represent the N observations and the rows are the p random variables, data are summarized by reducing the number of columns of the data matrix $[X]$ defining a number q ($q < p$) of artificial variables. Therefore, a matrix $[Y] \in \mathbb{R}^{q \times N}$ of new data composed of q variables uncorrelated with each other is obtained by a linear combination of the former:

$$[Y]_{q \times N} = [L]_{N \times q} [X]_{p \times N} \quad (4.4)$$

where $[L]$ is the principal components matrix while $[Y]$ is the transformed data matrix (score matrix). In order to obtain the described transformation, the eigen decomposition of the correlation matrix is performed, after normalizing the signals:

$$[C_X] = \frac{1}{N} [X][X]^T \quad (4.5)$$

$[C_X]$ is a square symmetric matrix giving the degree of linear relationship between each pair of elements belonging to the data set. The objective is then to maximize the variance in the directions containing the most significant information, represented by the diagonal of the covariance matrix, and to minimize the

redundancy of data and noise, represented by the covariance found in the non-diagonal elements. More in detail, the eigenvectors with the highest eigenvalues represent the most significant trends recognized in the dataset with the largest quantity of information.

Once the transformation is done, dimensionality reduction can be obtained by projecting the dataset onto the calculated eigenvectors corresponding to the first eigenvalue only. The main components can therefore be used to reconstruct the original dataset. In particular, it is possible to project back the $[Y]$ matrix onto the original space, and obtain the reconstructed data matrix $[\widehat{X}]$ as follows:

$$[\widehat{X}] = [Y][L]^T \quad (4.6)$$

It is thus possible to evaluate the accuracy of the PCA results by calculating the error between the original data and its reconstruction. More in detail, the average reconstruction error can be defined as the distance between the original data points and their projection onto a lower-dimensional subspace (ref. Figure 4.3). Considering a generic signal instance x and its reconstruction \widehat{x} , the reconstruction error E_x can be obtained as:

$$E_x = \sum_{i=1}^N \|x_i - \widehat{x}_i\|^2 \quad (4.7)$$

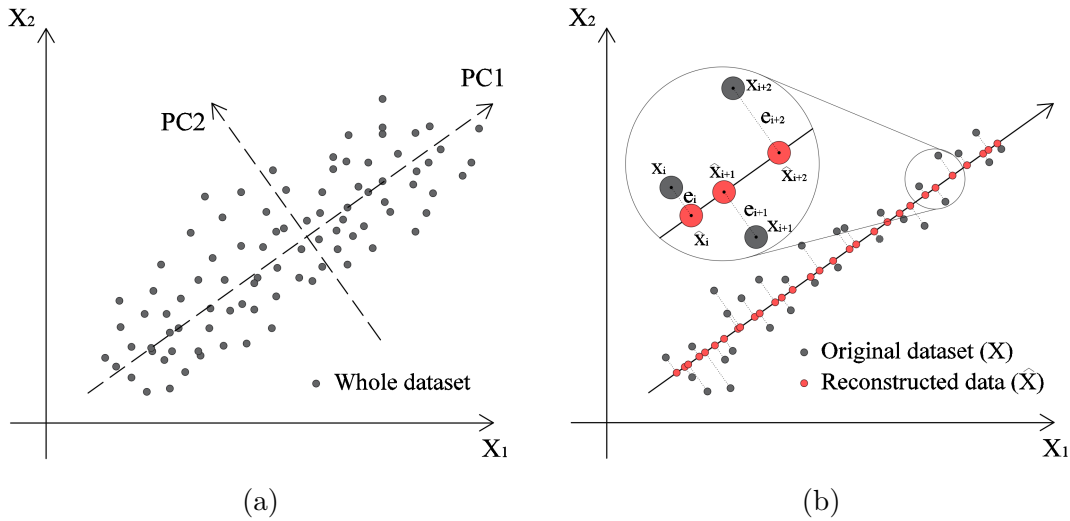


Figure 4.3: Principal Component Analysis. (a) PCA explanation in a two-dimensional feature space; (b) Projection of reconstruction error e_i

The reconstruction error has to be minimized in order to obtain a more accurate approximation of the original matrix $[X]$.

PCA is by definition a non-iterative process, which finds the best squared error fit through a linear representation. However, the following paragraph will illustrate how to integrate PCA into an iterative process aimed at finding the most suitable threshold values for identifying the excitation level of a structure, using as control parameter the reconstruction error E_x .

Iterative process

The proposed methodology integrates the PCA technique described in the previous paragraph within an iterative process aimed at automatically obtaining the two threshold values T_{WU} and T_T . In particular, as aforementioned, a training period of one month is considered. The proposed algorithm for automatic threshold selection based on the reconstruction error of the PCA is structured as follows:

1. Sensors samples are divided in slot of 100 samples (1 second long, which corresponds to the sampling frequency of accelerometers) and the STD value is obtained for each slot;
2. A compression level of the signal is defined, based on the desired level of accuracy for the PCA reconstruction algorithm;
3. An initial very low STD threshold is set. This value will be increased sequentially in a feedback-loop process;
4. All the STD values above the threshold are used as training set for the PCA while the slots under the threshold are discarded as noise. Figure 4.4 shows the application of the described selection process for a currently monitored bridge. In particular, Figure 4.4 (a) illustrates as an example vibration data collected during a time period of 2 hours and corresponding STD values obtained for each data slot of 100 samples. Moreover, Figure 4.4 (b) depicts the histogram distribution of STD data, together with a threshold that separates accepted samples from not accepted ones. As expected, STD data are lognormally distributed, with a large concentration of low values (corresponding to the signal noise) and a lower concentration of high values (corresponding to the dynamic energy in the signal). If the selected dataset has noise inside, the PCA algorithm will not be able to reconstruct it adequately, since by definition the signal noise is a random quantity without any pattern inside. This means that the reconstruction error will be higher. On the contrary, if the selected dataset is composed only of the dynamic response of the structure, the PCA will provide an adequate reconstruction of the input data and consequently the reconstruction error will be smaller. This implies that, as the threshold increases, the reconstruction error tends to decrease until the convergence condition is reached.

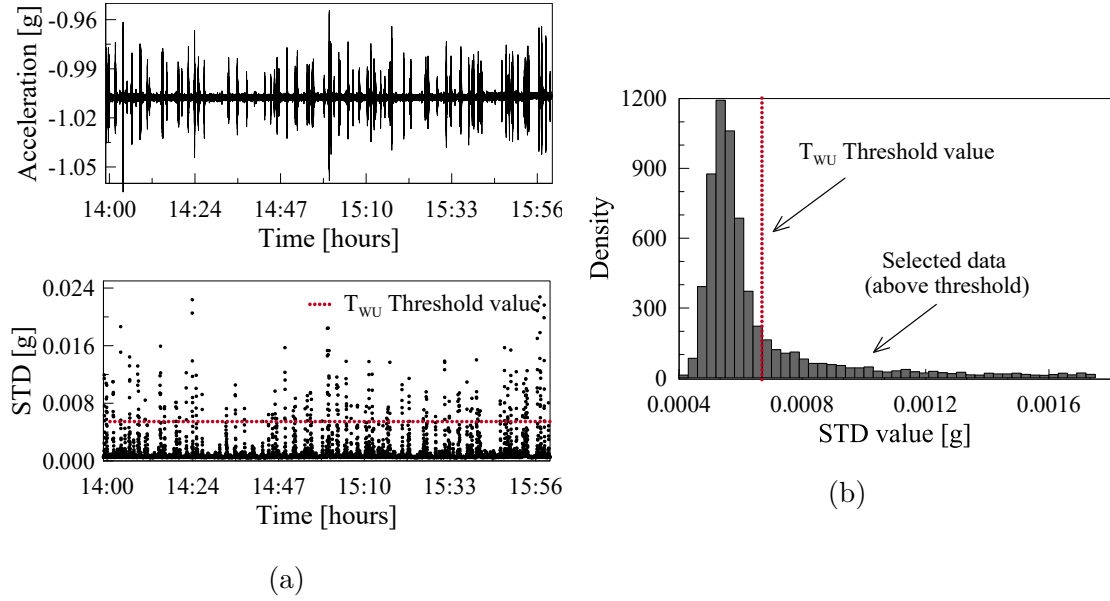


Figure 4.4: Principal Component Analysis example. (a) raw vibration data and corresponding STD values; (b) STD distribution

5. Selected data (above threshold) are used to train the PCA algorithm after removing windows behind the energy threshold;
6. The reconstructed data are compared with the original ones by evaluating the reconstruction error, according to the convergence condition (the partial sums become closer and closer to a limit number). If the convergence is reached, it is possible to exit the loop and define the threshold value. On the contrary, if the convergence is not reached, the threshold value is increased and the algorithm restart from point 4.

4.4.2 Time-Window Size

This paragraph illustrates the approach used for defining the minimum time-window (number of samples N_{min}) to perform an accurate dynamic analysis of the monitored structure.

As aforementioned, when dealing with the acquisition and storage issue, a fundamental aspect is the definition of a proper (minimum) time-window of continuous and synchronized acceleration time-series to be used for obtaining accurate modal parameter estimates. The definition of the most appropriate time-window mostly rely on empirical evaluates and typically vary from few minutes up to one hour for each time window. The evaluation of the most suitable size must be carried out taking into account varius parameters, which are:

- sensor buffer memory, which is the holding place for data recorded by each sensing device. In fact, when the system wake-ups after exceeding the T_{WU} threshold, data are temporarily stored in the sensor local memory in order to evaluate the excitation level of the entire set of data composed of N_{min} samples. Thus, it is necessary that sensor buffers have sufficient storing capacity to contain N_{min} samples and to provide extra memory to be used in case of anomalous events.
- frequency resolution, which is related to the decrease of Leakage error in the frequency domain and can be defined as the capability of distinguishing close frequency components as separate spectral peaks. The frequency resolution can be obtained as the ratio

$$F_r = \frac{F_s}{N} \quad (4.8)$$

where F_s is the sampling frequency and N is number of data points used for spectral analysis. Since the sampling frequency is a constant value for each sensor (equal to 100 Hz in this case), the frequency resolution depends only on the length of the window used for the spectral analysis (the window size represents the number of samples and thus the duration of the signal). It follows that, with reference to equation 4.10, if higher resolution is required, a longer record must be used.

- time resolution, which is the discrete resolution of a measurement with respect to time. The time resolution is by definition inversely proportionate to the frequency resolution and is defined as:

$$T_r = \frac{N}{F_s} \quad (4.9)$$

this means that the longer the window, the less images of the signal evolution in time are available.

- signal to noise ratio, which is a comparison between the level of the desired signal with the level of background noise. In particular, the larger the signal excitation, the smaller the window size needed to perform an accurate modal identification.

These requirements could create very challenging demands to the hardware architecture, asking for very long data sets. It is therefore necessary to find a

solution that can match all these needs, while ensuring a good accuracy of the analysis results.

Considering the frequencies we are interested in, some consideration can be made.

First of all, MEMS accelerometers have limited buffer memory, able to store at most 256 kB of data without generating overflow problems. Thus, considering a sampling rate of 100 Hz on three measuring axes, this means a maximum of 426 seconds of data (about 7 minutes). This value must be reduced by considering an extra memory to be used in case of exceptional events.

Secondly, working with civil engineering structures such as bridges, the minimum identifiable frequency variation that is expected in case of damage is in the order of 0.005 Hz. This means that, considering a sampling frequency of 100 Hz, a window size of at least 20000 samples (about 3min20sec) is required to obtain a frequency resolution of 0.005 Hz.

Finally, the acquisition and storage procedure described in paragraph 4.4.1 allows to select only sufficiently excited time-windows, increasing the signal to noise ratio value. In this way, limiting the presence of signal noise and selecting only the most excited time-series, the accuracy of modal identification is considerably improved. Moreover, acceleration records are post-processed with different type of algorithms that work in the frequency or in the time domain, which take into account that the noisy part of the signal has to be decreased as much as possible. This can be achieved in the frequency domain by splitting the whole signal in smaller windows of length N_w that are used for the computation of the Pwelch of the total record and thus averaging out the noisy component of the measured acceleration. Instead, in the time domain, this can be achieved by computing the Auto and Crosscorrelation functions between all the different acceleration channels by delaying one signal with respect to another, step by step from a minimum ΔT (equal to zero) up to a maximum (ΔT_{Max}), but not overtaking the total length of the recorded acceleration signal.

For all the above-mentioned consideration and in order to considerably improve the accuracy of modal identification, the minimum number of samples N_{min} has been chosen as:

$$N_{min} = 33000samples \quad (4.10)$$

corresponding to a time-window of about 5min30sec. In this way, a frequency resolution of 0.003 Hz is obtained and about 58 kB of memory are left for any sudden and exceptional event.

4.4.3 Sudden Events Threshold

This paragraph describes the methodology implemented to determine the T_{SE} threshold value, used for recognizing sudden events that could affect the monitored structure. In particular, exceptional events such as earthquake, landslides, explosions and so on, can be identified by detecting anomalous acceleration values that are not normally assumed by the structure under standard operating conditions. Statistical analysis is thus a critical component in determining which acceleration value can be considered anomalous or exceptional. Since the nature and type of the possible sudden event are unknown, threshold values cannot be determined based on a priori information. They can therefore be determined adaptively, starting from data collected during a “training phase” and then adjusted as the amount of data increases over time (during the first few months of monitoring).

The proposed methodology uses statistical analysis to identify vibration data that appear to be rare or exceptional given the available dataset. It is important to highlight that the aim of this approach is to make sure that observations relating to sudden events are properly stored and processed. This means that the values identified by the proposed algorithm can be anomalous events as well as exceptional traffic conditions or outliers. But, the method described in this paragraph is helpful in shedding light on rare events, regardless of their nature, properly storing the related time-series and triggering more in-depth analysis.

The population used for the statistical analysis is composed, for each sensor, by all the samples collected during the first month after the installation of the monitoring system. In particular, as the main goal is highlighting the presence of any abnormal behaviors in terms of vibration energy, the standard deviation (STD) value has been chosen as reference parameter. Indeed, the STD, calculated every 100 samples (once per second), represents the dispersion of a set of data relative to its mean that is the measure of the energy contained in the vibration signals collected by each sensor. This means that, if a sudden event occurs, the variation of data around the mean would increase drastically due to the strong impulse recorded.

In order to define the T_{SE} threshold value, the Interquartile Range Method was used. The Interquartile Range (IQR), also known as midspread, is a method widely used in descriptive statistics for measuring the statistical dispersion ([66]). It is obtained as the difference:

$$IQR = Q_3 - Q_1 \tag{4.11}$$

where Q_3 and Q_1 are the 75th and the 25th percentiles respectively. In other words, the IQR can be clearly seen on a box plot on the data (Figure 4.5).

The IQR can be used to find samples that are far from the mean value, by defining limits that are a factor k of the IQR below the 25th percentile or above

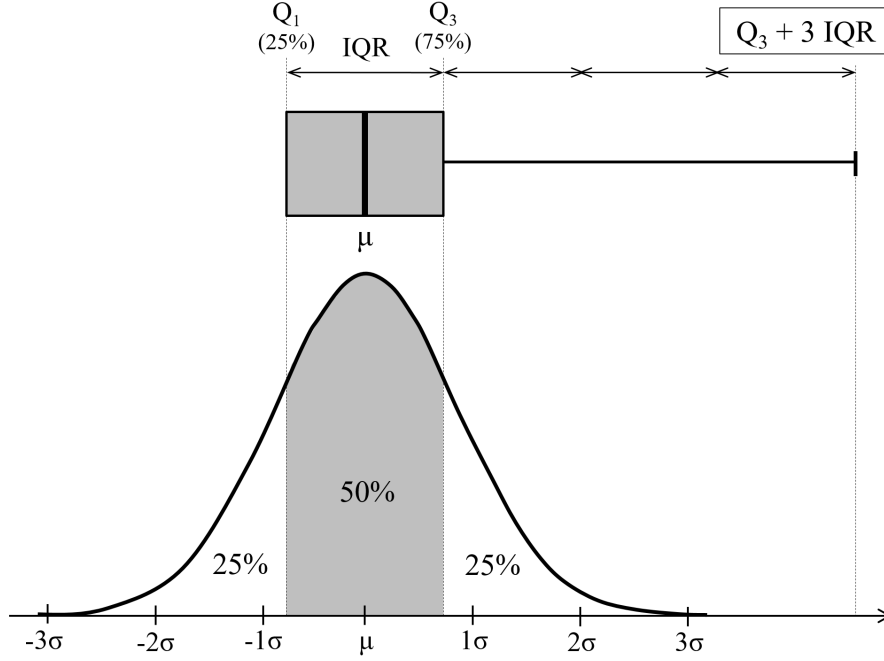


Figure 4.5: Boxplot of the InterQuartile Range (IQR)

the 75th percentile. k factor is usually put equal to 1.5 for outliers but, for extreme “far out” observations, a k factor of 3 can be used.

IQR approach has been applied to STD values calculated for the whole dataset and pre-filtered to eliminate the noisy windows.

In particular, the implemented automatic procedure includes the following steps, summarized in Figure 4.6:

1. the whole considered dataset (one month of data) is subdivided in n slots of 100 samples (one second), such that the algorithm can elaborate a slice of data within time and memory limits. Windows are not overlapped; however, the method can be extended to the case where a certain level of overlap is expected;
2. calculate the modulus m_i , in order to take into account the contribution of all axes (ref. equation 4.2);
3. calculate the standard deviation (STD) value for each window;
4. pre-filter the obtained STD values through the procedure described in paragraph 4.4.1, in order to discard all windows containing a noisy signal (below the T_{WU} threshold) and keep only those in which environmental excitation is recognized;

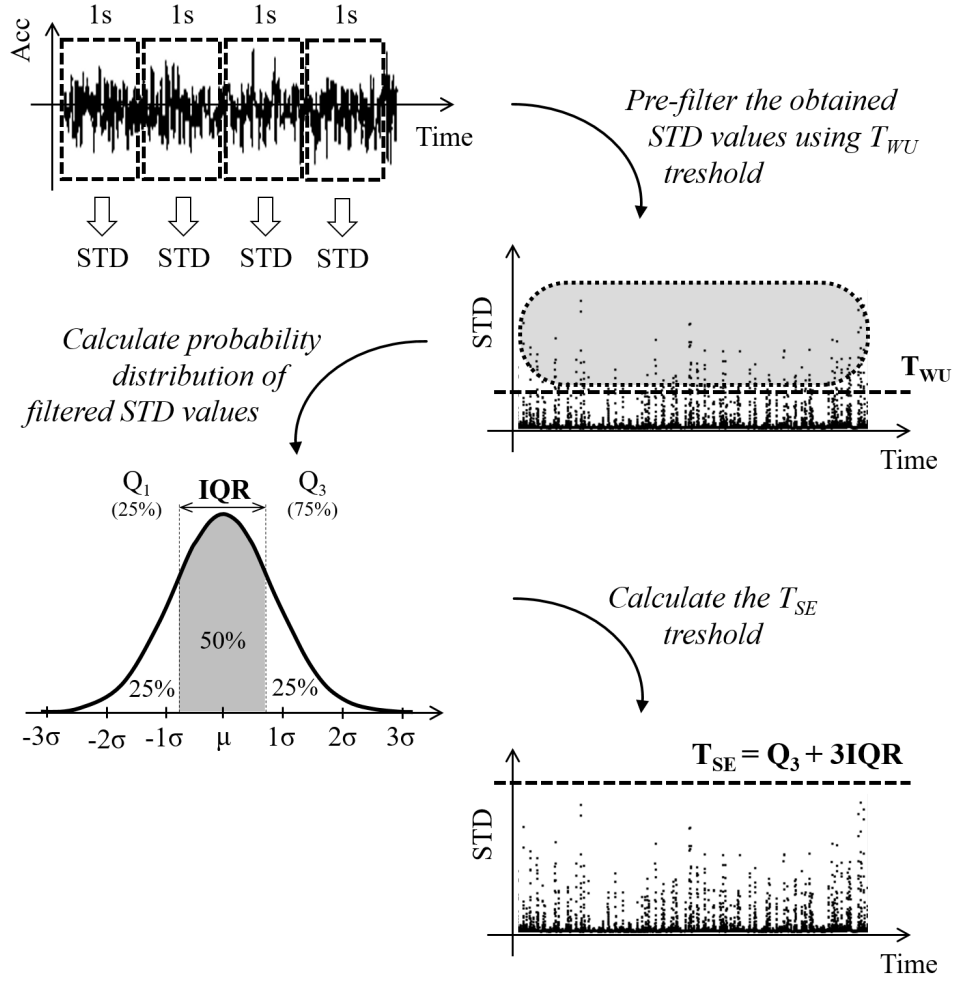


Figure 4.6: InterQuartile Range (IQR) procedure

5. calculate the probability distribution of filtered STD values;
6. calculate the 75th and 25th percentiles of the selected dataset and compute the IQR as the difference between the two percentiles;
7. calculate the T_{SE} threshold as:

$$T_{SE} = Q_3 + 3IQR \quad (4.12)$$

It is important to underline that the identification of sudden and anomalous events is aimed on one hand at properly storing the time series relating to the

event and on the other at triggering further more detailed analyzes (ref. Paragraph 4.5). Regarding the data storage, once the event has been identified, it is necessary to send to the IoT cloud and store not only the time windows exceeding the T_{SE} threshold, but a wider time interval at the turn of the event. It is in fact essential to keep a record of both the instants preceding and following the event, in order to better analyze its nature and effects on the structure.

Considering that the effects of a sudden event on the structure arise after the event, a not symmetrical time window with respect to the event has been considered. In particular, taking into account the minimum time-window of 5min30sec defined in paragraph 4.4.2, it was decided to store:

- if $\Delta t_{out} \leq 3min30sec$:

$$\Delta t_{bef} = 1min00sec$$

$$\Delta t_{aft} = 4min30sec - \Delta t_{out}$$

- else if $\Delta t_{out} > 3min30sec$:

$$\Delta t_{bef} = \Delta t_{aft} = 1min00sec$$

where Δt_{out} is the time window in which the standard deviation is beyond the T_{SE} threshold while Δt_{bef} and Δt_{aft} are the stored time windows before and after the event respectively. It is important to underline that the IoT gateway always stores the last 3 minutes of data in its local memory, which are continuously overwritten as a new dataset is collected. This means that if the T_{SE} threshold is exceeded, the previous 1 minute of data is always available.

4.5 Multilevel damage detection procedure

This paragraph illustrates the proposed multilevel decision approach to be applied to a distributed sensor network for identifying damages in civil engineering structures. The “multilevel” attribute indicates that various methods, having different approaches, reliability and robustness in detecting damages, have been integrated in a diagnostic framework, able to perform an "information fusion". As aforementioned, when dealing with a network of structures (hundreds of structures) instrumented with a network of sensors, the main objective is just to identify a damage occurrence, postponing the localization and the extension evaluation to in-depth and subsequent analyzes.

An extensive literature is available on all the methods developed over the years for identifying damages in civil engineering structures. However, no method is capable of providing by itself a reliable, comprehensive and robust answer to all the classical monitoring questions about whether, where and how serious the failure is.

For this reason it is essential to merge all the information coming from different methods and, at the same time, integrate data from all sensors of the network, which can be considered as many eyes looking at the same physical phenomenon. In facts, dealing with complex structural systems, it is important to take into account both the behavior of the structure working as a whole and the behavior of the structure composed by many elements or subsystems. The main challenge for detecting a system damage is thus recognize the global or local symptoms shown when a structural change occurs over time. Moreover, the intrinsic nature of failure mechanisms must be considered. For civil engineering structures, damages could be caused by a sudden change of state or a slow change of state.

Sudden change of state refers to all that cases in which the whole structure or a part of it breaks almost instantly, with little or absent elastic and plastic deformations. The failure can be caused by exceptional natural events, such as earthquakes or a landslide, by man-made events, such as explosions or road accidents, or finally by the achievement of the ultimate strength of a structural element that has a brittle behavior, such as the breakage of a prestressing tendon or shear failures in beams. In all these cases, if a dynamic monitoring system is installed on the system, a strong excitation would be recorded by accelerometers and, if the sudden event causes a damage to the structure, a modification of the structural behavior (and therefore of the modal parameters) would be observed. This means that it is necessary to have an indicator able to detect the occurrence of the sudden/brittle event, which would trigger more detailed analyzes aimed at assessing the health status of the structure following the event.

Slow change of state refers to all that cases in which the whole structure or a part of it experiences significant plastic deformation before breaking. Therefore, the damage evolves slowly over time. This means that it is necessary to monitor the evolution of some significant parameters over time, in order to highlight any evolutionary trend that could indicate a progressive damage of some element of the structure (or the structure as a whole).

Based on these considerations, the monitoring system could be smart enough for indentifying both types of failure. In this regards, the proposed multilevel methodology has the objective of recognizing the symptoms generated as a result of faults (ductile or brittle) and to identify their local or global nature. More in detail, the multilevel methodology is based on 3 different levels of alert, aimed at providing a robust damage detection framework able to detect any abnormal condition, avoiding false alarms as much as possible. The three implemented levels of alert are defined as follows:

1. Level 1: the first level of alert is verified in real-time (once per second) inside the sensor node. It is aimed at highlighting any abnormal behavior in terms of vibration energy. Being computed at sensor level, it is computationally inexpensive, considering the limited resources available inside the low-end

devices. The reference parameter is the standard deviation (STD) value, which is a measure of the energy contained in the vibration signals collected by sensors. The first level of alert aims at ensuring the continuous and real-time control of the structure, in order to identify any sudden and brittle event and trigger the subsequent level checks;

2. Level 2: The second level of alert is computed inside the IoT gateway and it is normally checked once a day or when level 1 is exceeded. It makes use of an unsupervised machine learning algorithm (described in detail below) for detecting damages, having knowledge of the normal condition of the system. The main idea is to combine the physical parameters (level 3) with statistical pattern recognition approaches, in order to take full advantage of the system resources for building a damage detection framework as robust and reliable as possible. The level 2 check is based on a data-driven model (an autoencoder, which is a type of artificial neural network, is used), constructed by learning - in an unsupervised manner - a representation (encoding) of a given dataset. Once performed the learning process, the neural network would try to produce, for each new dataset coming from sensors, a representation as close as possible with respect to the original input. The reconstruction error has been chosen as reference parameter for identifying damaged conditions. This means that, if the structure is undamaged, the reconstruction error will be more or less constant over time while, in case of damages, the reconstruction error would increase dramatically, being the autoencoder unable to reconstruct data.
3. Level 3: The third level of alert is computed inside the IoT Cloud and it is normally checked once a week or when levels 1 or 2 are exceeded. Reference parameters are natural frequencies, which are intrinsic characteristic of the structure. The choice of the weekly check is motivated considering that the type of phenomenon to be observed (damages) are ductile in nature and therefore their evolution is very slow over time. This means that it is possible to save computational cloud resources, while ensuring continuous monitoring of any sudden events (level 1). An OMA algorithm is used to identify natural frequencies, as described in the following paragraphs.

The following diagram (Figure 4.7) summarizes the proposed multilevel procedure:

The three described alert levels are interrelated to each other and are able to take into account the spatial distribution of the sensor network. In particular, as aforementioned, information on the structural health status must be provided by a number of sensors, which are part of the network of devices installed on the structure. In fact, if a damage occurs in the structure, be it localized or global, a number of sensors would record it. Let's take the example of a simply-supported 10

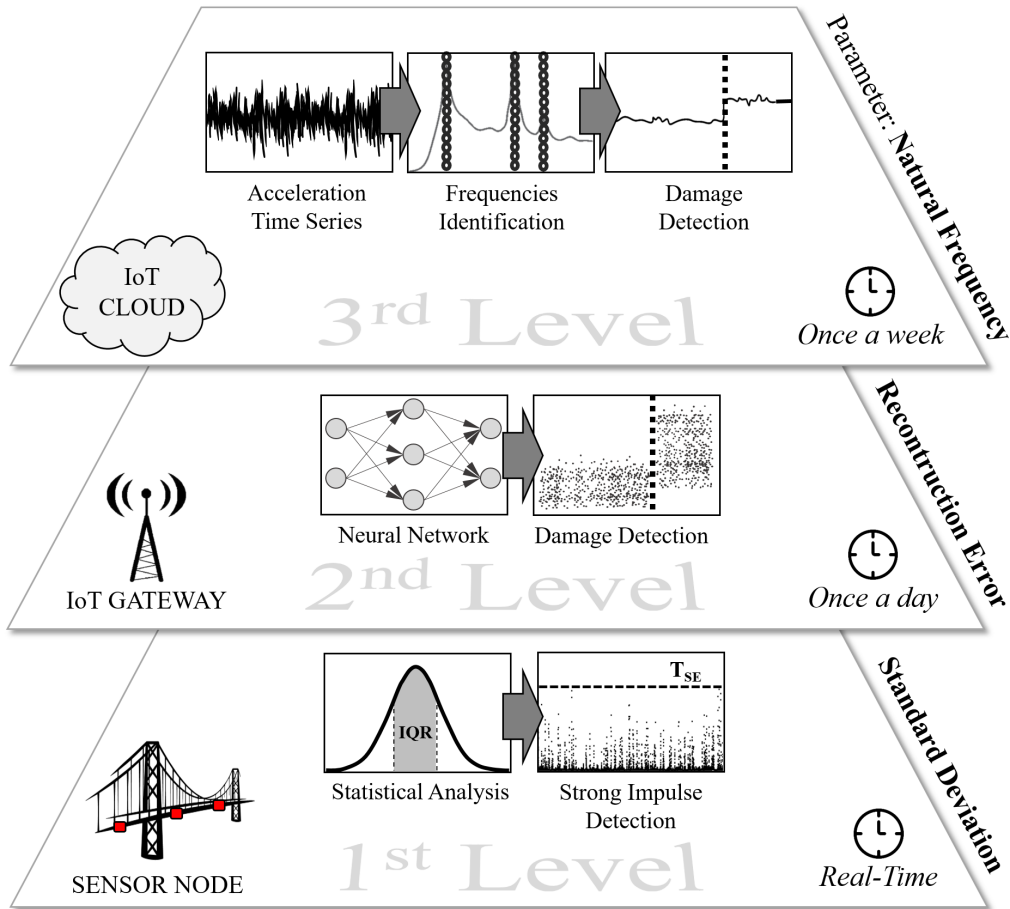


Figure 4.7: Proposed Multilevel damage detection procedure

span bridge. If a beam belonging to the first span suffers damage, several sensors of that span should be involved in recording the event while those installed on the other spans should not notice anything. This means that spatial logics are needed to identify and localize damages in complex structures with many independent elements. The proposed methodology takes into account the following two spatial logics:

1. sensor groups: sensor groups are defined according to the geometry of the structure. In order to automatically define the groups, a procedure based on sensor names has been developed. Indeed, each sensor is given a name which depends on its specific position on the structure. In this way it is possible to identify sensors close to each other and sensors distant from each other. Sensor groups are mainly used to identify localized damages;
2. minimum percentage of sensors: a minimum percentage of sensors outside the

threshold is defined to consider an alert level reached.

Summarizing the above, the multilevel methodology includes a real-time check carried out through alert level 1, a daily check according to alert level 2 and a weekly check through alert level 3.

In particular, *Level 1* assesses in real-time the occurrence of sudden events of a brittle nature. If level 1 is exceeded, which means that either a group of sensors or the minimum percentage of sensors has exceeded the pre-defined STD threshold, a triggering signal is generated and levels 2 and 3 are immediately activated.

- if at least one of levels 2 or 3 are exceeded, which means that either a group of sensors or the minimum percentage of sensors has exceeded the pre-defined thresholds, an ALARM message associated with a phone call is automatically generated, indicating the group or percentage of sensors out of threshold;
- if, on the other hand, no other threshold is exceeded, a WARNING message is automatically generated, indicating the group or percentage of sensors out of first level threshold.

Level 2 assesses once per day the evolution of damages of a ductile nature. If level 2 is exceeded, which means that either a group or the minimum percentage of sensors has exceeded the pre-defined threshold, a triggering signal is generated and level 3 are immediately activated.

- if level 3 is exceeded, which means that either a group or the minimum percentage of sensors has exceeded the pre-defined thresholds, an ALARM message associated with a phone call is automatically generated, indicating the group or percentage of sensors out of threshold;
- if, on the other hand, no other threshold is exceeded, a WARNING message is automatically generated, indicating the group or percentage of sensors out of second level threshold.

Level 3 assesses once per week the evolution of damages of a ductile nature. If level 3 is exceeded, which means that either a group or the minimum percentage of sensors has exceeded the pre-defined threshold, an ALARM message associated with a phone call is automatically generated, indicating the group or percentage of sensors out of threshold.

The two automatically generated alert messages, WARNING and ALARM type, are defined as follows:

WARNING: the warning message refers to anomalous conditions which are not connected to structural deficiencies and would thus require further investigation to be clarified. No actions are therefore required;

ALARM: the alarm message refers to significant anomalous conditions which are potentially connected to structural damages or failures. An on-site inspection is required together with more in-depth data analysis.

The following paragraphs detail all the procedures used for the three defined levels of alert.

4.5.1 First alert level - Sudden Events Threshold

The first alert level is computed in real-time (once per second) within the sensor node and it is aimed at verifying that no abnormal vibrational levels occur (with respect to the standard dynamic behavior of the structure). The procedure and all the steps followed for defining the threshold values is detailed in paragraph 4.4.3.

4.5.2 Second alert level - Machine Learning Approach

As aforementioned, the second level of alert implies the application of an unsupervised machine learning algorithm for identifying anomalies in the structure.

Artificial Neural Network (ANN) can be defined as brain-inspired systems, able of learning how to perform specific tasks, replicating the way humans learn. In recent years, neural networks have increasingly been used as damage detection tools for structural health monitoring purposes. Several examples can be found in literature, [56], [27], [13].

In this dissertation, a machine learning algorithm has been implemented for classifying the structure state of health based only on data representing the standard behaviour of the system, that is, the undamaged condition. This technique, called unsupervised learning, allows the model to discover information and learn on its own, without any supervision. Indeed, considering that in real cases data from a damaged scenarios are not available, the main idea is to train the network for reconstructing the healthy state of the structure in order to detect any novelty, which would be flagged as damage.

For the applications described in this work, an autoencoder has been used. An autoencoder is an artificial neural network that is able to generate a new dataset by first compressing input data into a space of latent variables and subsequently reconstructing the output on the basis of the information acquired. In particular, an autoencoder learns how to reconstruct the input data x from a reduced encoded representation, to output data \hat{x} which are as close to the original input as possible.

With reference to Figure 4.8, the 4 main parts that characterize an autoencoder are the following:

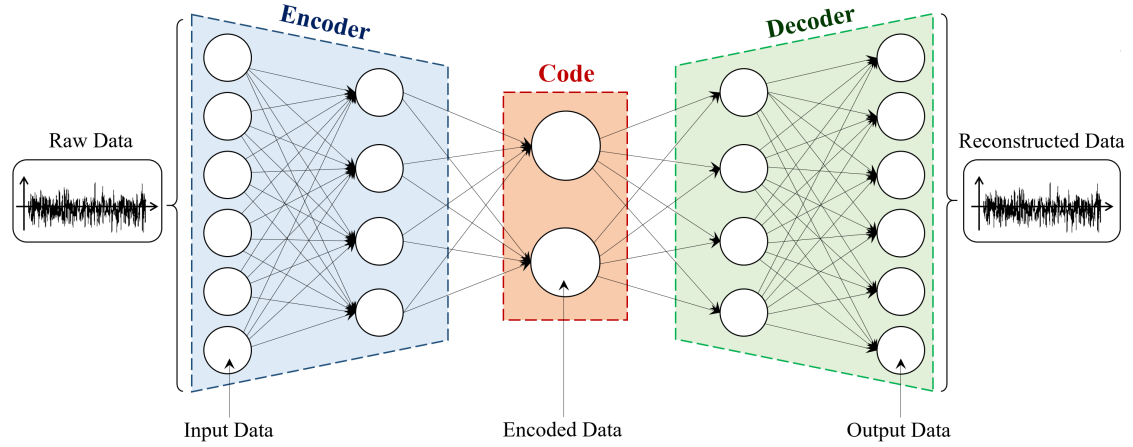


Figure 4.8: Autoencoder architecture

- **Encoder:** the encoder is the stage in which the model takes the input layer and reduces its dimension by compressing it in an encoded representation;
- **Code:** the code stage, also known as *bottleneck* or *latent representation*, contains the compressed representation of the input data, that is, the information needed to traverse the full network, through the lowest possible dimensions of the first layer;
- **Decoder:** the decoder is able to reconstruct the data from the encoded representation to be as similar as possible to the original dataset.
- **Reconstruction Error:** the reconstruction error measures how close the output data is to the input data, that is how well the autoencoder is working. The autoencoder objective is therefore the minimization of this parameter.

The autoencoder approach works very well if input data are correlated because the encoding operation relies on the correlated features to compress the data. Based on this assumption, the steps followed in the second alert level are as follows:

1. Define the autoencoder architecture: in this work, an autoencoder has been designed as a feedforward network, having 1 layer in both the encoder and decoder, without considering the input and output (Figure 4.8). The number of hidden layers has been chosen considering both training and generalization error. Indeed, few hidden units have shown to perform better than more hidden units, which return low training error but high generalization error due to overfitting and high variance. Acceleration time series recorded by accelerometers installed on the structure in the 3 measurement directions x , y , z are used as input data. The output data are also acceleration time

series. The number of nodes in middle layers is automatically set according to the input size (i.e. number of sensors), so that a suitable compression level is guaranteed. More in detail, the number of hidden neurons per layer has been set as 80% and 50% of the input size. The number of hidden units has been obtained by training several networks and estimating the training and generalization error of each. In particular, better performances have been observed having a large first layer and thinner last layer (code). Indeed, the first large layer allow the net to compute powerful representations of acceleration data, which help the code computing denser representations. The rectified linear units (ReLU) has been used as activation function, since it allows model to learn faster and perform better. Moreover, BackPropagation algorithm (BP) has been used to train the model.

2. Define a training dataset: to perform the autoencoder training, it is necessary to select a training dataset, which can be defined as a set of "examples" used to fit the parameters of the model. Indeed, the autoencoder learns from this training dataset and then it would able to predict the output from an input not encountered during its training. The choice of the suitable training dataset is therefore essential for the performance of the network. In this work, a dataset comprising acceleration time series collected by each sensor node has been used as training dataset. In particular, in order to prevent the autoencoder from overtraining and to take into account environmental influences, different traces have been considered. In particular, the training dataset has been assembled using several time series belonging to the first month of monitoring and collected at different times (day, night, week, weekend), in order to take into account all the possible scenarios that can occur in standard operating conditions.
3. Validating and Testing the network: validating and testing the trained ANN using an appropriate dataset, in order to obtain the final model to be used for damage detection. More in detail, from the training dataset, two samples of data are held back, in order to use them for validating and testing the neural network after the training process is completed. The validation dataset is mainly used for model selection, that is for optimizing model's hyperparameters. On the other hand, once the final model is defined, test dataset is used to give an unbiased evaluation of the ANN performances.
4. Define a threshold level for the reconstruction error: once the autoencoder has been trained, in order to use the trained network as a tool for damage detection, a threshold level has to be defined for the reconstruction error, chosen as key parameter, representative of the quality of the reconstruction. More in detail, a threshold value equal to 0.1% of the reconstruction error

is automatically set with reference to the average of the reconstruction error obtained throughout the training phase.

The described process allows to check the health of the structure once per day. Indeed, Autoencoders are used to predict the structure vibration signals under environmental and operational conditions, assuming a given state of preservation of the bridge. Any discrepancy between predicted and measured responses can be interpreted as a modification in the structural behaviour and therefore can be linked to damages. In practical terms, this means that, for each new dataset collected by sensors, the prediction made by the trained neural network is compared with the time histories recorded by the monitoring system and the reconstruction error between prediction and real data is calculated. If the reconstruction error is higher than the preset threshold (0.1% of the average error obtained during training), an automatic alarm signal is generated.

4.5.3 Third alert level - Frequency in time

The third level of alert is computed inside the IoT Cloud and it is normally checked once a week or when levels 1 or 2 are exceeded. The main goal is to identify the modal parameters, more specifically natural frequencies, of the monitored structure from the collected dynamic responses, in order to use them for assessing the current structural health condition. For this purpose, it is therefore essential to process real-time data coming from sensors through robust and powerful algorithms, able to perform an automatic and reliable frequency identification. Special attention must be paid to environmental influences (temperature, wind, etc.) which can lead to variations in the dynamic response of the structure.

Based on the above, the proposed methodology includes, for this level of check, the following automatic steps, summarized in Figure 4.9:

- collecting and storing real-time vibration data coming from sensors installed on the monitored structure. Signals are collected under normal operating conditions and thus excitation sources are assumed to be "white noise";
- preprocess the incoming data, according to what has been described in chapter 3;
- applying OMA methodologies (in this specific case, Cov-SSI method was chosen) for the identification of the selected dynamic parameters. In particular, natural frequency values are obtained once a week or when levels 1 or 2 are exceeded;
- removing environmental influences, especially temperature, on the modal parameters. Indeed, the effect of external factors may lead to relevant fluctuations that can generate false alarms and, at the same time, mask modifications

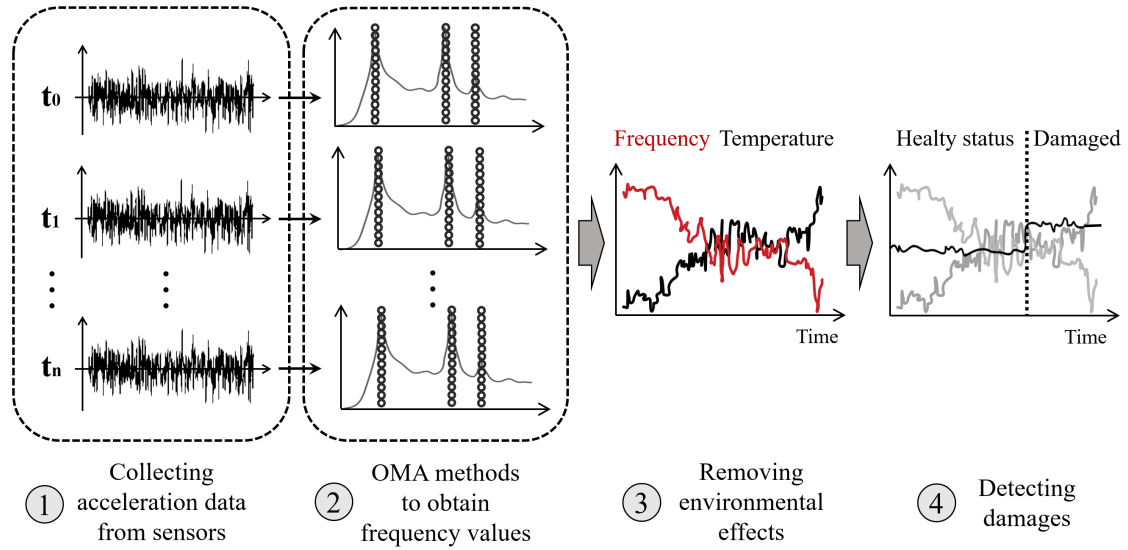


Figure 4.9: Main processing steps of the third alert level - Evolution of natural frequencies

due to damages. The issue of removing environmental influences on modal parameters is widely addressed in the literature [42], [35] and a number of significant methodologies have been developed for this purpose. However, for a first version of the proposed methodology, a linear regression approach has been implemented for removing temperature influence on frequency values. Nonetheless, improvements can be made by using more sophisticated methodologies;

- evaluating the evolution of natural frequency values over time, detecting any anomalies in the monitored structure. More in detail, frequency values are compared to a pre-set threshold value, in order to identify any reduction in stiffness.

As regards the threshold values, these should be set specifically for each structure, according to the expected damage scenarios. However, as widely explained at the beginning of this chapter, the purpose of the proposed methodology is to provide a complete data-driven method, able to automatically generate system health indicators without any specific analysis on the monitored structure. For this reason, a threshold of $0.1Hz$ is automatically set for any structure when the monitoring system is installed. The reason for choosing this threshold value is justified by the following considerations:

- The entity of frequency shifts due to damages is strongly influenced by the associated mode shapes. Indeed, the frequency shift Δf_i is usually larger for

the higher modes compared with the lower modes. However, since the civil engineering structures to which this methodology is directed (bridges) have in general low frequency values (in the range 0-12/15 Hz), it is possible to assume a single Δf_i threshold for all frequencies, which correspond to the minimum detectable frequency shift.

- Numerical modeling of the most typical damages that can occur in the analyzed structures (mainly bridges) allowed to identify the minimum frequency variation that can be observed following a damage. However, this result was compared with the minimum frequency variation detectable by the automatic algorithm, in order to limit false alarms as much as possible.

Notwithstanding, this threshold can be updated if specific analyzes are performed for a particular structure.

Chapter 5

Continuous Monitoring - Case Studies 1

5.1 Chapter Introduction

This chapter describes a significant case study of continuous monitoring systems applied on an highway bridge located in northern Italy. In particular, the main objective is to illustrate how the proposed methodology allowed the identification of anomalous conditions in this structure, which was and still is continuously monitored. Indeed, the monitoring framework described in chapter 4 is currently implemented on about 20 bridges, providing real-time information on their health status.

5.2 Dynamic monitoring of a box composite highway bridge

In this paragraph, the application of a SHM system to a real operating bridge is described, in order to demonstrate the potential of the proposed methodology for the continuous and automated monitoring of structures. More in detail, the structure under examination is being monitored continuously through a dynamic monitoring system since September 2017.

Vibration signals are acquired by a network of MEMS tri-axial accelerometers installed on the pre-stressing tendons of the bridge. These sensors are g-sensitive and their behavior is influenced by environmental factors so a pre-processing is required in order to remove environmental and operational effects on the measured dynamic properties. The fully automated monitoring process, described in detail in chapter 4, comprehends three main steps: (i) pre-processing data at node and gateway level, (ii) sending and storing data in an IoT Cloud, (iii) processing real-time data in the IoT Cloud.

A database of statistical and dynamic features of every monitored element has been therefore continuously updated since the system was put in operation, representing an interesting case study in how the issues of big data management and damage detection strategies in a SHM perspective can be overcome through the integration of IoT technologies and OMA methodologies.

In a first part of this paragraph, a description of the monitored bridge and monitoring elements is reported. Afterwards, the application and operation of the automated monitoring strategy is presented. Finally, results from 2 years of monitoring are illustrated, emphasizing the most relevant outcomes regarding the damage detection methodology presented in this dissertation. Part of this work was already published in [8].

5.3 Bridge Description

The monitored structure is a highway concrete bridge located in Italy. The bridge, opened to traffic in 2006, is a composite box girder in which the concrete webs are replaced with corrugate steel plates to reduce the self-weight and simplify the construction. Mixed prestressing (internal/external) was used to strengthen the structure. Two abutments are supporting the bridge at the end points and five concrete piers clamped into the girder are holding up the 6 spans. The bridge is 590 m long and it is characterized by four equally spaced continuous spans with a length of 120 m each, one continuous span with a length of 70 m and one simply supported end span 40 m long. The main girder has a cross-section height varying from 6.0 m (at the bearings) to 3.0 m (on the centerline of each span). A single expansion joint is present at pier P5, holding together the two separated decks while absorbing temperature-induced expansion and contraction of bridge materials. The structural details of the bridge are shown in Figure 5.2 while a 3D bridge view is shown in Figure 5.1.

The bridge is strengthened by both internal and external pre-stressing. More in detail, the pre-stress of the structure is provided by means of bonded tendons arranged in the upper flanges of concrete slab and unbonded external tendons composed of 27 strands placed in the hollow section of the box girder. The external pre-stressing tendons are encapsulated within a protective polyethylene duct where a grout is injected to protect the cable. Detailed information about tendons geometric and mechanical characteristics are listed in Table 5.1. Moreover, Figure 5.3 schematically shows the geometry and positioning of the pre-stressing tendons.

During an inspection carried out inside the box girder, some tendons were found broken; the failure point was identified for all tendons at an upper location, near the anchorages. The origin of this phenomenon was found in an incorrect grout composition that caused an accelerated corrosion of the strands. The investigations carried out on the failed cables have shown that, at break points, the steel

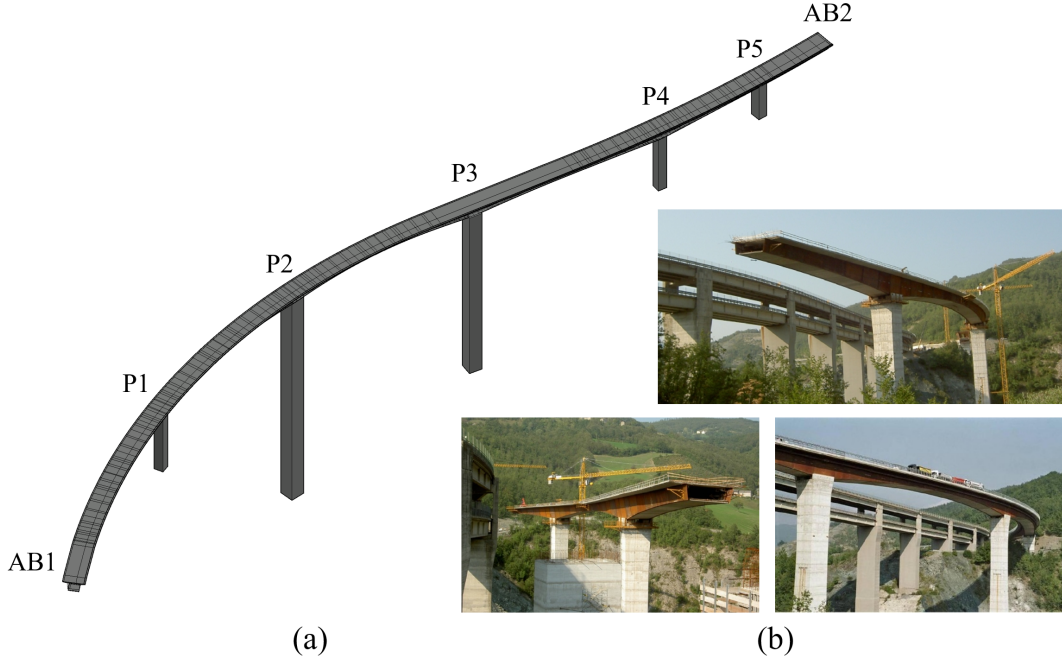


Figure 5.1: (a) Bridge 3D view. (b) Pictures of the bridge both under construction and in operating conditions.

Table 5.1: Geometric and mechanical characteristics of external pre-stressing tendons

Characteristic	Unit	Value
Num strands	-	27
Internal diameter	mm	110
External diameter	mm	115
Area	mm^2	139
Yield strength f_{yk}	N/mm^2	1670
Tensile strength f_{tk}	N/mm^2	1860

strands were completely corroded and the ducts were empty of grout near the anchorage plate. Indeed, the problem related to the corrosion of steel tendons in post-tensioned structures due to the lack of grout in the ducts is widely addressed in the literature [9], [1].

The assessment of failed external post-tensioned tendons led to the installation of a continuous monitoring system with the aim of identifying tendons condition during the service life of the structure and possibly anticipating future collapse of the tendons. Moreover, the long-term dynamic monitoring system allows checking the effects of the heavy daily traffic traveling on the bridge as well as understanding

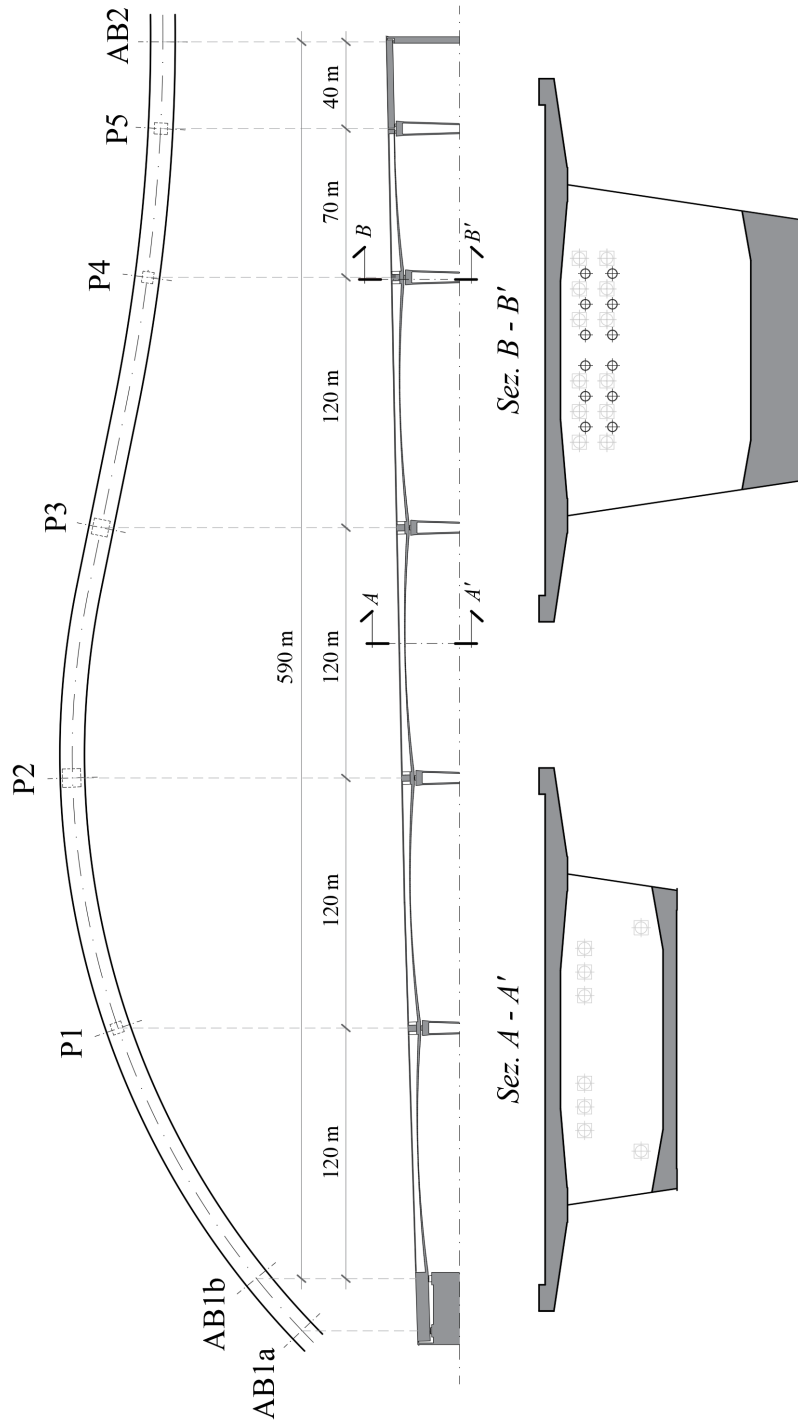


Figure 5.2: Structural details of the bridge: plan view, elevation and two different cross-sections (at the bearings and on the centerline of the span).

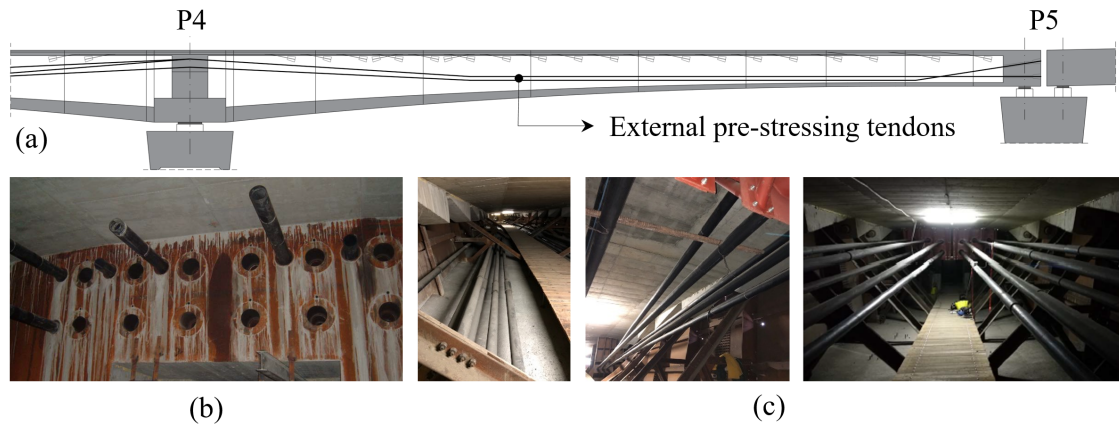


Figure 5.3: External pre-stressing tendons layout. (a) External pre-stressing drawings; (b) picture of one anchorage of external tendons; (c) external tendons positioning inside the bridge.

the dynamic response of the bridge under operational conditions. The bridge is in fact crossed every day by a large number of heavy vehicles, so special attention has to be paid to the dynamic interaction between traffic and bridge as well as to the consequences on the structural performance of the bridge during its service life.

5.4 Monitoring System Description

The monitoring system was installed between June and September 2017, being fully active since 20 September 2017. External tendons were instrumented with 88 MEMS tri-axial accelerometers, 2 for each monitored tendon. These MEMS accelerometers are ultra compact low-power three-axis linear accelerometers that include a sensing element and an IC interface able to take information from the sensing element and to provide a corresponding analog signal. Accelerometers have a dynamically user selectable full-scale of $\pm 2g / \pm 6g$ and they are capable of measuring accelerations over a maximum bandwidth of 1.8 kHz for all axes. They operate with a noise spectral density of $50\mu g / \sqrt{Hz}$ and a sensitivity of $V_{dd}/5$ [V/g], considering a full scale of $\pm 2g$ and a Vdd (power supply) of 3.3V.

A long lasting preliminary experimentation has allowed assessing the accelerometer performances, which were fit for the high expected excitation levels, especially produced by the heavy traffic travelling on the bridge both during day and night, with just a small reduction during the weekends.

As mentioned in paragraph 4.3, each tri-axial MEMS accelerometer provides data in the 3 orthogonal directions (x, y, z), oriented as shown in Figure 5.4. The x axis is the transversal direction of the deck, y axis is parallel to the longitudinal

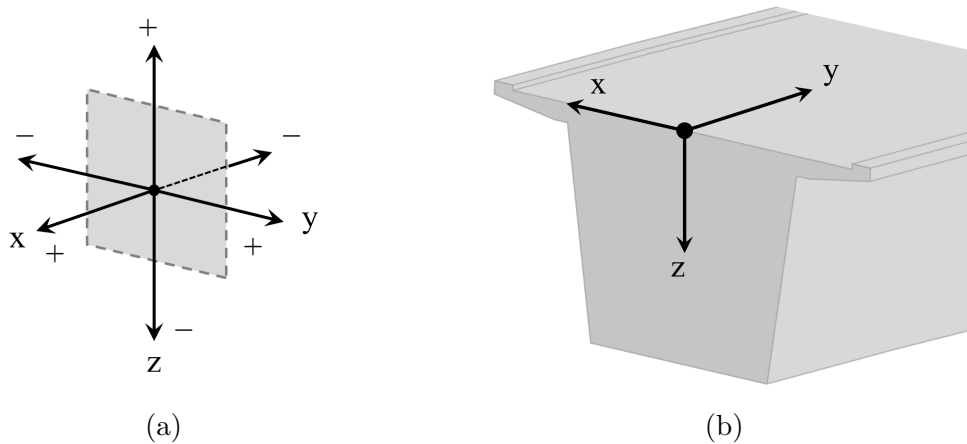


Figure 5.4: Accelerometer coordinate system: (a) Signs convention; (b) Measurement axes (x, y, z) orientation

extension of the tendon and z axis corresponds to the vertical direction.

The system was properly designed in order to cope with the monitoring needs, integrating sensor nodes with an IoT gateway and a Data Center, also known as IoT Cloud, as explained in detail in paragraph 4.3.

In this specific case, each of the 88 sensor nodes is equipped with a tri-axial MEMS accelerometer, a microcontroller and a sensor of humidity and temperature, in order to collect environmental data which must be taken into account when processing accelerometric data (especially temperature). The tri-axial accelerometers are characterized by a range of ± 2.5 g and a bandwidth of 50 Hz; preliminary tests carried out before designing the monitoring system proved the adopted MEMS sensors to be effective in measuring tendons vibration, whose frequency range in the order of 40 Hz can be considered enough to get any eventual damage detection. To increase accuracy, acceleration data are sampled at the sensor level at 25.6 kHz, filtered down and down sampled to finally obtain a sampling rate of 100 Hz; this sampling frequency is the maximum allowable sampling rate per channel, due to the data streaming limitation through the network. The measurement nodes are placed in 10 cross-sections of the bridge, close to the steel protection screens as shown in Figure 5.5. More in detail, the devices are placed on top of the pre-stressed cables and fastened to it (Figure 5.5).

Once collected, acceleration data are encoded by the microcontroller into a CAN BUS driven network and sent to a local IoT gateway. The acceleration, temperature and humidity time series coming from the 88 measurement nodes are then sent to the cloud monitoring infrastructure. Indeed, the monitoring system is connected to the internet via a 5 GHz point-to-point Wi-Fi link between an access point located at one end of the bridge and an "Ubiquity Nano M5" station located at the P2 pier, halfway between the viaduct ends. An Ethernet cable connects the station to the

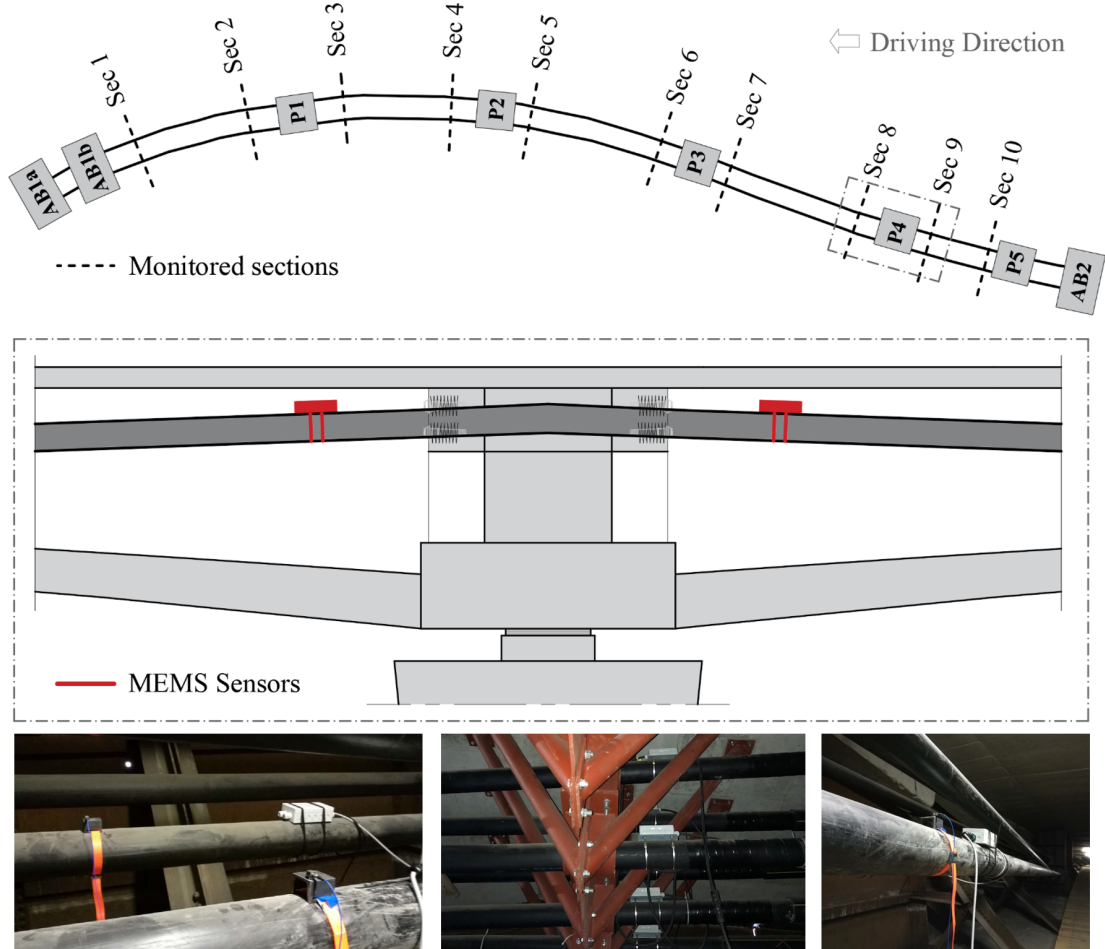


Figure 5.5: Sensor nodes positioning on the pre-stressing tendons

two IoT gateways installed on the bridge: one for the sensors installed on the left side, one for those installed on the right side of the bridge.

Data are then available to be accessed, downloaded or processed on a IoT cloud environment. Considering that the amount of stored data is of noticeable dimensions, the main challenge when designing the system was to elaborate this huge amount of information in the shortest time by using cloud resources at best. Taking advantage of the high parallelism (up to 1000 simultaneous executions) available in the IoT cloud, data composed by time series of length T seconds can be subdivided into m slot of T_w seconds such that the algorithm can elaborate a slice of data with low time and memory consumption.

The main challenge is, then, exploiting all the potentiality of the monitoring system, avoiding waste of resources. Being aware of the capacity and limits of the different components, a strategy for early detection of tendon damage has been developed. The description of the methodology and some interesting results are

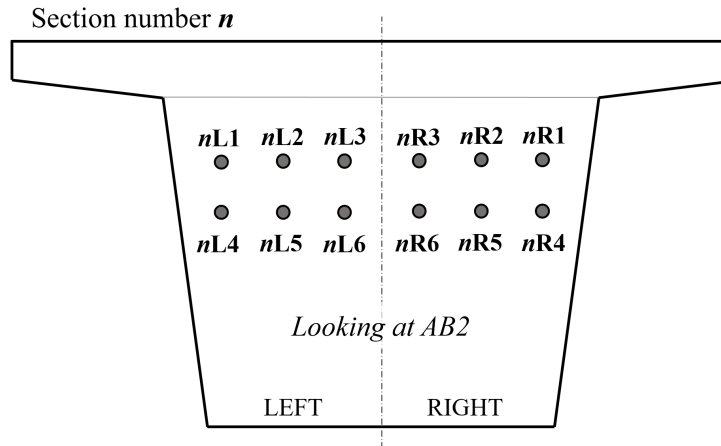


Figure 5.6: Tendons naming convention

shown in the following.

5.4.1 Naming Convention

For confidentiality reasons, a fictitious naming convention is adopted to describe the various elements belonging to the monitoring system. As aforementioned, the measurement points were placed in 10 cross-sections of the bridge, starting from the abutment called AB1 up to the abutment called AB2, as shown in Figure 5.5.

A maximum of 12 tendons can pass through each of the cross sections. The cables are numbered from 1 to 6 distinguishing those installed on the right side of the bridge and those installed on the left side of the bridge, as illustrated in Figure 5.6. Sensors installed on each tendon are then named according to the following nomenclature:

$$\langle \text{Section} \rangle [\text{Circuit}] \langle \text{sensor number} \rangle$$

where:

- $\langle \text{Section} \rangle$ - identifies the transversal cross-section to which the sensor belongs and varies from 1 to 10. In each span there are 2 transversal sections, near the piers;

Circuit - identifies the circuit to which the sensor belongs and can be Left (L) or Right (R); the reference system is looking towards the abutment AB2 (back to abutment AB1);

- $\langle \text{sensor number} \rangle$ - indicates the cable on which the sensor is installed, according to the aforementioned convention.

Below is a summary table of all sensors installed on the structure.

Span	Section	Tendon number	Sensor name	
			Left	Right
AB1 - P1	1	1	1L1	1R1
	2		2L1	2R1
	1	2	1L2	1R2
	2		2L2	2R2
	1	3	1L3	1R3
	2		2L3	2R3
	1	4	1L4	1R4
	2		2L4	2R4
	1	5	1L5	1R5
	2		2L5	2R5
	1	6	1L6	1R6
	2		2L6	2R6
P1 - P2	3	1	3L1	3R1
	4		4L1	4R1
	3	2	3L2	3R2
	4		4L2	4R2
	3	3	3L3	3R3
	4		4L3	4R3
	3	4	3L4	3R4
	4		4L4	4R4
	3	5	3L5	3R5
	4		4L5	4R5
	3	6	-	-
	4		-	-
P2 – P3	5	1	5L1	5R1
	6		6L1	6R1
	5	2	5L2	5R2
	6		6L2	6R2
	5	3	5L3	-
	6		6L3	-
	5	4	5L4	-
	6		6L4	-
	5	5	5L5	-
	6		6L5	-
	5	6	5L6	5R6
	6		6L6	6R6
P3- P4	7	1	7L1	-
	8		8L1	x
	7	2	7L2	7R2
	8		8L2	8R2
	7	3	-	7R3
	8		-	8R3
	7	4	-	-
	8		-	-

	7		-	7R5
	8	5	-	8R5
	7		-	7R6
	8	6	-	8R6
	9		9L1	-
	10	1	10L1	10R1
	9		9L2	9R2
	10	2	10L2	10R2
	9		9L3	9R3
P4- P5	10	3	10L3	10R3
	9		9L4	-
	10	4	10L4	-
	9		-	-
	10	5	-	-
	9		-	9R6
	10	6	-	10R6

Table 5.2: Naming convention of all sensors installed on the bridge

5.5 Preliminary analysis

Before the installation of the monitoring system, some preliminary analyses were carried out.

Firstly, given that the objective of the monitoring system was to check continuously the health status of the external prestressing tendons of the bridge, a preventive evaluation of the expected damage scenario was carried out. In particular, based on the observations made during the inspection, it was proved that the tendons breakage was caused by a corrosive phenomenon. More in detail, an important lack of grout, together with oxidation marks on strads and a relevant reduction of the tendon cross section was observed. The localized absence of grout in the duct, due to an incorrect grout composition which led to a bleeding of the grout during construction, causes a local corrosion attack in the form of pitting in the upper part of the tendons. As the corrosion proceeds, the individual strands begin to break. The breakage of a number of strands leads to a reduction of the pre-stress force and therefore to a consequent reduction of the tendon stiffness. Consequently, a decrease in cable stiffness would produce an abrupt reduction of its own natural frequencies.

This means that, as soon as the system is installed, it is possible to carry out a preliminary evaluation of the health status of each tendon only by comparing the expected theoretical frequencies with the measured ones.

Ambient vibration measurement were collected in a first stage of the monitoring process, without disturbing the normal use of the bridge. More in detail, time

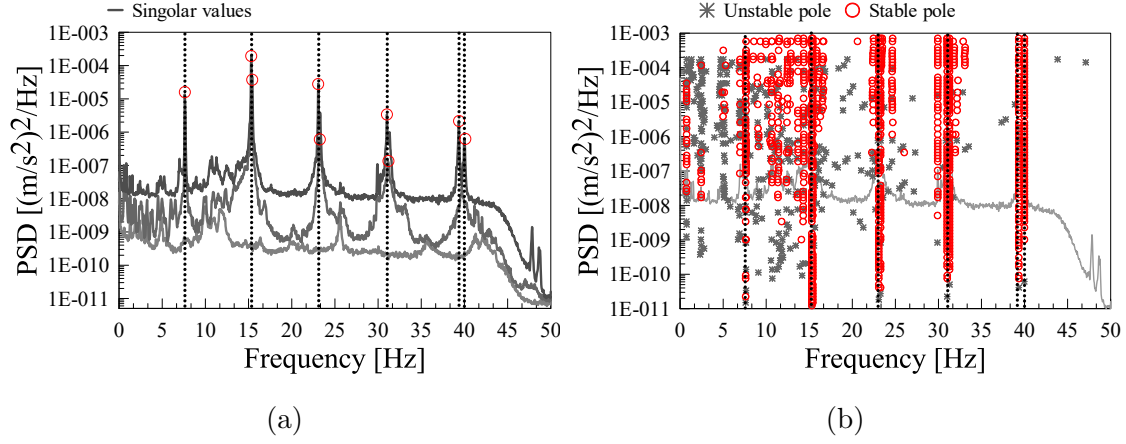


Figure 5.7: Comparison between (a) Frequency Domain Decomposition and (b) Covariance-driven Stochastic Subspace Identification Method for frequency identification

series were collected for each tendon during a 24 hours time period, before the fully operation of the monitoring system was reached. Modal parameters, in particular resonant frequencies, were identified using two OMA identification techniques, described in detail in chapter 3: Frequency Domain Decomposition (FDD) and Covariance-driven Stochastic Subspace Identification (Cov-SSI) methods. The use of these methodologies was aimed at verifying that the results were consistent between them. Results from both methods are shown in Figure 5.7 for one of the sensors installed on the bridge.

Table 5.3: Identified Natural Frequencies

Mode	Frequency [Hz]
1	7.614
2	15.293
3	15.408
4	23.068
5	23.275
6	31.005
7	31.278
8	39.316
9	39.971

As it can be seen from Figure 5.7 resonant frequencies, summarized in Table 5.3,

were clearly identified (indicated with dashed vertical lines) between 0 and 50 Hz. In particular, both methods allowed the identification of all the extremely close modes of the axially symmetric cables (vibrating in two orthogonal planes). However, for the preliminary analysis carried out at the installation of the monitoring system, only the fundamental frequency was considered. This is justified by the fact that, since the monitored element is a cable, the theory of the vibrating string can be applied. Consequently, whatever the initial conditions are, tendon vibration will always be periodic and more precisely it will be given by the superposition of (in general infinite) elementary harmonic vibrations, each characterized by a specific harmonic frequency. All these harmonic frequencies are integer multiple of the first fundamental frequency. This means that any observation made on the fundamental frequency can be considered valid also for all the identified modes, being multiples of the first natural frequency.

At the same time, knowing the length and mass of each tendon, it was possible to calculate the theoretical first frequency using the following expression:

$$f_i = \frac{1}{2L_i} \sqrt{\frac{T_i}{m_i}} \quad (5.1)$$

where L_i , m_i and T_i are respectively the length of the cable, its mass and the axial force acting on it. In the case of tendons injected with cement mortar, only stress variations are taken into account, as mass and length losses are not physically acceptable. It is important to underline that the axial force and the length of each tendon were measured in situ before the installation of the monitoring system and therefore they can be considered as known quantities.

Tables 5.4 and 5.5 shows a comparison between the expected first natural frequency for each tendon and the value measured in September 2017, immediately after installing the monitoring system.

Span	Sensor	Tendon Length [m]	Tendon Mass [kg/m]	Numerical Frequency [Hz]	Measured Freq 09/2017 [Hz]	Frequency Variation [Hz]
AB1 - P1	1L6	18,32	46,30	8,60	8,58	0,02
	1L5	18,35	46,30	8,59	8,60	-0,01
	1L4	18,35	46,30	8,53	8,30	0,23
	1L3	20,93	46,30	7,55	6,98	0,57
	1L2	20,89	46,30	7,55	7,55	0,01
	1L1	20,93	46,30	7,49	7,48	0,02
	1R6	18,24	46,30	8,64	8,53	0,11
	1R5	20,75	46,30	7,60	7,53	0,07
	1R4	20,69	46,30	7,56	7,35	0,22
	1R3	20,83	46,30	7,59	7,25	0,34
	1R2	20,74	46,30	7,61	7,60	0,01

5.5 – Preliminary analysis

	1R1	20,70	46,30	7,57	7,56	0,01
P1 - P2	3L5	20,76	46,30	7,68	7,70	-0,01
	3L4	21,07	46,30	7,58	7,52	0,07
	3L3	21,09	46,30	7,50	7,41	0,09
	3L2	21,06	46,30	7,53	7,35	0,18
	3L1	21,10	46,30	7,54	7,38	0,17
	3R6	20,93	46,30	7,62	7,54	0,08
	3R5	20,89	46,30	7,63	7,62	0,01
	3R3	20,98	46,30	7,54	7,47	0,07
	3R2	20,89	46,30	7,59	7,55	0,04
	3R1	17,58	46,30	9,05	9,04	0,01
P2 - P3	5L6	21,03	46,30	7,57	7,41	0,17
	5L5	21,06	46,30	7,56	7,37	0,19
	5L4	21,06	46,30	7,58	7,56	0,02
	5L3	20,49	46,30	7,71	7,71	0,01
	5L2	21,05	46,30	7,52	7,43	0,09
	5L1	21,09	46,30	7,53	7,45	0,08
	5R4	20,84	46,30	7,65	7,53	0,12
	5R3	20,37	46,30	7,76	7,70	0,06
	5R2	20,59	46,30	7,69	7,61	0,08
P3 - P4	7L2	20,91	46,30	7,56	7,51	0,05
	7L1	20,31	46,30	7,81	7,80	0,02
	7R5	20,91	46,30	7,61	7,43	0,18
	7R4	20,89	46,30	7,63	7,46	0,17
	7R2	20,91	46,30	7,57	7,40	0,17
	7R1	20,91	46,30	7,59	7,40	0,20
P4 - P5	9L3	20,91	46,30	7,65	7,47	0,18
	9L2	20,88	46,30	7,66	7,59	0,07
	9L4	17,89	46,30	8,95	8,62	0,33
	9L1	17,43	46,30	9,21	-	-
	9R2	18,41	46,30	8,69	8,18	0,51
	9R4	20,97	46,30	7,63	7,49	0,14
	9R1	20,92	46,30	7,67	7,51	0,16

Table 5.4: Comparison between numerical and measured frequencies - odd sensors

Span	Sensor	Tendon Lenght [m]	Tendon Mass [kg/m]	Numerical Frequency [Hz]	Measured Freq 09/2017 [Hz]	Frequency variation [Hz]
AB1 - P1	2L6	18,50	46,30	8,64	8,53	0,11
	2L5	18,53	46,30	8,64	8,44	0,20
	2L4	21,07	46,30	7,58	7,37	0,22
	2L3	21,11	46,30	7,58	7,07	0,52
	2L2	21,06	46,30	7,60	7,53	0,07
	2L1	20,81	46,30	7,50	7,44	0,07

	2R6	20,96	46,30	7,63	7,56	0,07
	2R5	20,92	46,30	7,65	7,49	0,16
	2R4	20,87	46,30	7,65	7,26	0,40
	2R3	21,01	46,30	7,62	7,09	0,53
	2R2	20,92	46,30	7,65	7,41	0,24
	2R1	20,88	46,30	7,48	7,40	0,08
P1 - P2	4L5	18,09	46,30	8,83	8,84	-0,01
	4L4	18,09	46,30	8,85	8,86	-0,01
	4L3	21,10	46,30	7,51	7,53	-0,01
	4L2	20,75	46,30	7,65	7,65	0,00
	4L1	21,10	46,30	7,55	7,61	-0,06
	4R6	20,95	46,30	7,62	7,58	0,04
	4R5	20,91	46,30	7,64	7,63	0,01
	4R3	21,00	46,30	7,55	7,52	0,03
	4R2	20,91	46,30	7,60	7,56	0,04
	4R1	20,57	46,30	7,75	7,69	0,06
P2 - P3	6L6	20,93	46,30	7,62	7,26	0,36
	6L5	20,92	46,30	7,62	7,30	0,32
	6L4	20,89	46,30	7,65	7,51	0,14
	6L3	20,99	46,30	7,54	7,30	0,24
	6L2	20,92	46,30	7,58	7,33	0,25
	6L1	20,92	46,30	7,61	7,53	0,08
	6R4	18,35	46,30	8,71	8,32	0,39
	6R3	20,99	46,30	7,54	7,53	0,01
6R2	20,92	46,30	7,58	7,46	0,13	
P3 - P4	8L2	20,86	46,30	7,59	7,50	0,09
	8L1	20,25	46,30	7,85	7,87	-0,02
	8R5	18,39	46,30	8,66	8,49	0,17
	8R4	20,92	46,30	7,63	7,52	0,11
	8R2	20,93	46,30	7,57	7,42	0,15
	8R1	20,95	46,30	7,59	7,47	0,12
P4 - P5	10L3	7,19	46,30	21,78	21,69	0,09
	10L2	7,15	46,30	21,90	21,87	0,04
	10L4	7,20	46,30	22,04	22,02	0,02
	10L1	7,10	46,30	22,03	22,00	0,03
	10R2	7,67	46,30	20,42	19,79	0,63
	10R4	7,51	46,30	21,15	21,08	0,07
	10R1	7,15	46,30	21,88	21,86	0,02

Table 5.5: Comparison between numerical and measured frequencies - even sensors

By analyzing the discrepancy between the theoretical values and the measured quantities, it was possible to obtain an indication about the cables with potential stiffness reduction. In particular, in tables 5.4 and 5.5 those tendons for which the difference between the theoretical frequency value and the measured one was higher than 0.3 Hz (red lettering) have been highlighted using red font. These tendons,

given the significant frequency difference with respect to the expected theoretical values, could present corrosive phenomena that had already caused the breakage of one or more strands before the installation of the monitoring system. This means that these cables are more likely to break than the others, having already lost some of their stiffness before installing the monitoring system. For this reason, particular attention was paid to these structural elements.

5.6 Methodology

In order to effectively detect any damage in the analyzed structure, the methodology described in chapter 4 has been applied. The aim was to provide, through a permanent and long-term monitoring system, an early-stage alert of anomalous conditions that should trigger more detailed analysis or inspections. In the case of tendons, detecting the breakage of a strand could allow the prior replacement of the cable and prevent it from breaking, that would have serious consequences on the entire safety of the bridge due to the enormous release of energy. In fact, as aforementioned, the corrosive phenomenon causes a progressive collapse of the strands until the break of tendon is reached.

The proposed and adopted methodology is based on three levels of alarm (ref. chapter 4, fully exploiting the potentiality of the monitoring system, where the interaction between the different sites of computational capability has been used to produce an alert for the maintenance. The main idea was to have a damage detection framework organized as follows:

- Level 1: the first level of alert, that should be computationally inexpensive, is verified in real-time (once per second) inside the sensor node. It is aimed at highlighting any abnormal behavior in terms of vibration energy.
- Level 2: The second level of alert is computed inside the IoT gateway and it is normally checked once a day or when level 1 is exceeded. It makes use of an unsupervised machine learning algorithm for detecting damages, having knowledge of the normal condition of the system.
- Level 3: The third level of alert is computed inside the IoT Cloud and it is normally checked once a week or when levels 1 or 2 are exceeded. Reference parameters are natural frequencies, which are intrinsic characteristic of the structure. The main goal is to verify whether the reported anomalous condition was actually a structural damage or not.

In this way, the monitoring system is sufficiently robust and reliable, able to automatically detect any structural damage and at the same time identify abnormal conditions that are not necessarily attributable to structural problems.

The first level of alarm is verified at node level, and its main output is highlighting the presence of any abnormal behavior in terms of tendons vibration energy. The reason for this choice is to be found in the brittle nature of the strand failure, which is associated with the release of a large amount of energy that would be perceived as an impulse by the accelerometers. A measure of the energy contained in the vibration signals collected by sensors is carried out by evaluating the standard deviation (STD) value during the preprocessing of data at node level. In fact, the standard deviation represents the dispersion of a set of values relative to its mean. This means that, if a strand breaks, the variation of data around the mean would increase drastically due to the strong impulse recorded.

According to the methodology described in chapter 4 and in order to set proper threshold values for each sensor, data were collected and analyzed for a training period of one month, where only data associated to a normal behavior of the structure have been taken into account. In this way, it was possible to define and set a range of acceptable values that the STD can assume under normal operating conditions of the bridge.

More in detail, thresholds values were obtained with reference to the STD calculated by dividing the available time series in segments of 1 second (100 points), corresponding to the sampling frequency of the measuring instrument, 100 Hz. In particular, the procedure described in paragraph 4.4.3 has been followed.

The result of the training phase is showed in Figure 5.8, where T_{WU} and T_{SE} values, evaluated considering a training period of one month, are represented for one sensor of the structure. As a result of the training phase, all the sensors belonging to the last span on the right side of the bridge (between piers 4 and 5) were characterized by higher vibration levels with respect to the other four spans, which showed a similar behavior between them. This result is attributable to the geometric characteristics of these cables, which are shorter than the cables of the remaining spans (ref. Table 5.5).

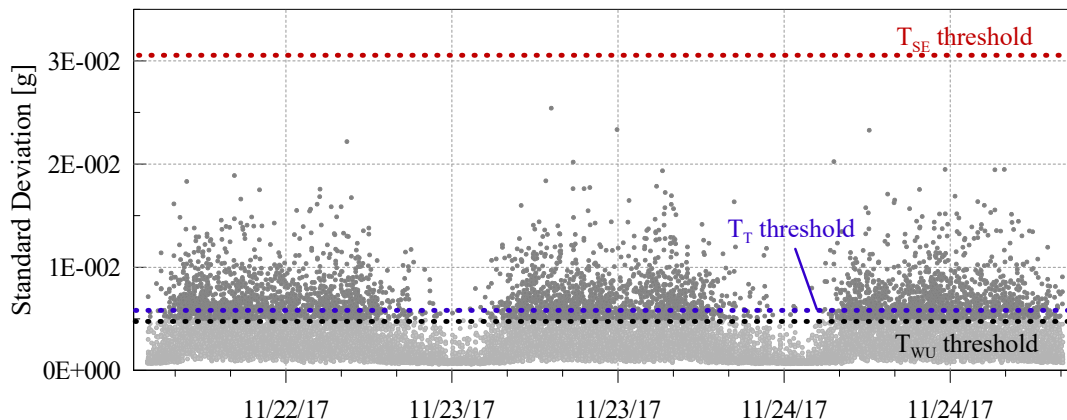


Figure 5.8: Threshold values for one sensor installed on the structure

If the first level of alarm is reached, the IoT node sends an alert message to the IoT gateway and cloud. The analysis is then moved to the gateway and cloud environment, where a deeper insight in the portion of abnormal data is conducted, with the aim of distinguishing high level of energy associated to exceptional operational loading (such as exceptional maintenance works on the bridge, earthquakes, ...) from that associated to the release of energy due to the failure of a strand.

The second level of alarm allows to check the health of the structure by means of an Artificial Neural Network (ANN). More in detail, when a warning signal is generated by the IoT node, the autoencoder check is activated inside the IoT gateway, with the aim of identify any change in the structural behaviour.

More in detail, a threshold equal to 0.1% of the reconstruction error is automatically set within the IoT gateway. This threshold is checked with reference to the average of the reconstruction error values once a day.

Together with the second level check, the third level of alarm, which is based on a physical interpretation of the vibration data in the frequency domain, is activated. In particular, when a warning is triggered by the IoT node or gateway, meaning that the first and/or second level threshold has been exceeded, data are sent to the cloud where a OMA algorithm is activated to check if a changing in the tendon natural frequencies occurred. In order to identify the natural frequencies of tendons, the Covariance-driven Stochastic Subspace Identification (Cov-SSI) method has been adopted (ref. chapter 3). In this specific case, in order to define significant threshold values, the following procedure was followed:

- The axial force reduction corresponding to a strand breaking has been calculated, considering that a strand collapse produces a reduction of the tendon cross section;
- The fundamental frequency shift associated with the obtained variation in the tendon stress was calculated, considering the mass and length of the cable as constants;
- A threshold corresponding to about 70% of the obtained frequency shift has been set;
- A similar threshold value has been set for the remaining natural frequencies, as multiples of the threshold value obtained for the fundamental frequency.

Therefore, once the third level check procedure is activated on the cloud, following the overcoming of the first and/or second level of alert, the algorithm identifies the natural frequency values through the chosen OMA method (Cov-SSI) and compares them with the pre-set threshold values.

An alarm is activated if three of the identified frequencies exceed the preset thresholds for three successive identifications, carried out at time intervals of 5

minutes. In this case, a report is sent to the infrastructure manager, signaling the anomaly.

5.7 Monitoring Results

This section summarizes the main results obtained from the large-scale monitoring system installed on the pre-stressed concrete bridge, as described in the previous paragraphs. In particular, experimental results obtained under normal operating conditions are presented.

As aforementioned, the dynamic monitoring system has been in continuous operation since September 2017, therefore collecting a large database of acceleration time series. It should be highlighted that the bridge was opened to traffic for the entire monitored period; the traffic was and still is mainly composed of passenger cars as well as small and heavy trucks.

5.7.1 Statistical Analysis of Dynamic Signals

The dynamic input of the structure is very variable and is significantly higher at day, with intensive traffic, than during the night or weekends. Two examples of acceleration time series recorded during the night and during the day are illustrated in Figure 5.9, in order to show the difference between the level of acceleration observed in the two different scenarios.

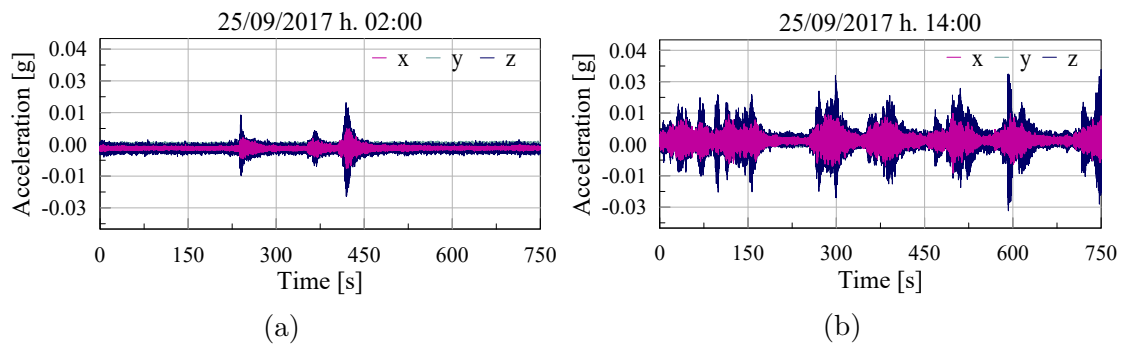


Figure 5.9: Acceleration time series collected from one sensor (a) during the night, (b) during the day.

The average acceleration value recorder for the three directions is close to a constant value for all the sensors installed on the bridge (about 0 g for x and y directions, about 1 g for the z direction), resulting from an average of periodic and almost symmetrical oscillations of the cable.

The process of trend recognition has been carried out on acceleration time series by using mean and standard deviation values, calculated within the sensor node

every 100 readings (once per second). In particular, for each measured direction (x , y , z), the signal is pre-processed by applying a high pass filter and mean (μ) and standard deviation (σ) values are then obtained from the filtered data.

Standard deviation has been considered as a good indicator of the average vibration activity induced by traffic loads, wind and/or other external agents under standard or exceptional conditions. In addition, maximum and minimum values have been considered as relevant for detecting possible anomalous behaviors of the tendons. Figure 5.10 and Figure 5.11 show the variation of the aforementioned parameters (standard deviation, maximum and minimum acceleration values) for the reference direction z (the most excited one) of some sample sensors, located in position 1 on the left side of the bridge for all the monitored sections, calculated over a time period of one month.

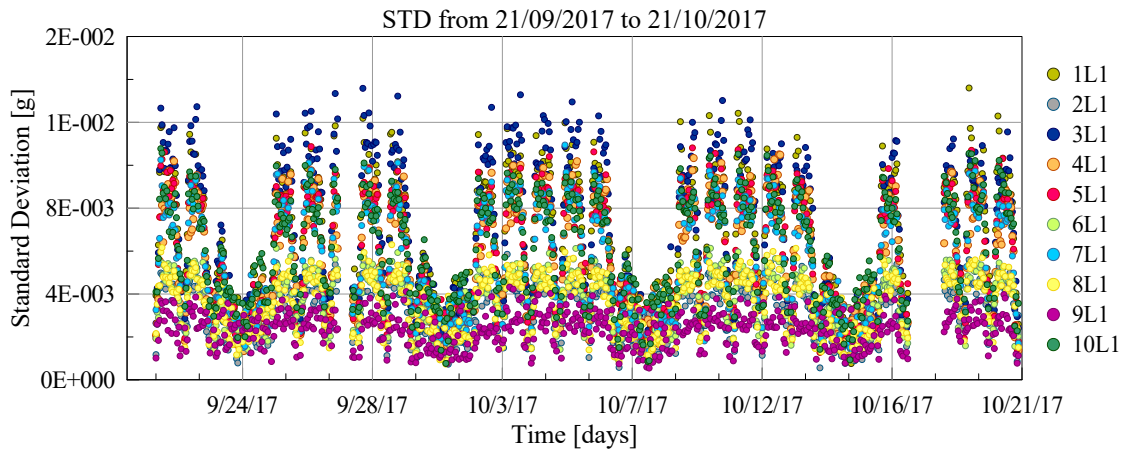


Figure 5.10: Standard Deviation (STD) evolution in time.

The day-night traffic cycle is clearly recognized: the maximum vibrations are mainly recorded during the day hours (from 6 a.m. to 10 p.m.) with an appreciable decrease at night (from 10 p.m. to 6 a.m.). Moreover, the x and z axes are the most excited ones, with respect to the y axis. This is indicative of an elliptical vibration of the cable in the x - z plane, which is orthogonal to the longitudinal development of the tendons. Y direction shows in fact reduced vibration levels (one order of magnitude smaller than x and z directions), meaning that it has a lower sensitivity with respect to traffic variations and environmental noise. Figure 5.10 and Figure 5.11 display also the weekly tendon vibration response. Indeed, higher acceleration values can be observed from Monday to Friday with a significant reduction in traffic during the weekend.

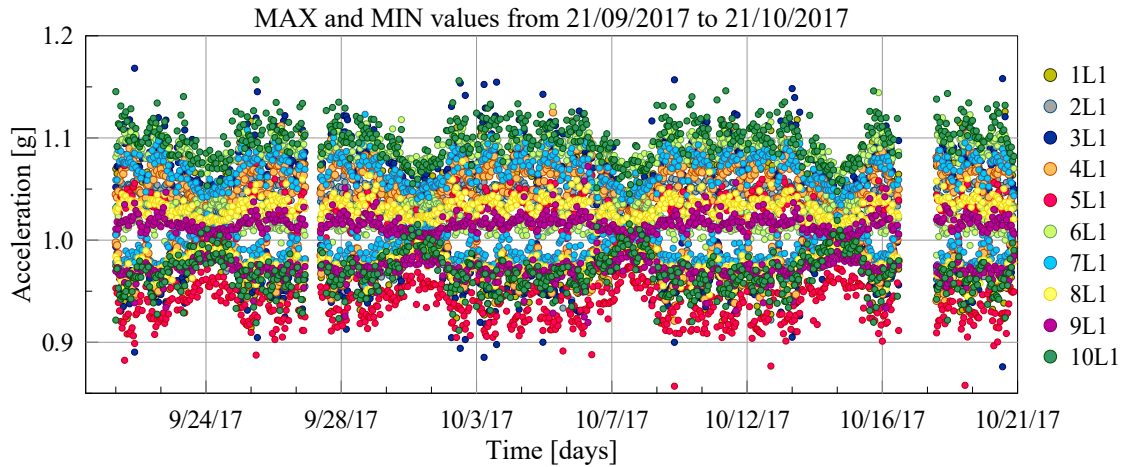


Figure 5.11: Maximum and minimum acceleration values calculated over a time period of one month.

5.7.2 Environmental effects

The influence of environmental factors on frequency values is a well documented issue [48], [34]. With reference to what has been described in detail in chapter 4, the environmental variations, and in particular temperature variations, can have a strong influence on frequency values such as to lead to the exceeding of the pre-set thresholds, with the consequent generation of false alarms. On the other hand, if the environmental influences are not properly removed, structural changes due to damages can be masked by the variations of reference parameters caused by the temperature. For this reason, environmental influences must be removed from processed data within the automated process. With a view to a long-term and automated monitoring system, although other environmental and operational factors such as wind, humidity and traffic loading may also affect the resonance frequencies, temperature shows a far higher effect and therefore the only influence of the temperature is considered.

In order to characterize the correlation between temperature and modal parameters (mainly frequency), the evolution of frequencies in time has been observed during a training period of 6 months, from 21 September 2017 to 21 March 2018. The evolution in time of the third natural frequency with respect to temperature is illustrated in Figure 5.12 for one sensor installed on the structure. The choice of the third natural frequency is motivated by the fact that frequency variations are amplified and therefore more clearly recognizable in modes at higher frequencies than the fundamental frequency. The correlation between frequency and temperature is however the same observed for the other frequencies.

Figure 5.12(a) shows an average temperature of about 20°C, ranging from a minimum value of about 5°C to a maximum value of about 30°C. By comparing

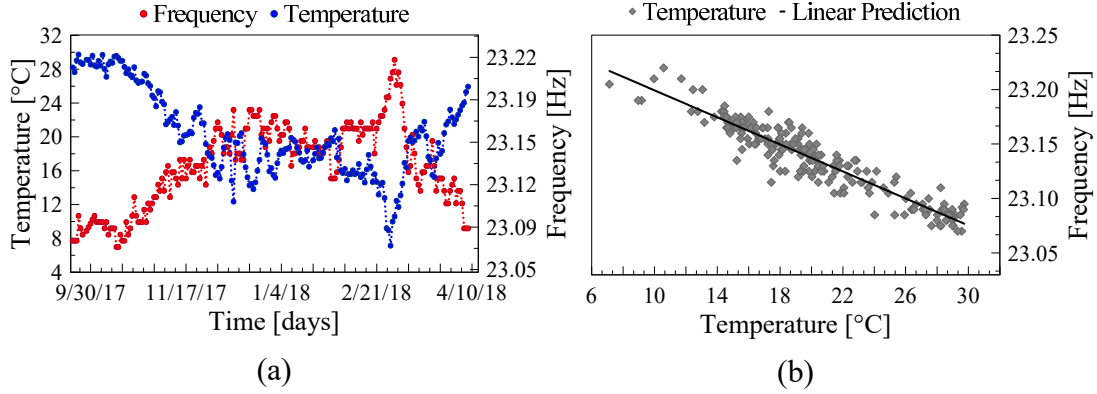


Figure 5.12: Correlation between temperature and frequency. (a) Temperature and Frequency evolution over time (b) Temperature vs Third natural frequency

temperature and frequency trends, it is possible to observe that there is an explicit inverse correlation between them over the selected time period. Indeed, for the selected sensor, frequency increases from September 2017 to November 2017, when temperature falls. The relation between natural frequencies and temperature may be further clarified by Figure 5.12(b).

The interdependence between temperature and frequency values has been examined by performing a linear Pearson correlation analysis. Pearson Correlation Coefficient (PCC) measures the linear correlation between two random variables. In order to assess the interdependence between temperature (T) and frequency values (f_i), PCC (ρ_{Tf}) was calculated as follows:

$$\rho_{Tf} = \frac{\text{cov}(T, f)}{\sigma_T \sigma_f} \quad (5.2)$$

where cov is the covariance, σ_T is the standard deviation of T and σ_f is the standard deviation of f .

The correlation between two statistical variables can be mainly of three types:

- if $\rho_{Tf} > 0$, temperature and frequency are directly correlated;
- if $\rho_{Tf} = 0$, temperature and frequency are uncorrelated;
- if $\rho_{Tf} < 0$, temperature and frequency are inversely correlated.

Furthermore, depending on the value that the correlation coefficient assumes, the following types of correlation can be distinguished:

- if $0 < |\rho_{Tf}| < 0.3$, there is a weak correlation;

- if $0.3 < |\rho_{Tf}| < 0.7$, there is a moderate correlation;
- if $0 < |\rho_{Tf}| > 0.7$, there is a strong correlation.

Consequently, if two variables are independent, meaning that no linear correlation can be identified between them, the correlation coefficient is equal to 0 whereas, if the two variables are perfectly linearly correlated, the correlation is 1 or -1.

PCC has been calculated for all the sensors installed on the bridge.

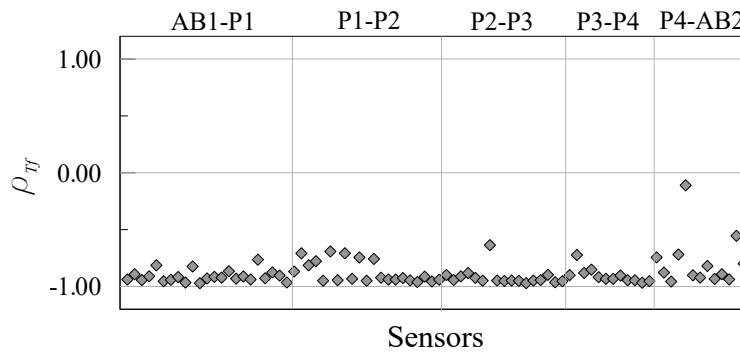


Figure 5.13: Pearson Correlation Coefficient calculated for all the sensors

Figure 5.13 shows the Pearson Correlation Coefficient ρ_{Tf} (y axis) calculated for all the sensors installed on the structure (x axis). As can be seen, 90% of the sensors showed a ρ_{Tf} value lower than -0.7, indicating a strong inverse correlation between the evolution of natural frequencies and temperature.

Therefore, given that all sensors showed a strong linear correlation between frequencies and temperature, a linear regression model was used to remove the environmental influence from frequency data. The implemented regression model has been incorporated in the automatic and real-time processing of the data collected at the bridge.

Results from the regression model are illustrated in Figure 5.14, where the time evolution of the third natural frequency before and after removing the environmental influences is represented. As it can be seen, the resulting trend is almost constant for the entire monitored period. Moreover, it could be noted that no particular anomalies in peaks evolution have been observed over time. All the frequencies are included in a range between 23.12 Hz and 23.16 Hz, without values clearly outside the normal oscillations around a constant mean value. Moreover, by observing the histograms associated with data before and after the removal of the thermal influences, it is clearly shown that the range of variation of the natural frequencies is considerably reduced after the application of the regression model.

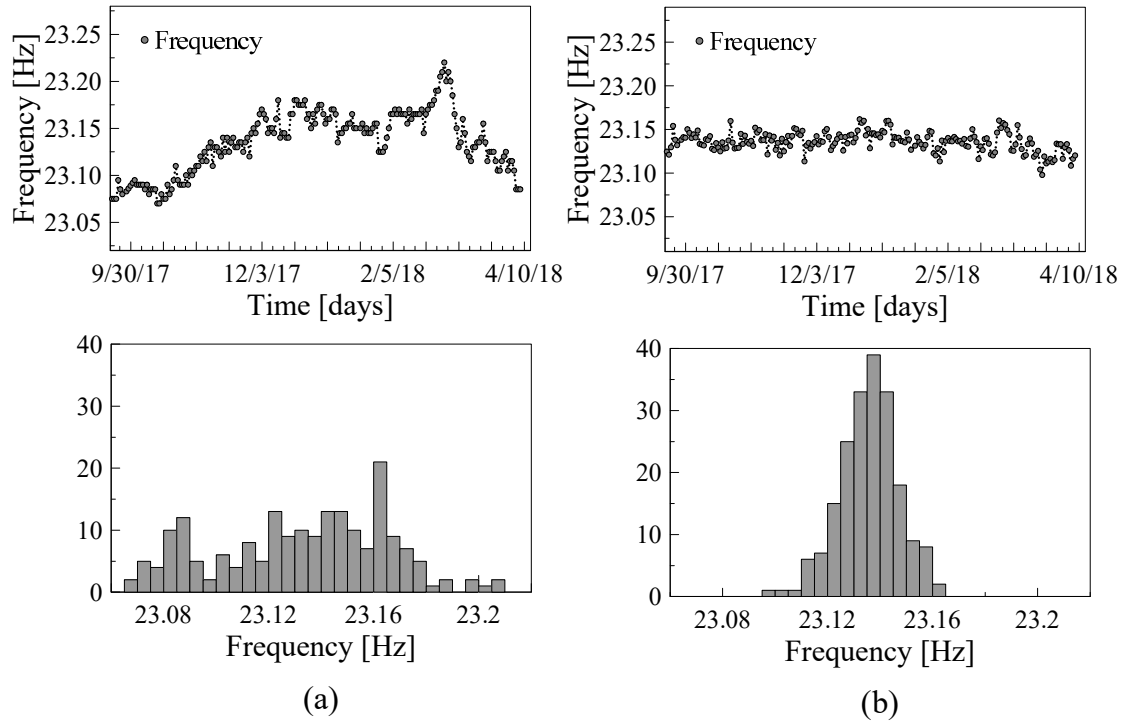


Figure 5.14: Third natural frequency evolution over time and relative histogram. (a) before removing the thermal influence (b) after removing the thermal influence

5.7.3 Damage Detection

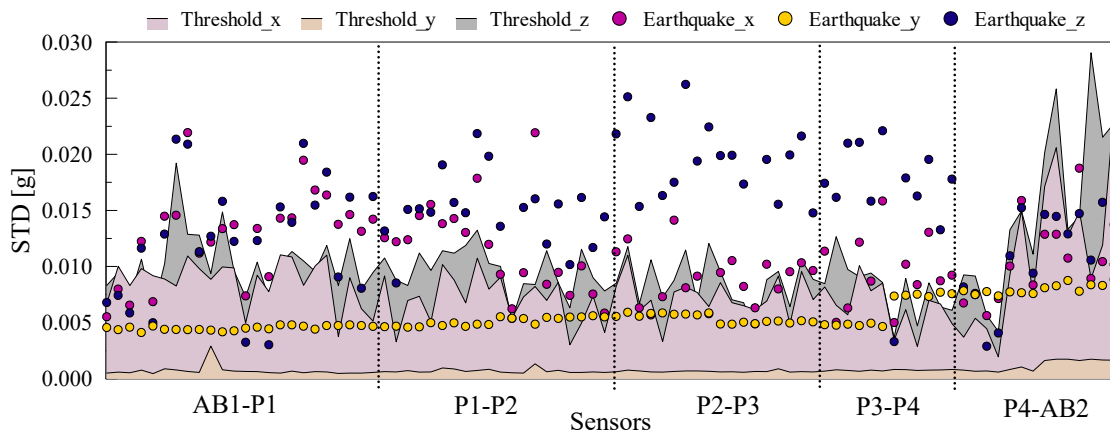
This section illustrates the main events observed during the monitoring period, with particular focus on the damages automatically detected by the long-term and real-time monitoring system described in the previous paragraphs. It is important to emphasize that the presented methodology allows the automatic identification of damages using 3 levels of alert, defined through specific threshold values which have been implemented respectively within the gateway and the cloud environments, after a data pre-processing (for the reduction of thermal effects for example) executed within the sensor node.

The proposed strategy has been adopted for monitoring the integrity of tendons in the period between September 2017 and July 2019. In this time period, three main events occurred, being detected by the automated monitoring system. The three events, called for simplicity event 1, 2, 3, will be described in detail in the following sub-sections.

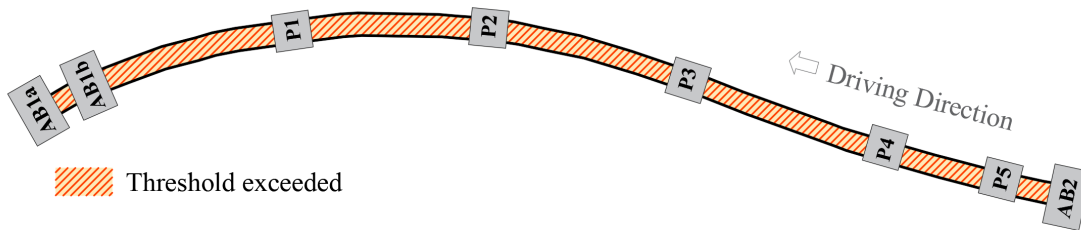
Event 1 - Earthquake

The first significant event was recorded in November 2017. Indeed, on 19/11/2017 the first level threshold was exceeded by all the sensors of the structure. No alarm was produced by the automatic monitoring system but, since all the sensors had exceeded the first level of thresholds, more in-depth analyses were carried out.

Figure 5.27 shows the STD values (calculated as described in chapter 4) on November 19, 2017, which exceeded the first level threshold values set for each sensor. As illustrated in Figure 5.15 (a) and in the corresponding plan view (Figure 5.15 (b)), all the sensors showed STD values significantly higher than the pre-defined thresholds, indicating an anomaly condition that covered the whole bridge.



(a) Standard Deviation (STD) registered during the earthquake by all the sensors in the 3 measurement directions x, y, z



(b) Standard Deviation (STD) registered during the earthquake by all the sensors in the 3 measurement directions x, y, z

Figure 5.15: Sensors that exceeded the first level threshold during the earthquake (a) STD values, (b) Plan view

In particular, by analyzing the individual measurement directions x, y and z (Figure 5.15), it is possible to observe that the y direction, which normally shows very low standard deviation values, recorded STD values comparable to the x and

z directions. This observation excluded the possibility that the recorded anomalous behavior was associated to the excitation caused by exceptional traffic conditions on the bridge, as the y direction would not have been affected as it was.

Once the first level threshold was exceeded, levels 2 and 3 were activated.

However, neither level 2 nor level 3 have exceeded the predetermined threshold, indicating that no changes to the intrinsic characteristics of the structure have occurred.

Figure 5.16 illustrates the evolution of the third natural frequency for some of the monitored tendons during the period under analysis (section 2R). A focus on this graph around the date in which the event occurred shows that frequencies did not change during the considered time period, remaining constant for all the tendons, meaning that no structural changes happened on those elements. Indeed, when the first level threshold was exceeded, the second level check was automatically activated on the cloud for all tendons, in order to verify the frequency trend at the alerted time instant, but no frequency shifts were observed.

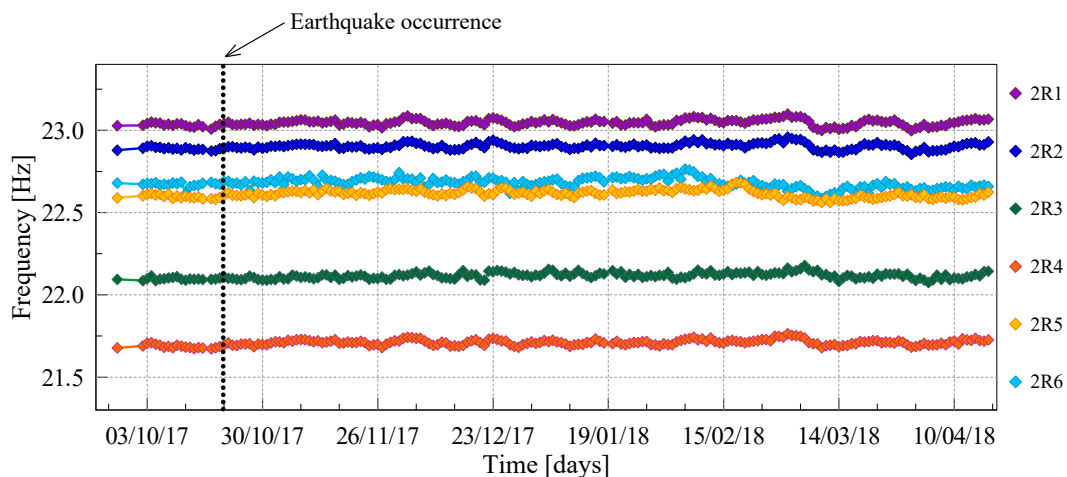


Figure 5.16: Frequency evolution over time - Section 2R

The overcoming of the first level threshold for all the sensors was in fact justified by the occurrence of an earthquake in the vicinity of the structure. In particular, an earthquake of magnitude 4.4 occurred at about 50 km from the bridge. The hypocentral depth was estimated to be 32 km.

The STD values calculated on acceleration data recorded by sensors during the earthquake were, of course, out of bounds, due to the considerable amount of energy contained in the signal following the seismic input. In fact, as known, standard deviation is only related to the signal amplitude that, in this case, was extremely high due to the seismic shock. Figure 5.17 shows the time series recorded by two sensors installed on the bridge respectively at the center of the deck and near the abutment AB1.

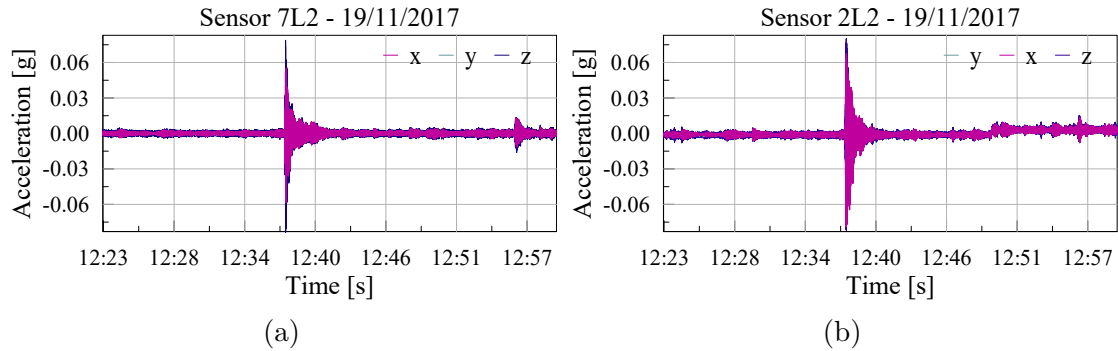


Figure 5.17: Acceleration time series collected during the earthquake (a) sensor 7L2, (b) sensor 2L2.

By looking at Figure 5.17 it is possible to note the large amount of energy released during the earthquake, especially in the y direction, which justifies the overcoming of the first level of thresholds.

However, it is worthwhile to mention that the second threshold was not exceeded and no shifts in natural frequencies were observed; consequently, the automatic anomaly detection procedure did not report any structural alarms, demonstrating the reliability and robustness of the implemented methodology.

Event 2 - Strand breakage

On December 2017 another significant event occurred on the monitored structure. In particular, the first level threshold was exceeded by some sensors installed in the first span of the bridge, as shown in Figure 5.27.

The event was recorded mainly by one of the sensors installed in the first span, as highlighted in the graph, where it is possible to observe that sensor 1L3 reached the highest standard deviation level. At the same time, all the sensors installed in the remaining spans did not show anomalous STD values, indicating that the event triggering the alarm affected only the first span of the bridge (AB1-P1).

Following the first level alert, the second (autoencoder) and third (natural frequencies) alert levels were automatically activated by the monitoring system on the IoT gateway and cloud for all the sensors that exceeded the first threshold check. As a result of the second level analysis, one of the tendons located in the first span (AB1-P1) of the monitored bridge exceeded both the second and third threshold levels, indicating a possible structural damage.

As aforementioned, the second level of alert takes advantage of an unsupervised machine learning algorithm (more specifically an autoencoder) to detect changes in structural behavior which is characterized by several variables. The reference parameter is the reconstruction error, which is used to measure how well the decoder is performing. Figure 5.18 shows the trend of the reconstruction error for sensor

1L3 from the beginning of December 2017 until 15/12/2017.

As can be observed from the graph, the reconstruction error assumes almost constant values around 0.8% from the beginning of the monitoring period until 09/12/2017. On 09/12/2017 a sudden increase in the reconstruction error has been detected, passing from an average value of 0.8%, to values of around 0.95%, thus exceeding the preset threshold value equal to 0.1% of the reconstruction error mean value.

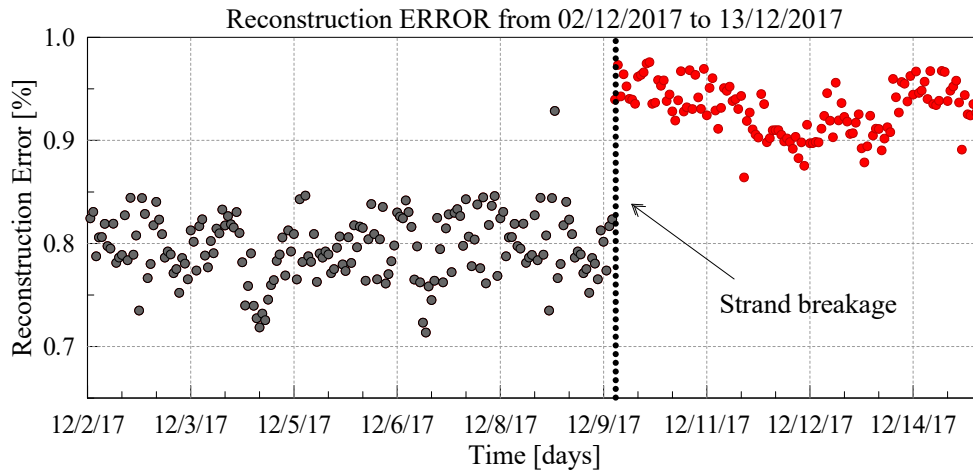


Figure 5.18: Reconstruction Error at the anomalous event - sensor 1L3

This sudden shift indicated that the autoencoder was no longer able to reconstruct the vibration signal with the same accuracy as before due to a change in the intrinsic characteristics of the structural element, which affects the dynamic characteristics of the signal collected by sensors.

Moreover, as regards level 3, a shift in frequency values was detected for cable L3 located in span AB1-P1, left side of the bridge. Figure 5.19 shows the PSDs calculated for sensor 1L3 before (black line) and after (red line) the anomalous event. A sudden right shift of natural frequency values can be clearly observed, meaning that a damage occurred in of the tendon.

Moreover, 5.20 shows the evolution over time of the third natural frequency obtained for all the sensors affected by the anomaly, with the indication of the date on which the event occurred.

As can be observed from the graph, tendon L3 of the span AB1-P1, on which sensors 1L3 and 2L3 are installed, showed a significant shift in fundamental frequency value of about $0.33Hz$, corresponding to the expected frequency reduction in case of failure of one of the strands of the cable. The registered shift in frequencies could thus be caused by the failure of one of the strands of the tendon L3, that exceeded the second level threshold. Indeed, as aforementioned, a strand break

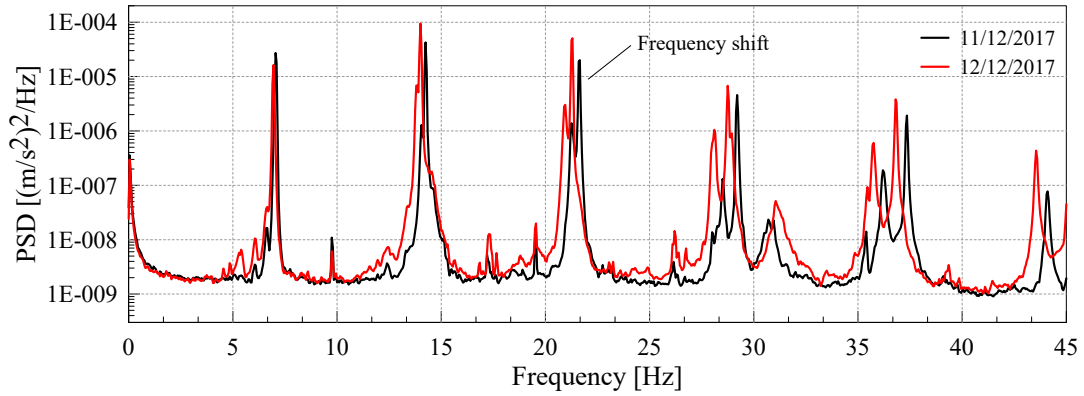


Figure 5.19: PSD calculated for tendon L3 before and after the anomalous event- Significant shift in fundamental frequency values

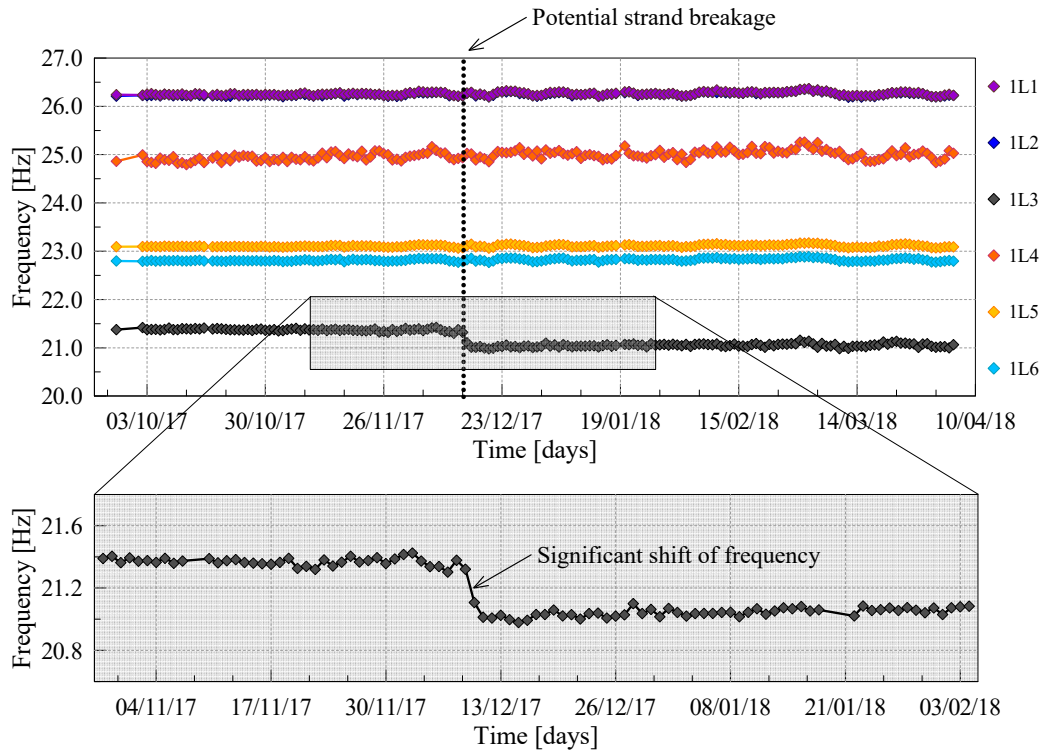


Figure 5.20: Frequency evolution over time - Section 1L - with zoom on sensor 1L3 which showed a significant shift in fundamental frequency values

causes a partial loss of prestress force in the tendon, which results in a stiffness reduction of the element itself. This reduction in tendon stiffness translates into a reduction of natural frequencies as a function of the severity of tendon damage

(the number of strand breaks) and the location of the damage.

Moreover, if a strand breaks, a significant amount of vibrational energy would be released, being recorded as a dynamic input by the immediately nearby sensors. In fact, by looking more in detail at which sensors showed STD levels above-average, the following could be observed:

- Section 1

The monitoring section 1 is located at the abutment AB1. In this section, the highest standard deviation values have been recorded and therefore it is supposed to be potentially closer to the point where the strand breakage occurred. The sensor 1L3, installed on the tendon L3 in this section, registered strong vibration levels in the 3 directions of measurement x, y, z.

In particular, with reference to Figure 5.21 (a), it can be observed that some sensors in close proximity to sensor 1L3 registered STD levels considerably higher than the pre-set threshold values in y and z directions, while in x direction the anomaly was observed only on 1L3 sensor. This observation could be justified by the fact that the possible breakage of one strand of the L3 tendon generated a vibration impulse along the y and z axes, being a phenomenon that develops mainly in the longitudinal direction of the cable. This impulse was then transmitted to the deviator (located at the abutment AB1) and therefore to the tendons close to L3. It is thus understandable that there is no particular evidence of the event in the x direction in the cables located near tendon L3.

- Section 2

The monitoring section 2 is located at the pier P1. The sensor 2L3, installed on the tendon L3 in this section, registered strong vibration levels only along y and z directions, while no anomalies were observed in x direction. With reference to Figure 5.21 (b), it can be observed that some sensors in close proximity to sensor 2L3 registered STD values considerably higher than the pre-set threshold values in y and z directions. This observation, as explained before, could be justified by the fact that the strand breakage generates a vibration impulse mainly in the longitudinal direction of the cable. This impulse was then transmitted to the deviator (located at the pier P1) and therefore to the tendons located close to cable L3.

It is important to stress that this tendon showed frequency values considerably lower than the expected theoretical ones already when the monitoring system was installed. In fact, with reference to Table 5.4, it is possible to notice that, in September 2017, a fundamental frequency of 6.98 Hz was identified against the expected 7.55 Hz, evaluated considering the length and stress of the cable obtained from the in situ measurements carried out before the installation of the monitoring

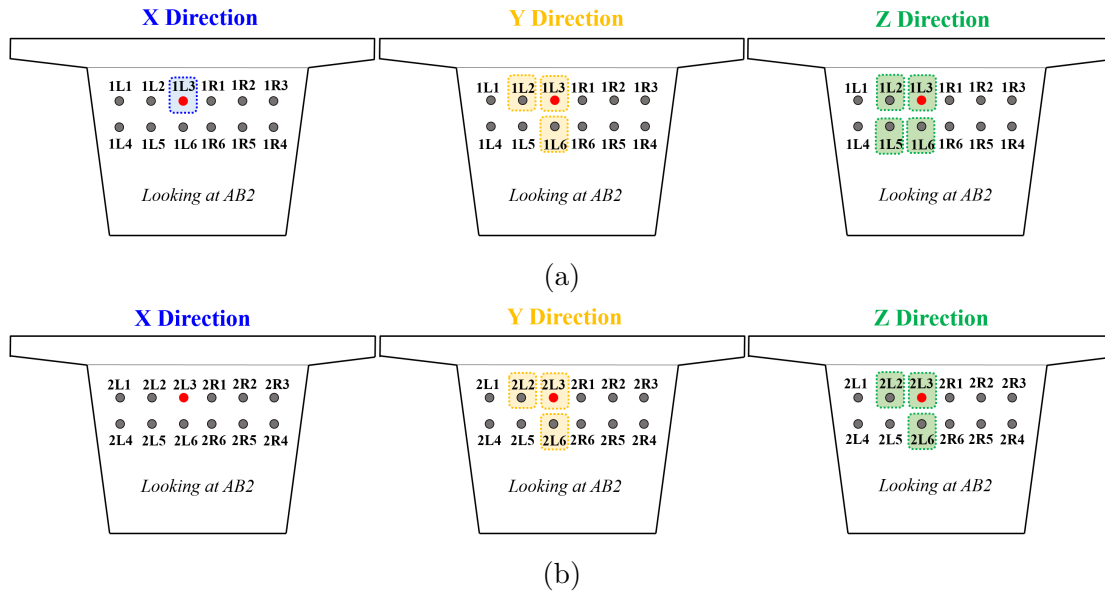


Figure 5.21: Sensors that exceeded the T_{SE} threshold along the 3 measurements axes x, y, z. (a) Section 1, (b) Section 2

system. This means that, at the time of system installation, there was a difference between experimental and theoretical frequencies of about 0.57 Hz. This could indicate that, already in September 2017, there was a corrosive phenomenon in progress that could have caused the breaking of some strands of the cable. In particular, this frequency shift would correspond to the breaking of 4 strands, with an associated reduction in the tendon axial force of about 15%. Based on these considerations, the hypothesis according to which the frequency shift observed in December 2017 was caused by the break of a strand seems realistic.

Following the exceeding of the second threshold level, an alert communication was sent to the infrastructure manager, who arranged an inspection of the L3 tendon. During the inspection, the protective envelope of the tendon showed visible swelling near the monitoring section 1 (at the abutment AB1), as showed in Figure 5.22, indicating a localized increase in volume of the cementitious grout injected in the tendon duct to encapsulate and protect the tendon itself.

However, no maintenance or replacement actions were carried out on the alerted tendon immediately after the inspection, which took place in February 2018.

Event 3 - Tendon breakage

At the beginning of April 2018, the first threshold level was exceeded by all the sensors installed in the first span of the bridge (between abutment AB1 and pier P1) and by some sensors installed in the second span (between piers P1 and P2), as

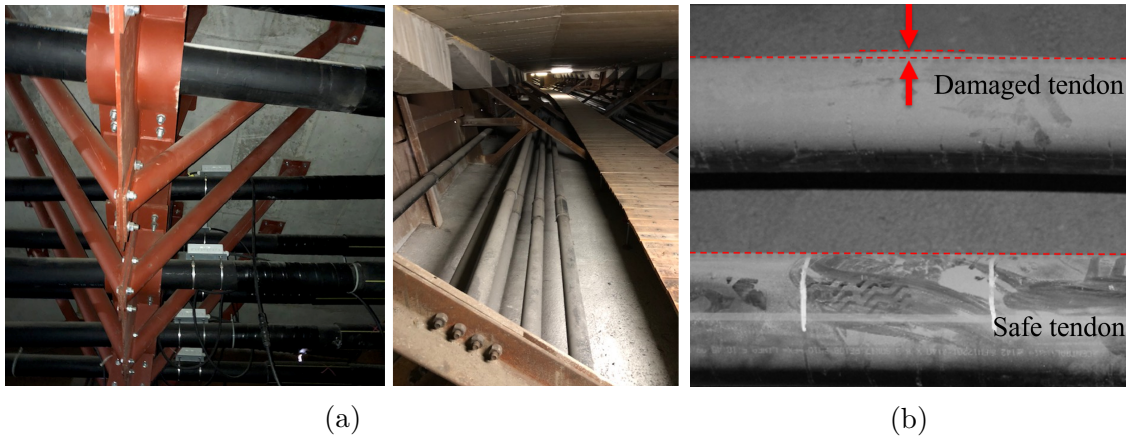


Figure 5.22: Inspections carried out in February 2018. (a) Inspected tendons, (b) localized increase in volume of the damaged tendon compared with safe one.

highlighted in Figure 5.23 (a) and Figure 5.23 (b). Moreover, a monitoring system malfunction alert was generated because of the breakdown in data flow from all the sensors on the left side of the first span (AB1-P1) of the bridge.

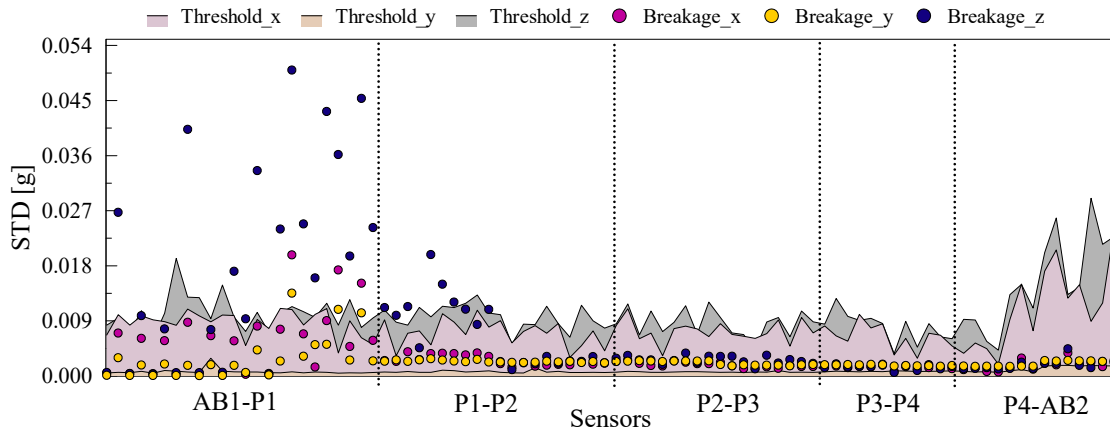
More in detail, a strong impulse was recorded by all the sensors belonging to sections 1 and 2 and in particular:

- *Section 1* - all the sensors installed on the right side (1R) of the span AB1 -P1 recorded a strong impulse, which caused the first alert level to be exceeded, while the sensors installed on the left side (1L) interrupted transmitting data to the IoT cloud at the anomalous event (ref. Figure 5.24);
- *Section 2* - all sensors installed in section 2 recorded a strong impulse, which caused the first alert level to be exceeded, except for sensors 2L3 and 2L6 which recorded a significant mean shift in the acceleration time series at the anomalous event (ref. Figure 5.25).

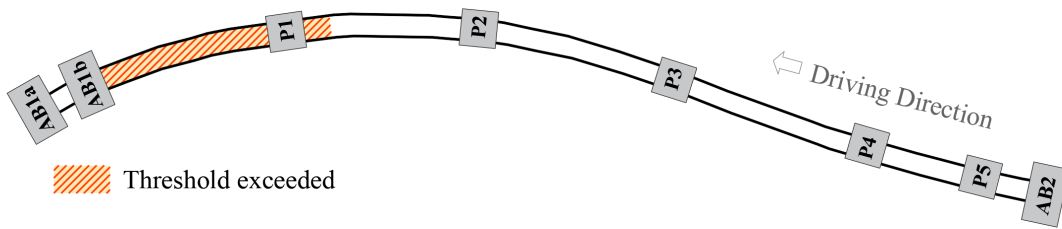
Following the first level alert, the second and third alert levels were automatically activated by the monitoring system on the IoT gateway and cloud for all the sensors that exceeded the first threshold check. However, as a result of the second and third level analysis, no anomalies were detected.

Nevertheless, considering that many sensors belonging to the same section affected by the anomalous event of December 2017 were no longer reachable by the IoT cloud and all the others exceeded the first level threshold, a specific visual inspection was performed inside the box girder.

During the inspection, cable L3 was found broken, as shown in the Figure 5.26. The accelerometers installed on the tendon that suffered the breakage are sensors 1L3 and 2L3.



(a) Standard Deviation (STD) registered by all the sensors in the 3 measurement directions x, y, z, during the breakage of one tendon in the first span of the bridge (AB1 - P1)



(b) Plan vien representing bridge areas exceeding the first alarm level threshold - tendon breakage april 2018

Figure 5.23: Sensors that exceeded the first level threshold during the tendon breakage (a) STD values, (b) Plan view

The breakage of the L3 tendon caused the cutting of the system cable connecting all the sensors installed of the left side of section 1 (whose readings were therefore interrupted) and the detachment of two sensors installed on section 2, 2L3 and 2L6, as aforementioned. The break point of the tendon was located inside the abutment AB1.

Based on the inspection outcomes and on the analysis conducted for the potential breakage of a strand belonging to the same cable in December 2017, it is possible to assume that the breakage was caused by the achievement of the ultimate tensile strength of the tendon, induced by the loss of a critical number n of strands. More in detail, the most realistic hypothesis is the following:

1. One of the strands composing the tendon L3 broke at section 1;

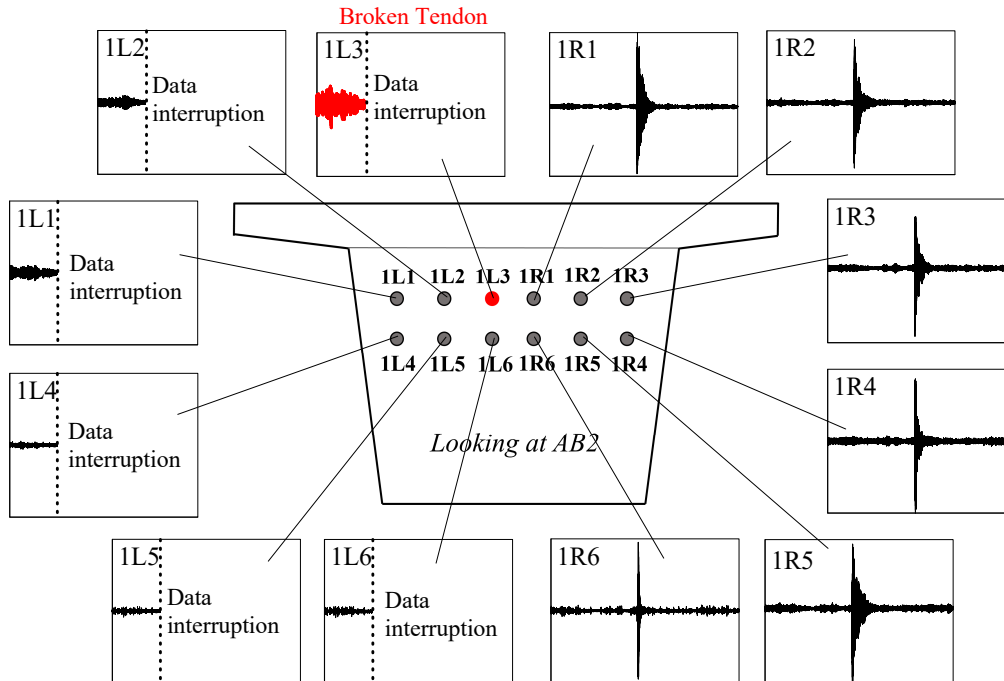


Figure 5.24: Acceleration time series related to the tendon breakage - Section 1

2. The strand breakage caused the achievement of the ultimate steel tensile strength in the remaining strands (therefore assuming that a number m of strands have already broken and the latter was just the $m + 1$ th strand);
3. The tendon broke in a section located inside the abutment AB1;
4. The energy released during the occurrence of the sudden tendon break caused the cable to 'slide' inside the abutment until it stopped due to the friction with the concrete. At the same time, the sliding of the tendon produced the left power cable to break in section 1 and sensors 2L3 and 2L6 to detach from the tendon duck in section 2.

The breakage of the L3 cable was extremely relevant because it confirmed even more the effectiveness of the proposed methodology, which identified the state of damage of this cable in December 2017, when a change in the modal parameters of the structure was observed.

Figure 5.27 summarizes the 3 main events recorded during the monitoring period and described in detail above. In particular, the trend of the STD value from from 01/10/2017 to 05/05/2018 is represented for each sensor installed on the structure. The standard deviation (STD) value, calculated every 100 samples (once

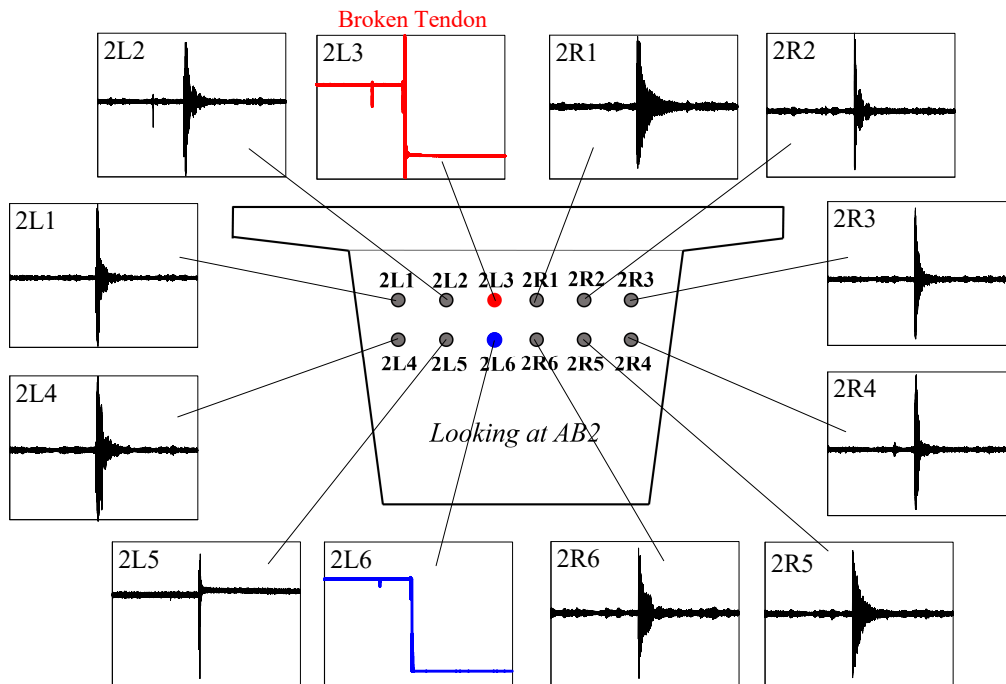


Figure 5.25: Acceleration time series related to the tendon breakage - Section 2

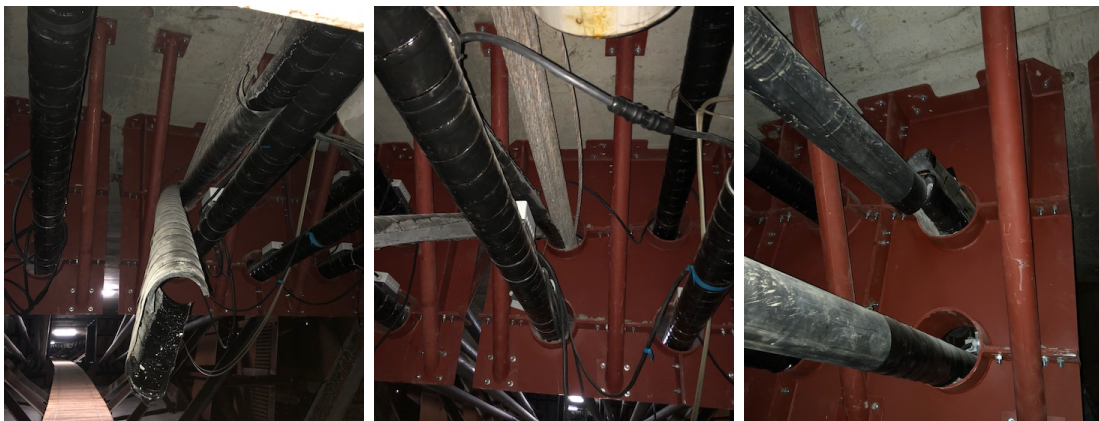


Figure 5.26: Broken tendon

per second) with respect to the signal modulus, as described in detail in Chapter 4, was chosen as reference parameter for the first alert level. This parameter is aimed at highlighting any abnormal behaviours in terms of vibration energy.

In order to detect the most significant events occurred on the structure during the monitoring period of time and to identify the areas involved for each event, the maximum STD value recorded by each sensor has been considered for each

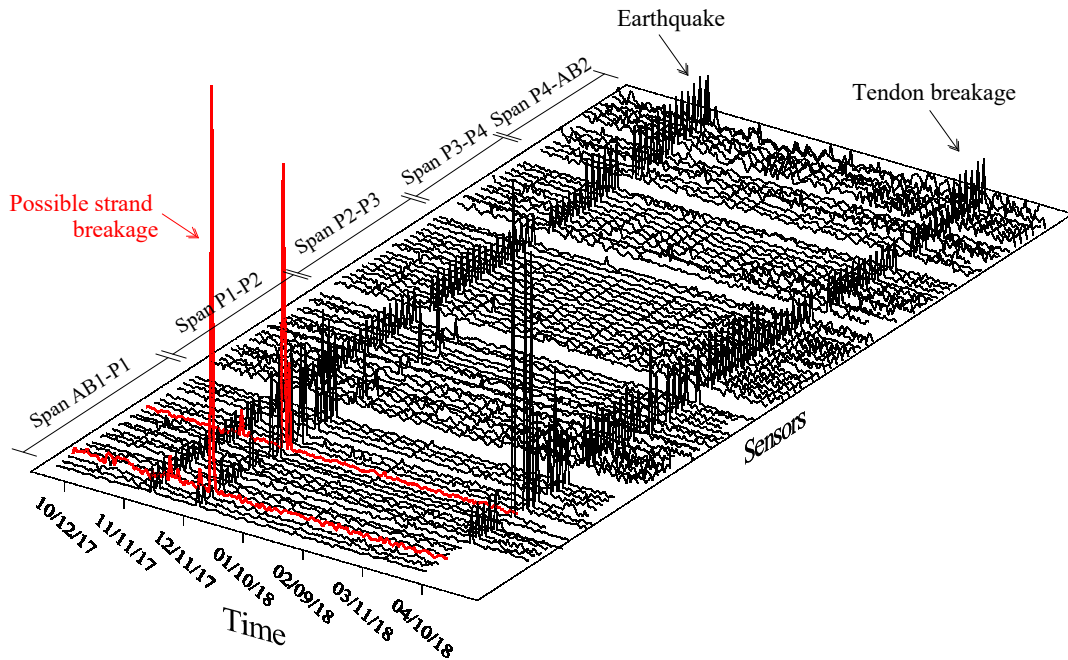


Figure 5.27: Evolution of the STD values calculated for each sensor in the monitoring period from 01/10/2017 to 05/05/2018 - identification of three main events

monitoring day. Figure 5.27 clearly illustrates three days (events) with STD values considerably higher than the standard behavior:

- on November 19, 2017, all the sensors recorded STD values that exceeded the T_{SE} threshold. It is noteworthy that the extent of the overcoming is comparable between all the sensors, which is in line with the phenomenon that triggered the first alert level, that is the earthquake.
- anomalous STD values were afterwards recorded on 09/12/2017, exceeding the first alarm level. As we can infer from the graph, the event mainly affected the span AB1-P1, where the highest STD values have been observed. Span P1-P2 also recorded STD values outside the threshold, even if of a lesser extent, while the remaining spans did not record the event. This is consistent with the hypothesized strand breakage.
- finally, in early April 2018, another significant event was recorded by all the sensors of the structure. In particular, some sensors of the AB1-P1 span have stopped sending data to the cloud while the remaining sensors of the same

span have reported STD values significantly above the T_{SE} threshold. On the other hand, all the remaining spans recorded STD values exceeding the threshold, even if with lower values.

5.8 Final Remarks

This chapter describes the application of the methodology proposed in this dissertation to a significant case study, concerning the monitoring system installed on the external tendons used to pre-stress a concrete highway bridge located in norther Italy.

The chapter started with the description of the dynamic monitoring system installed on the highway bridge, for the continuous and automated monitoring of the pre-stressing tendons. This application is completely innovative both for the monitoring system itself, which has been designed for allowing the continuous monitoring of the structure through a large number of sensors for several years, and for the type of application, in which sensors have been installed directly on the external prestressing tendons, with the aim of predictive maintenance of these elements subjected to a gradual corrosion process due to an incorrect grout composition. The main challenge in designing and managing such a monitoring system has been the full exploitation of all the potentialities of the implemented infrastructure, being aware of the capacities and limits of the different components and avoiding waste of resources. For this reason, some important aspects associated with the design and management of dynamic monitoring systems for large civil engineering structures were discussed together with the description of the solutions adopted for the analyzed bridge. In this regard, the operation of the installed monitoring system for more than two years demonstrated its robustness and reliability.

Afterwards, some preliminary analyses were carried out to evaluate the health state of the structure (and especially of tendons) at the installation of the monitoring system. These preliminary ambient vibration tests were essential for understanding the state of the structure before installing the sensors.

Once the preliminary analyses were carried out, the proposed methodology was applied in order to detect any damage in the monitored structure. Appropriate threshold values have been automatically generated by the system and the implemented framework has been activated for the permanent and long-term monitoring of the bridge, in order to ensure an early-stage alert of any anomalous condition.

Subsequently, the main results obtained during the monitoring period were presented. Firstly, some statistical analyses were performed in order to understand

excitation trends (e.g. traffic, wind..). For this purpose, the large database collected during the years allowed to clearly recognize day-night and week-weekend traffic trends. Moreover, differences were also identified between the excitation levels of the 3 measurement axes x , y and z . After that, the influence of environmental and operational variables on the modal parameters has been addressed and removed through a linear regression model, which have been automatically calibrated for each monitored tendon. The implemented model permitted to minimize the effects of environmental and operational factors on natural frequencies, thus allowing to correctly detect the frequency shift caused by damages.

Finally, real damage scenarios observed during the monitoring period have been described. In particular, 3 different events have been detailed:

- the first significant event concerns an earthquake that occurred in November 2017. This event caused the first level threshold to be exceeded by all the sensors of the structure, triggering more in-depth analysis (levels 2 and 3 were activated). However, neither level 2 nor level 3 were exceeded, indicating that no damages occurred to the monitored structural elements. This event has proven the effectiveness of the implemented automatic multilevel methodology, capable of distinguishing real damage scenarios from anomalies that do not generate structural problems;
- the second meaningful event is the potential breakage of a strand within one of the monitored cables. In particular, the first level threshold was exceeded by some sensors installed in the first span of the bridge in December 2017. Following the first level alert, the second and third checks were automatically activated by the monitoring system and, as a result of the these deeper analysis, one of the tendons exceeded both the second and third threshold levels, indicating a possible structural damage. This event is particularly relevant as it allowed the automatic and reliable identification of a structural anomaly which affected one of the monitored tendons.
- On april 2018 the cable that had suffered the damage in December 2017, was found broken. The relevance of this event is very high if referred to what has been observed previously. In fact, it demonstrated that the event recorded in December 2017 was actually related to the breaking of a tendon's strand and therefore represented an unequivocal symptom of the degradation of the structural element. This occurrence has highlighted the potentiality of the monitonoring system for the early detection of degradation processes on the structure and thus, the preventive maintenance operations.

To sum up, it was demonstrated that the proposed methodology allowed the continuous, automatic and reliable evaluation of the state of health of the monitored

structure over time, effectively detecting changes of the modal parameters that are indicators of the occurrence of structural degradation which, in this specific case, corresponded to the breakage of one or more strands inside the prestressing tendon.

Chapter 6

Continuous Monitoring - Case Study 2

6.1 Chapter Introduction

This chapter describes a meaningful case study of continuous monitoring systems applied on a concrete highway bridge located in northern Italy. As for the previous case study, the main goal is demonstrating the potential of the proposed methodology for the identification of anomalous conditions in this structure, which was and still is continuously monitored.

6.1.1 Dynamic monitoring of a pre-stressed highway bridge

An interesting case study of a damaged operating bridge located in Italy is illustrated in this chapter. In particular, the structure under examination is being monitored continuously through a dynamic monitoring system since March 2019, after some visual inspections that revealed that one span of the structure was in a state of advanced deterioration. Following more in-depth analysis, strengthening works were planned on the damaged span, through the adoption of external prestressing tendons. In particular, this type of intervention improves the ultimate bearing capacity and thus the performances of the bridge, increasing the lifespan and durability of the structure. In order to track the behavior of the bridge during and after the maintenance procedure, a series of triaxial accelerometers were installed on the structure. The very short time needed for the restoration works only allowed to set up a line of sensors in each span, for a check on natural frequencies and modal damping, and only roughly accounting for the mode shapes. All the same, this has been considered a very important chance to compare a damaged and undamaged bridge behavior.

The measurements started before the strengthening works so that a dataset representative of a damaged state was collected. The opportunity to have evidence

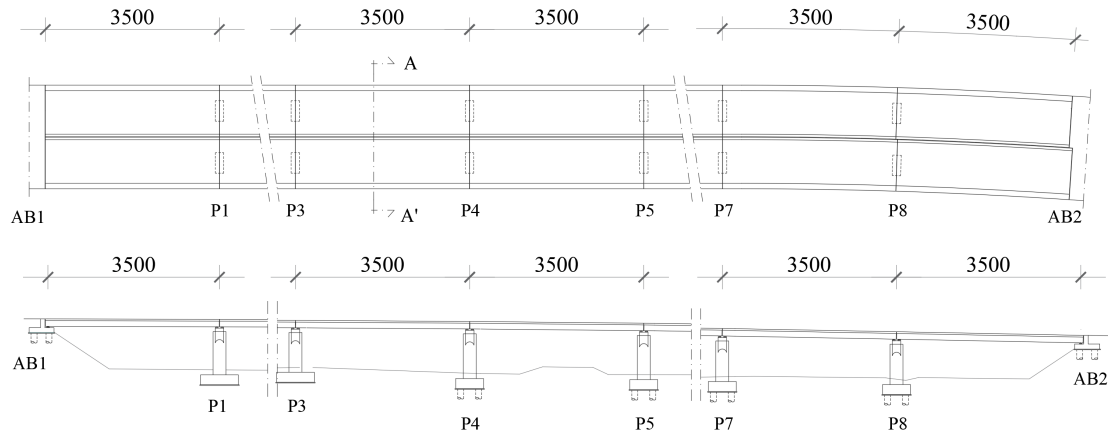


Figure 6.1: Plan and elevation view of the monitored bridge

of a damaged structure is extremely important especially in case of civil structures, for which data referred to the damaged state are usually not available.

In a first part of this chapter, a description of the monitored bridge and monitoring elements is reported. Afterwards, the application and operation of the automated monitoring strategy is presented. Finally, a very clear representations of the state of the structure before and after the maintenance works is illustrated, emphasizing the most relevant outcomes regarding the damage detection methodology presented in this dissertation.

6.2 Bridge Description

The monitored structure is a pre-stressed concrete bridge from the early 1965s, located in northern Italy. This bridge, due to its geometric and design features, can be considered as representative of many highway infrastructures in Italy. In fact, pre-stressed concrete was a very common way of designing bridges at that time.

The structure is composed by two independent roadways, each characterized by nine simply supported pre-stressed concrete spans. Each span is 35.0 m long, corresponding to a support distance of 33.9 m. The cross-section is a pre-stressed reinforced concrete slab with a constant height in the longitudinal direction of about 1.5 m. Two abutments are supporting the bridge at the end points and nine concrete piers are holding up the nine simply supported spans. Figure 6.1 and Figure 6.2 show the plan view, elevation and cross-section of the bridge.

The individual spans are constrained such as to guarantee an isostatic behavior with regard to vertical actions, while the horizontal (longitudinal) actions are transmitted to the abutments by means of two kinematic chains, one for each way. A single expansion joint, aimed at absorbing temperature-induced expansion and

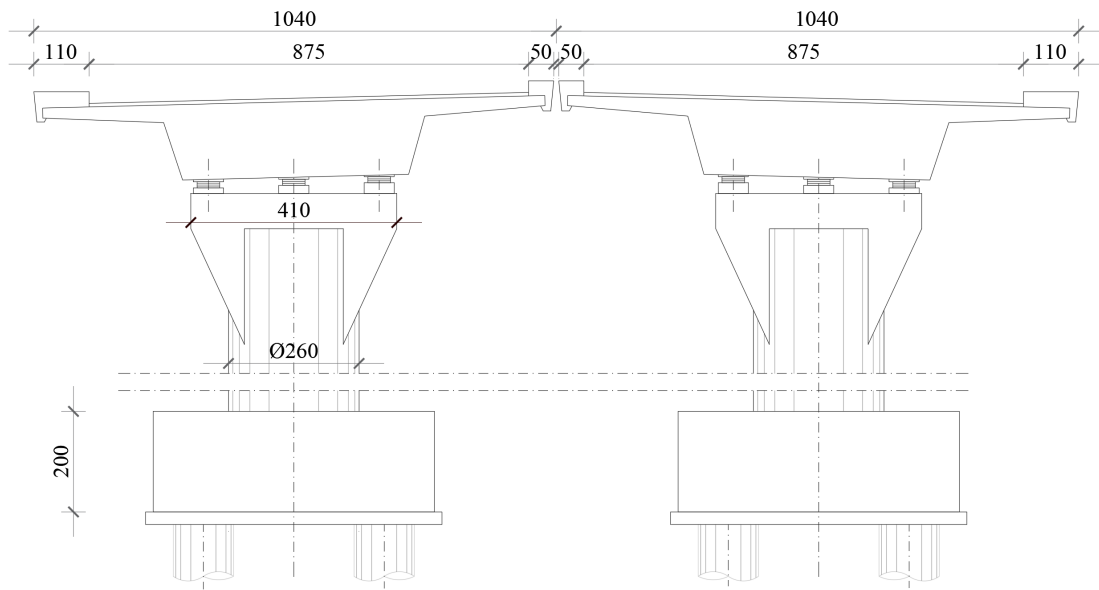


Figure 6.2: Cross-section of the monitored bridge



Figure 6.3: Bridge pictures

contraction of bridge materials, is present at pier P5. The eight piers have a circular cross-section with a constant diameter of 2.60 m.

Internal prestressing was used to strengthen the bridge. In particular, the prestress of the structure is provided by means of 14+14 post-tensioned prestressing tendons, arranged symmetrically with respect to the centerline of the decks. Each tendon is composed of 12 strands with a nominal strand diameter of 0.6 inches.

In March 2019, some visual inspections were carried out on the bridge. During the investigation activities, damage evidences have been observed at span 6 (left way), which led to more in-depth analysis. In particular, moisture spots were observed on the lower surface of the deck, as shown in Figure 6.4. Furthermore, in an



Figure 6.4: Damage evidences highlighted during visual inspections

area close to the center line of the span, several transversal and longitudinal cracks, which extended to full width and continue on the lateral sides of the transversal section, were highlighted. Water infiltrations inside the tendon ducts were also hypothesized.

In order to deepen the health conditions of the structure and inspect the tendons, two windows, approximately 20 cm wide along the transversal extension of the concrete slab, were opened straddling the center line of the bridge. Concrete demolition was deepened until reaching the prestressing tendons. The existing ducts were cut and partially removed so as to be able to evaluate the condition of the cables. Seven of the 28 tendons were found significantly corroded, with some broken strand wires (ref. Figure 6.4).

The assessment of the damaged state of the span 6, left way, led to the decision of carrying out strengthening works on the structure. At the same time, a continuous monitoring system was installed on the bridge, with the aim of checking the condition of the structure before and after the maintenance procedure.

6.3 Monitoring System Description

As aforementioned, the monitoring system was installed in March 2019, in order to characterize the behavior of the structure before and after the strengthening works. Each span of the bridge was instrumented with 5 MEMS tri-axial accelerometers, located at $1/4$, $1/3$ and $1/2$ of the bridge length, for a total number of 90 sensors installed on the entire structure, 45 for each of the two independent roadways. These MEMS accelerometers are ultra compact low-power three-axis linear accelerometers that include a sensing element and an IC interface able to take information from the sensing element and to provide a corresponding analog signal. Accelerometers have a dynamically user selectable full-scale of $\pm 2g / \pm 6g$ and they are capable of measuring accelerations over a maximum bandwidth of 1.8 kHz for all axes. They operate with a noise spectral density of $50\mu g / \sqrt{Hz}$ and a sensitivity

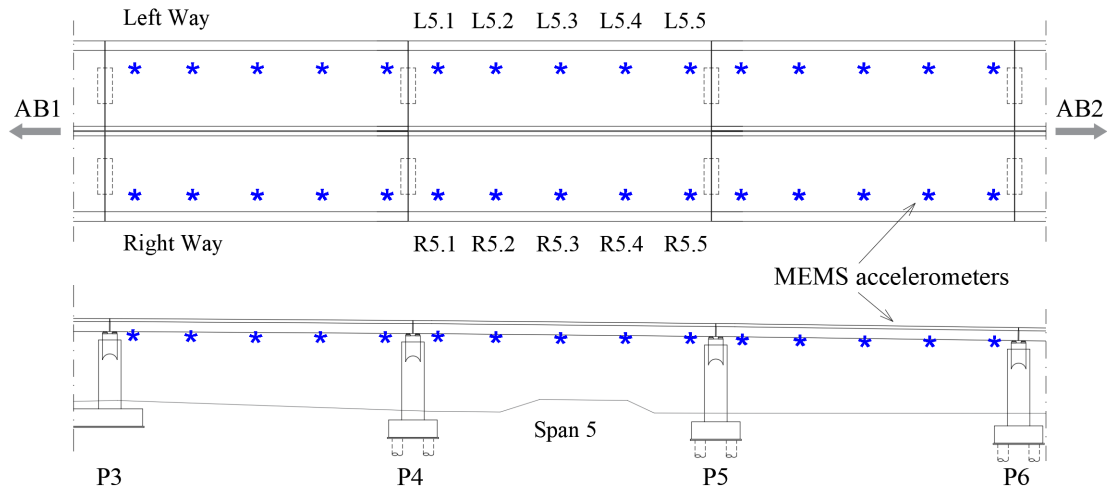


Figure 6.5: Sensors positioning on the bridge - Plan and elevation view

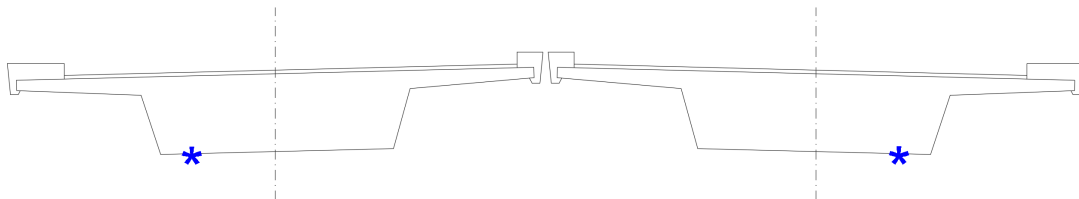


Figure 6.6: Sensors positioning on the bridge - Cross-section

of $V_{dd}/5$ [V/g], considering a full scale of $\pm 2g$ and a V_{dd} (power supply) of 3.3V.

Figure 6.5 and Figure 6.6 show the positioning of sensors on the bridge while Figure 6.7 depicts some pictures related to the installation of sensors.

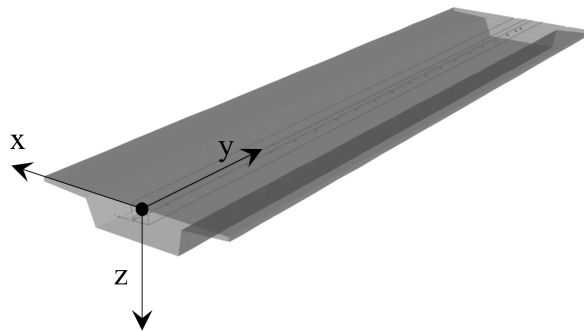
As mentioned in paragraph 4.3, each tri-axial MEMS accelerometer provides data in the 3 orthogonal directions (x, y, z), oriented as shown in Figure 6.8. The x axis is the transversal direction of the deck, y axis is parallel to the longitudinal extension of the bridge and z axis corresponds to the vertical direction.

This choice of this sensors layout deserves some deepening, as the use of MEMS allows to adopt a wider number of measurement points in a trade-off against their expected performances. Preliminary laboratory testing has allowed to fix the MEMS sensors features, not so far from those of more expensive instrumentation, anyway suitable for giving the needed information. Conversely, their low cost has allowed to have a very dense bridge sensing, which was considered of fundamental importance for the planned operation. Consequently, dealing with the huge data streaming represented the real challenge that forced a new data evaluation strategy (ref. Chapter 4).

Each of the 90 MEMS accelerometers (sensor nodes) was equipped with a 32-bit



Figure 6.7: Sensors installed on the bridge

Figure 6.8: Measurement axes (x, y, z) orientation along the deck

microcontroller and humidity and temperature sensors, in order to collect environmental information which must be taken into consideration for the correct analysis of the acceleration data. To increase accuracy, acceleration data are sampled at the sensor level at 25.6 kHz, filtered down and down sampled to finally obtain a sampling rate of 100 Hz.

Once collected, acceleration data are encoded by the microcontroller into a CAN BUS driven network and sent to a local IoT gateway, located between spans 5 and 6. The IoT gateway is connected to the IoT cloud, where data are available to be accessed, downloaded and processed, as illustrated in Chapter 4.

6.3.1 Naming Convention

For confidentiality reasons, a fictitious naming convention is adopted to describe the various elements belonging to the monitoring system.

The bridge develops starting from the abutment called AB1 up to the abutment called AB2. As aforementioned, the structure is composed by two independent roadways, called respectively "Right way" and "Left way", looking towards

the abutment AB2 (back to abutment AB1). Spans are named with progressive numbers from 1 to 9 for both directions. Sensors installed on each span are named according to the following convention:

<Direction> [Span] <sensor number>

where:

- <Direction> - identifies the roadway and can be Left (L) or Right (R);
- [Span] - identifies the span to which the sensor belongs and varies from 1 to 9 starting from abutment AB1 to the abutment AB2;
- <sensor number> - indicates the number of the transversal cross-section to which the sensor belongs and varies from 1 to 5, starting from abutment AB1 to the abutment AB2. In each span there are 5 transversal sections, located at 1/4, 1/3 and 1/2 of the span length.

Figure 6.5 shows the naming convention for the sensors installed on span 5 of the bridge, for both carriageways, which are also listed in Table 6.1.

6.4 Strengthening Works

As aforementioned, serious structural deficiencies were identified in the sixth span of the left roadway of the bridge, during an inspection campaign carried out in March 2019.

In particular, more in-depth investigations pointed out a significant loss of pre-stressing in the analyzed span, due to the breakage of a significant number of pre-stressing tendons in the concrete slab. The failure of pre-stressing tendons, as well as the high level of oxidation of the strand wires, was probably caused by a widespread corrosive phenomenon, as shown in Figure 6.4.

Following the identification of the damage, the infrastructure operator decided to carry out a reinforcement intervention on the bridge. In particular, the introduction of additional external pre-stressing tendons has been chosen as the method to strengthen the structure. This method has been widely used over the years as a means of strengthening or rehabilitating existing bridge which are considered inadequate to meet safety requirements. Indeed, the external post-tensioning has proved to be very useful in increasing the capacity of concrete span bridges [20], being at the same time a very efficient and economic solution that can be realized without affecting the normal operating conditions of the structure.

External pre-stressing tendons were thus placed outside the concrete section in May 2019 and the pre-stressing force was transferred to the concrete by means of end anchorages. In particular, an additional axial load combined with a hogging

Table 6.1: Naming convention of all the sensors installed on the bridge

Span	Left Side	Right Side	Span	Left Side	Right Side
1	L1.1	R1.1	6	L6.1	R6.1
	L1.2	R1.2		L6.2	R6.2
	L1.3	R1.3		L6.3	R6.3
	L1.4	R1.4		L6.4	R6.4
	L1.5	R1.5		L6.5	R6.5
2	L2.1	R2.1	7	L7.1	R7.1
	L2.2	R2.2		L7.2	R7.2
	L2.3	R2.3		L7.3	R7.3
	L2.4	R2.4		L7.4	R7.4
	L2.5	R2.5		L7.5	R7.5
3	L3.1	R3.1	8	L8.1	R8.1
	L3.2	R3.2		L8.2	R8.2
	L3.3	R3.3		L8.3	R8.3
	L3.4	R3.4		L8.4	R8.4
	L3.5	R3.5		L8.5	R8.5
4	L4.1	R4.1	9	L9.1	R9.1
	L4.2	R4.2		L9.2	R9.2
	L4.3	R4.3		L9.3	R9.3
	L4.4	R4.4		L9.4	R9.4
	L4.5	R4.5		L9.5	R9.5
5	L5.1	R5.1			
	L5.2	R5.2			
	L5.3	R5.3			
	L5.4	R5.4			
	L5.5	R5.5			

bending moment has been applied to the structure in order to improve the strength capacity of the structural members. This means that the application of external pre-stressing led to a structural system with an increased stiffness and reduced in-service deflections.

A total number of 24 externally mounted post-tensioned bars were anchored on each end of the inspected span, as shown in Figure 6.9.

However, the effectiveness and the corresponding effect given by the introduction of external pre-stressing tendons as bridge reinforcement method is not so easily assessable after tendons installation.

In the following paragraph, the main results deriving from the monitoring of the described bridge, before and after the intervention, will be presented in order to verify the change in structural stiffness, confirming the effectiveness of the adopted intervention in improving the structural properties.



Figure 6.9: External pre-stressing tendons installed for strengthening the structure

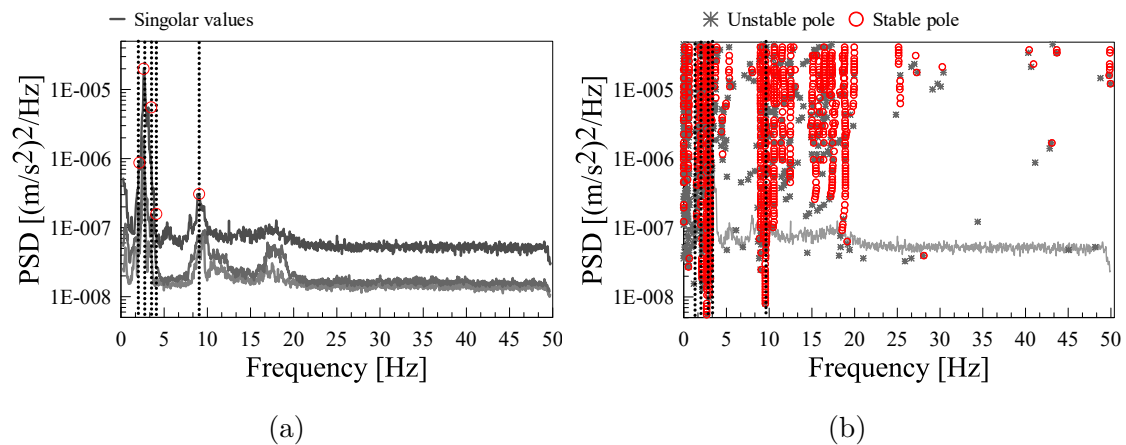


Figure 6.10: Comparison between (a) Frequency Domain Decomposition and (b) Covariance-driven Stochastic Subspace Identification Method for frequency identification

6.5 Preliminary analysis

In a first phase after installing the monitoring system, some preliminary analysis were carried out in order to identify the dynamic characteristics of the structure. More in detail, time series were collected for few weeks, before the reinforcement intervention. Modal parameters, in particular resonant frequencies and mode shapes, were identified using two OMA identification techniques, described in detail in chapter 3: Frequency Domain Decomposition (FDD) and Covariance-driven Stochastic Subspace Identification (Cov-SSI) methods. Results from both methods are shown in Figure 6.10 for one span of the bridge (span L5).

As it can be seen from Figure 6.10 resonant frequencies were clearly identified

(indicated with dashed vertical lines) between 0 and 15 Hz. These two methodologies have been used to verify the consistence of the estimates provided by the two approaches. However, for modal shapes reconstruction, only results from FDD method are shown.

With reference to Figure 6.10, it is possible to observe that the main frequency band is between 0 Hz and 15 Hz, therefore the analysis was limited to this interval. In particular, in the analysed frequency band, there are 5 alignments of stable poles. The identified frequencies are listed for all spans in Table 6.2 for the right side of the bridge and in Table 6.3 for the left side.

Table 6.2: Identified Natural Frequencies - Right spans

Span	Mode 1 [Hz]	Mode 2 [Hz]	Mode 3 [Hz]	Mode 4 [Hz]	Mode 5 [Hz]
R1	2.08	2.83	3.01	3.28	9.82
R2	2.08	2.74	2.93	3.30	9.65
R3	2.08	2.68	3.04	3.39	9.57
R4	2.08	2.70	3.05	3.40	9.61
R5	2.08	2.78	3.03	3.31	9.67
R6	2.08	2.72	3.01	3.28	9.69
R7	2.08	2.74	2.99	3.45	9.70
R8	2.08	2.79	3.01	3.27	9.68
R9	2.09	2.81	3.05	3.26	9.53

Table 6.3: Identified Natural Frequencies - Left spans

Span	Mode 1 [Hz]	Mode 2 [Hz]	Mode 3 [Hz]	Mode 4 [Hz]	Mode 5 [Hz]
L1	2.02	2.70	3.07	3.26	9.36
L2	2.06	2.71	3.01	3.24	9.42
L3	2.02	2.60	3.05	3.21	9.44
L4	2.02	2.64	3.07	3.24	9.45
L5	2.01	2.70	3.01	3.19	9.48
L6	2.01	2.19	2.64	2.80	8.71
L7	2.02	2.70	3.09	3.19	9.51
L8	2.01	2.61	3.08	3.21	9.32
L9	2.00	2.68	3.01	3.20	9.61

The local and global mode shapes were identified in the selected frequency range. Natural frequencies and mode shapes of the selected mode estimates are presented in Figure 6.11 for span L5, taken as an example; the remaining spans are

almost equivalent. It can be observed that mode shapes of very good quality were obtained.

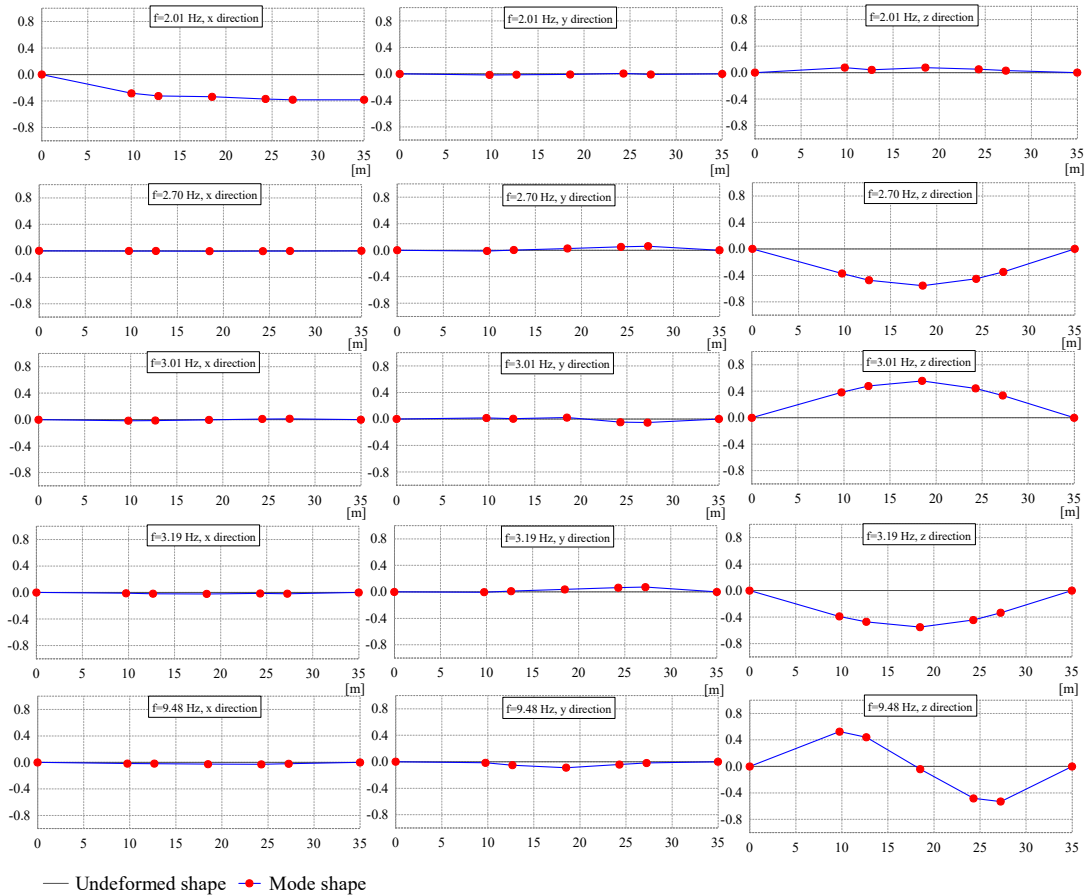


Figure 6.11: Results of the FDD analysis for the vertical and out-of-plane bending modes for L5 span

Figure 6.11 highlights that, among the five identified natural frequencies, only the first one is related to a lateral mode (mode 1) while the others are related to bending modes. Unfortunately, having only one longitudinal alignment of sensors, it is not possible to correctly reconstruct torsional modes. This fact justifies the existence of modes with different natural frequencies but similar bending mode shapes at the deck level, since some of these could be torsional.

By observing the frequency values listed in Table 6.2 and in Table 6.3 and represented graphically in Figure 6.12 for two spans, it is possible to observe that span L6 shows considerably lower frequency values than all the remaining spans of the structure, having values that are more consistent with each other.

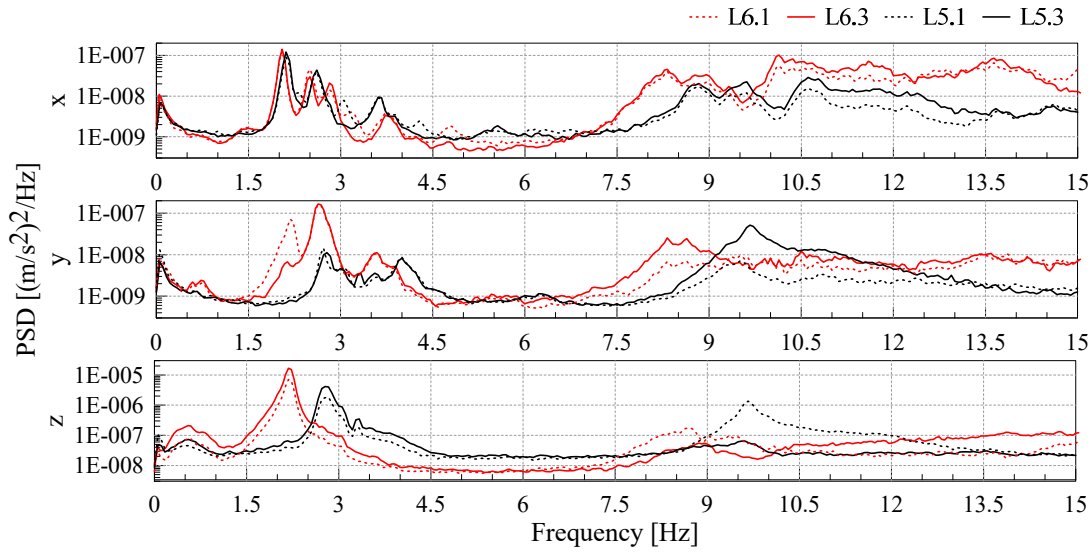


Figure 6.12: Comparison between PSD curves of some sensors installed on span L5 and L6 - axes x, y, z

Furthermore, Figure 6.12 illustrates the comparison between the Power Spectral Density (PSD) obtained for two sensors located at mid span and at bearings respectively, for spans L5 and L6.

Looking at the graph, it is evident the difference between frequency values of span L6 and those of span L5, representative of all the remaining spans of the structure. Indeed, natural frequency peaks of span L6 are significantly shifted to the left with respect to the nearby span L5. The significantly lower frequency values are symptomatic of the reduced deck stiffness due to the detected state of damage of span L6. In particular, it is possible to observe that frequencies of modes 2, 3, 4, 5 were significantly lower than those belonging to all the remaining spans, while the frequency linked to mode 1 did not show any particular difference when compared with the other spans. This evidence could be related to the nature of the damage identified in span L6. In fact, the partial loss of prestressing in the deck due to the tendon corrosion (has described in paragraph 6.2), may have generated a bending stiffness reduction in the damaged span. This means that all the flexural or flexural-torsional vibrational modes (modes from 2 to 5) were affected by the damage in a consistent way, with the associated natural frequencies reduction of about 0.4 - 0.8 Hz. The mode at frequency of 2.01 Hz instead, being connected to the out of plane stiffness of the structure, was not affected by the damage and therefore there were no obvious variations in stiffness compared to the other spans.

6.6 Monitoring Results

6.6.1 Statistical Analysis of Dynamic Signals

The acceleration time series coming from the dynamic monitoring system installed on the pre-stressed concrete bridge, sampled at 100 Hz, were statistically analyzed in order to identify similar trends and behaviors between the 18 spans of the bridge.

One of the first observations that can be made beforehand is that the dynamic input on the structure is extremely variable, depending on the traffic. Indeed, the accelerations measured during the day, with intensive traffic levels, are considerably higher than those measured during the night, with limited traffic. Figure 6.13 illustrates two examples of acceleration time series recorded during the night (a) and during the day (b).

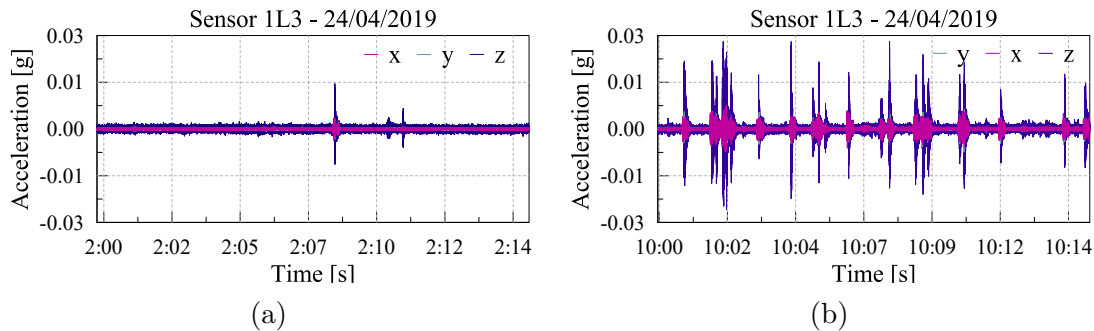


Figure 6.13: Acceleration time series collected from one sensor (a) during the night, (b) during the day.

Furthermore, a noticeable difference can also be observed by comparing vibrational levels recorded during the week and over the weekend. Standard deviation has been considered as a good indicator of the average vibration activity induced by traffic loads, wind and/or other external agents under standard or exceptional conditions. Figure 6.14 shows a comparison between the probability distribution of standard deviation values collected by sensor L1.3, chosen as an example, along the z axis during day and night hours for a weekly day (a) and during the weekend (b).

As it can be seen from Figure 6.14, there is a significant difference between the STD values recorded during the day and during night for a weekly day. Indeed, the maximum vibration levels are mainly recorded during the day hours with an appreciable decrease at night. On the other hand, this difference is not so marked during the weekend, where the vibrational levels between day and night are closer and lower if compared with those recorded during the weekly day, indicating reduced traffic levels.

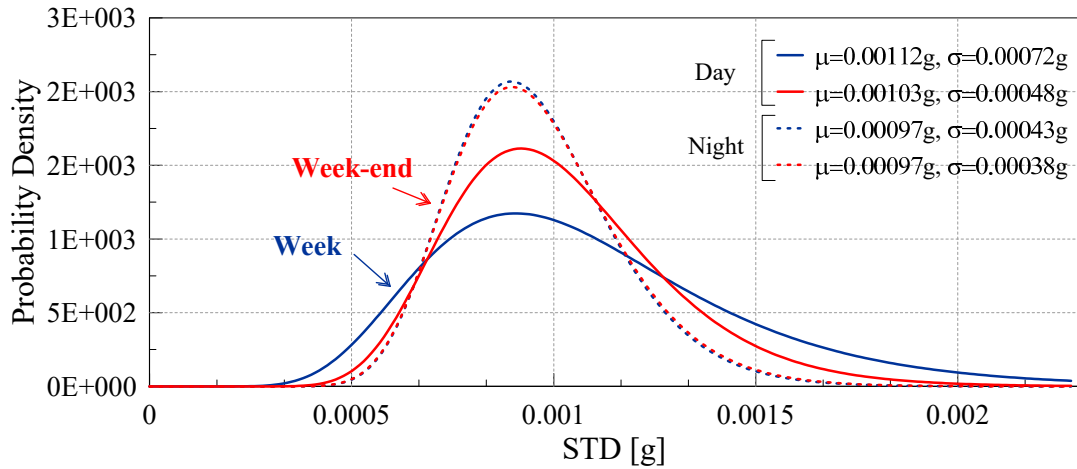


Figure 6.14: PDF of STD values collected along z axis during day and night hours - week and week-end

Another significant observation can be made with respect to the vibrational levels recorded along the 3 measurement axes x, y, z. More in detail, the potential difference between the 3 measurement axes needs to be addressed considering the position in which sensors are installed (corresponding to the different points of the deck). In particular, the acceleration recorded in the middle of the span and at supports, in the 3 measurement axes, would be different according to the dynamic modes. Figure 6.15 shows a comparison between the probability distribution of STD values collected from 01/06/2019 to 20/06/2019 for the 3 measurement directions x, y and z for both a sensor placed in the middle of the span (sensor L1.3) and a sensor installed at supports (sensor L1.1).

Figure 6.15 illustrates a significant difference between the 3 measurement axes. In particular, the probability distribution calculated for the z-axis shows a significantly higher mean and standard deviation value than the x and y axes for both sensors. Furthermore, it can be observed that the x-axis has a higher mean value than the y-axis, indicating a higher vibration amplitude. Moreover, no major differences can be detected between the two sensors of the structure.

This observations can be justified, with reference to natural frequencies and modal shapes identified in paragraph 6.5, through the following considerations. The lower modes of the bridge excited by traffic involve all 3 measurement directions, in a frequency range from 2 to 3.5 Hz (for all the spans of the structure). However, looking at Power Spectral Density (PSD) plot shown in Figure 6.12, it can be observed that most of the power is in the vicinity of the first eigenfrequency identified along z-axis, associated with the first flexional mode which involves, predominantly, the flexural stiffness (along z) of the structure. This means that the

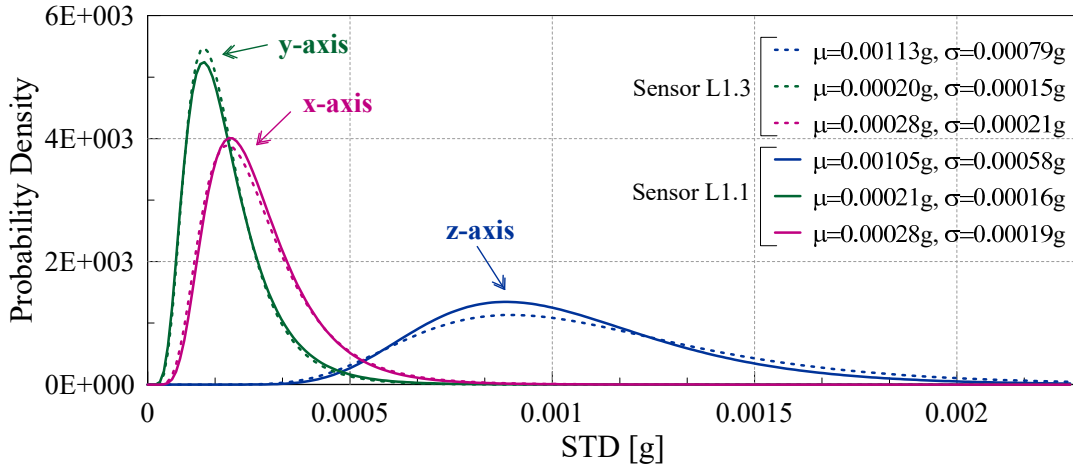


Figure 6.15: PDF of STD values collected from 01/06/2019 to 20/06/2019 - sensors L1.1 and L1.3; axes x, y, z

first mode along z-axis is the most excited one; thus, it makes sense that acceleration values recorded along z-axis are greater than those recorded by x and y axes. Similar considerations can be done by comparing x and y directions.

A very interesting comparison has been also made among all the spans of the structure, in terms of vibrational levels. Indeed, all the spans of the bridge have the same length and the same geometric characteristics. This means that, with the same input, the behavior of all spans should be about the same. However, some differences have been observed by comparing the undamaged spans with the damaged one (L6), before carrying out the reinforcement works.

In particular, the standard deviation values (STD) of the acceleration time series, collected along the z direction and calculated once per second, have been obtained for the time period between 01/04/2019 and 30/04/2019, that is before the strengthening intervention. Figure 6.16 and Figure 6.17 show a comparison between STD values obtained for all the spans of the left side of the bridge, so as to have the same input (traffic), for both sensors located in the center of the span and at supports.

Figure 6.16 shows a boxplot displaying the distribution of data based on the minimum, first quartile (Q1), median, third quartile (Q3), and maximum values. As can be seen, the minimum, first quartile, median and third quartile values are approximately comparable for all spans and for all sensors (installed both in the middle of the spans or at supports). However, with reference to maximum values, a difference between sensors installed on the L6 span and those installed on the remaining spans can be identified. Indeed, the same consideration can be made by observing Figure 6.17, in which span L6 shows STD values under traffic definitely higher than the other spans.

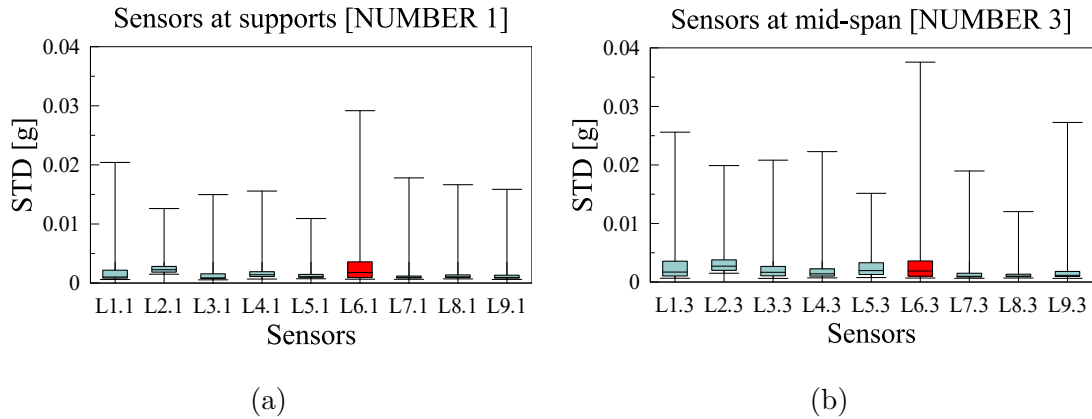


Figure 6.16: Boxplot of STD values along the z direction between 01/04/2019 and 30/04/2019; (a) sensors located at supports; (b) sensors located at mid-span

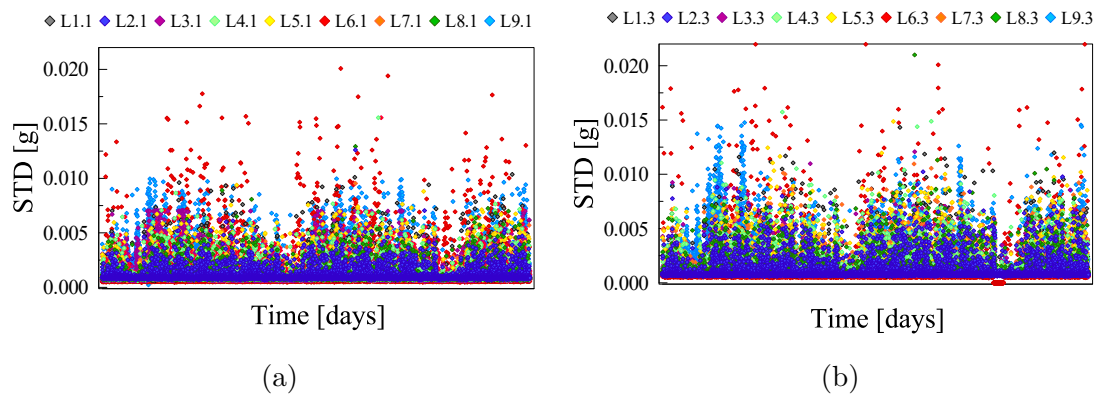


Figure 6.17: STD values along the z direction between 13/04/2019 and 25/04/2019; (a) sensors located at supports; (b) sensors located at mid-span

With reference to natural frequency values reported in Table 6.3, it is possible to correlate the higher vibrational levels to the lower bending stiffness of this span due to its state of damage. This could lead to the conclusion that larger acceleration amplitudes correspond to lower stiffness values.

6.6.2 Monitoring during the strengthening works

This paragraph summarizes the main results obtained during and after the reinforcement installation. More in detail, the proposed methodology has been applied for detecting the strengthening works and for comparing the bridge behavior before and after the installation of the external pre-stressing tendons.

As described in chapter 4, the proposed methodology allows the automatic identification of changes in the structural behavior, both in terms of natural frequencies and vibration response, using 3 levels of alert, defined through specific threshold values which are implemented for all the monitored structures respectively within the sensor node, the gateway and the cloud environment. Changes within the dynamic characteristics of structures are detected, for each alarm level, with respect to the standard behavior, that is, with respect to a behavior considered "normal", which corresponds to the installation of the monitoring system. Therefore, if the structure changes its behavior with respect to this standard condition, an alert signal is generated. This means that, even if the reinforcement works caused an increase in the stiffness of the structure, the behavior of the bridge after the intervention would be different than before; therefore, this case study has been effectively used to verify the effectiveness of the proposed methodology in identifying changes in structural properties.

The strengthening works took place on May 9th, 2019 and were entirely recorded by the accelerometers installed on the structure. During the restoration works the highway was open to traffic in both directions.

All sensors installed in span L6 recorded a strong impulse when tendons were tensioned, causing the first alert level to be exceeded.

Following the first level alert, the second and third alert levels were automatically activated by the monitoring system on the IoT gateway and cloud for all the sensors that exceeded the first threshold check. As a result, both the second and third threshold levels were exceeded for the selected span, indicating a possible variation of the modal parameters (stiffness) of the structure.

As regard the second level of alert (autoencoder check), activated by the IoT gateway following the first level alarm, it is possible to notice a remarkable increase in reconstruction error values for all sensors installed on span L6, following the reinforcement works.

More specifically, with reference to Figure 6.18 in which the trend of reconstruction error is shown for sensor L6.3 from April 21, 2019 to May 18, 2019, it is possible to observe that the reconstruction error assumes almost constant values around 1.05% from the beginning of the monitoring period until 09/05/2019. On 09/05/2019, when the reinforcement works took place, a sudden increase in the reconstruction error has been detected, passing from an average value of 1.05%, to values of around 1.22%, thus exceeding the preset threshold value equal to 0.1% of the reconstruction error mean value, indicating a variation in the dynamic behavior of the structure. As aforementioned, the second level of alert takes advantage of an unsupervised machine learning algorithm to detect changes in structural behavior which is characterized by several variables. The reconstruction error is thus used to measure how well the decoder is performing.

The underlined variation in reconstruction error mean value indicated that the autoencoder was no longer able to reconstruct the vibration signal with the same

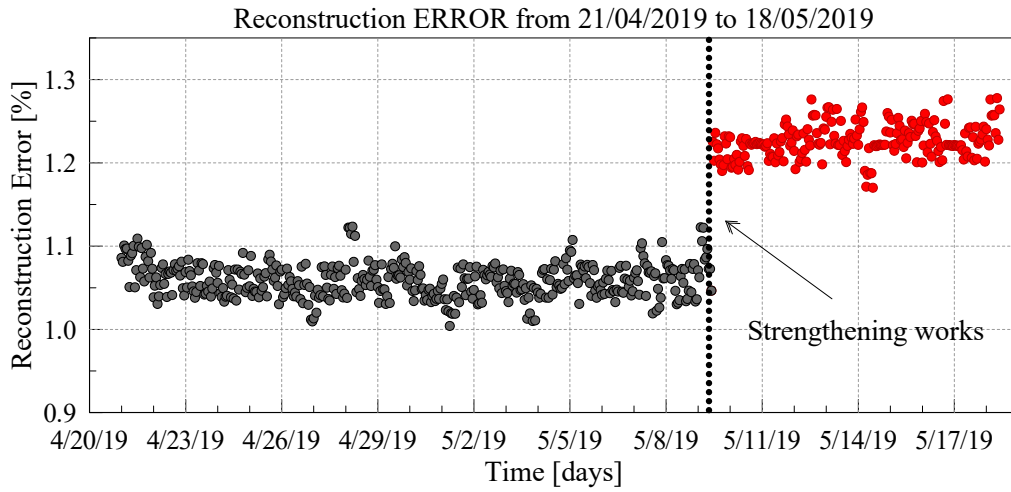


Figure 6.18: Reconstruction Error at the anomalous event - sensor L6.3

accuracy as before due to a change in the intrinsic characteristics of structural elements, which affects the dynamic characteristics of the signal collected by sensors.

On the other hand, the third level threshold was also exceeded. More in detail, a sudden increase in frequency values was detected in correspondence of the strengthening works, indicating a stiffening of the structure. In Figure 6.19, the trend of the resonant frequency, corresponding to the first four modes listed in Table 6.3, is reported over time.

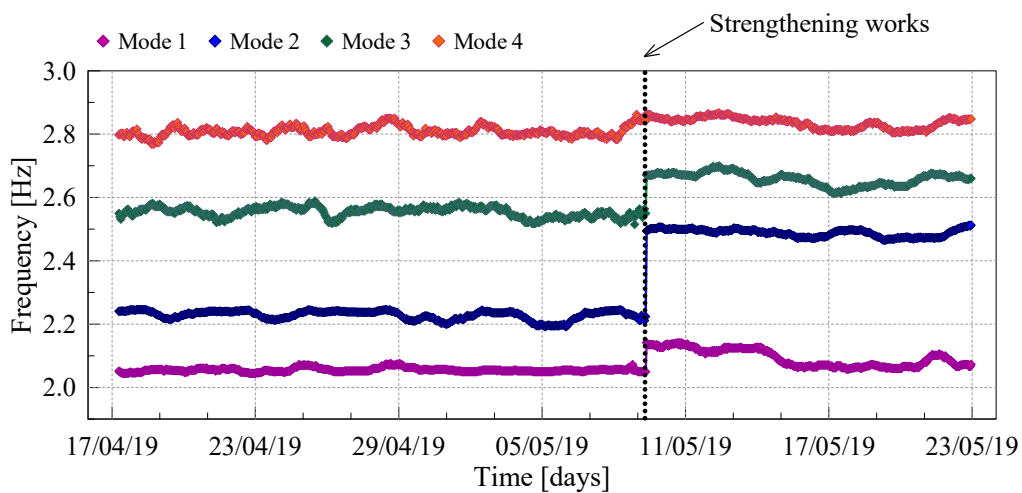


Figure 6.19: Frequency evolution over time at the reinforcement works

As can be observed from the graph, the reinforced span showed a significant shift

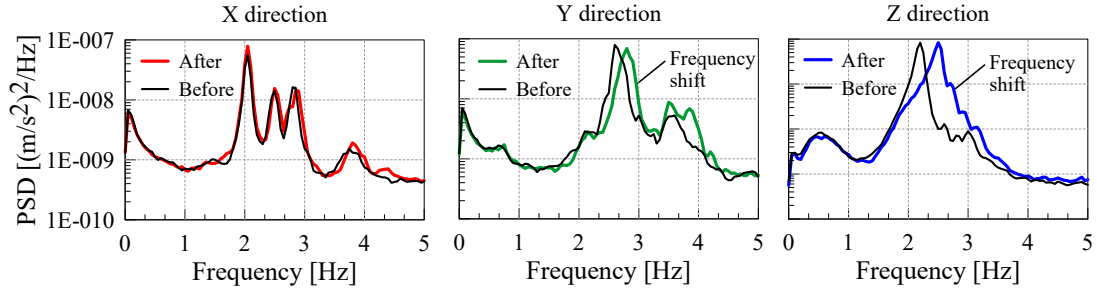


Figure 6.20: PSD calculated for the 3 measurement directions (x, y, z) before and after the strengthening works

in the frequency of the first bending mode (mode 2) of about $0.25 Hz$, indicating a stiffening of the structure. This variation is evident also by looking at the other frequencies, even if of a lesser extent. Moreover, the same phenomenon is clearly identifiable by analyzing the signal spectra. Indeed, since the signals are of random nature, the power spectral density (PSD) can be used to evaluate the system natural frequencies in a first stage. The choice of using PSD spectrum comes from the need of analysing the effect of the strengthening works along the 3 orthogonal directions (x, y z), in order to highlight the different stiffening contribution provided by the intervention. The averaging process has been carried out with a sub-records with a length of 200 s and overlap of 66% (Hanning window). The peaks of the PSD correspond to the natural frequencies of the structure under examination.

Figure 6.20 shows the PSDs calculated for the sensor located at mid span in the three directions x, y, z before and after the strengthening works (May 8th, 2019 and May 10th, 2019). It can be observed that the reinforcement caused a shift to the right of the natural frequencies of the span, meaning that a stiffening of the system occurred. It is noteworthy that this translation is more evident in the y and z directions, while in the x direction, transversal to the longitudinal extension of the viaduct, this variation is hardly recognized. This is consistent with the observation that external pre-stressing causes a flexural stiffening of the structure mainly in the y-z plane, with minor effect in the x-y plane.

Following the identification of the reinforcement works consequences on the structure using the methodology proposed in this thesis, a series of additional analyses were also carried out in order to evaluate the effect of externally mounted post-tensioned bars on the selected span.

Specifically, acceleration time series were averaged through a moving average smoothing procedure, in which each element of the series has been replaced by the average of n surrounding elements, where n is the width of the smoothing window. The average of the acceleration signal has been used for calculating the angular tilt along two orthogonal axes, x and y . Indeed, 3-axis accelerometers may also be

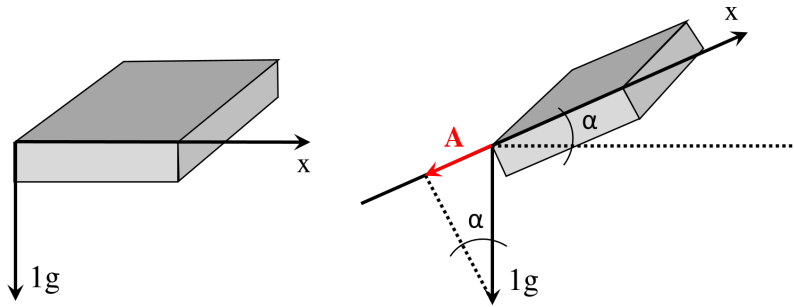


Figure 6.21: Tilt measurements using a single axis of the accelerometer

used for angular tilt calculation [43].

With reference to Figure 6.21, MEMS accelerometers measure, in static conditions, the projection of the gravity vector on the sensing axis. The amplitude of the sensed acceleration changes according to the sine of the angle α between the sensing axis and the horizontal plane:

$$A = g \cdot \sin(\alpha) \quad (6.1)$$

This means that, using equation 6.1, it is possible to estimate the tilt angle as:

$$\alpha = \arcsin\left(\frac{A}{g}\right) \quad (6.2)$$

where A is the measured acceleration and g is the Earth's gravity vector.

However, tilt is a static quantity; thus, it is necessary to average acceleration time series recorded by sensors installed on the structure (and subject to traffic input), on windows of at least 1 second, to obtain the equivalent static reading. Since sensors are most responsive to changes in tilt angle when the sensing axis is perpendicular to the force of gravity, only x and y axes have been considered.

As it can be observed from Figure 6.22, the averaged acceleration data along y axis highlighted an instantaneous shift in the tilt values when the external force was transferred to the bridge members. The shift is particularly evident for the two sensors located near the span ends and less visible from the sensor positioned at mid span, as expected. However, this result is very interesting especially with regards to sensor L6.3.

Indeed, pre-stressed concrete bridges are assumed to have an elastic structural behaviour during normal operating conditions. As a consequence, the middle point

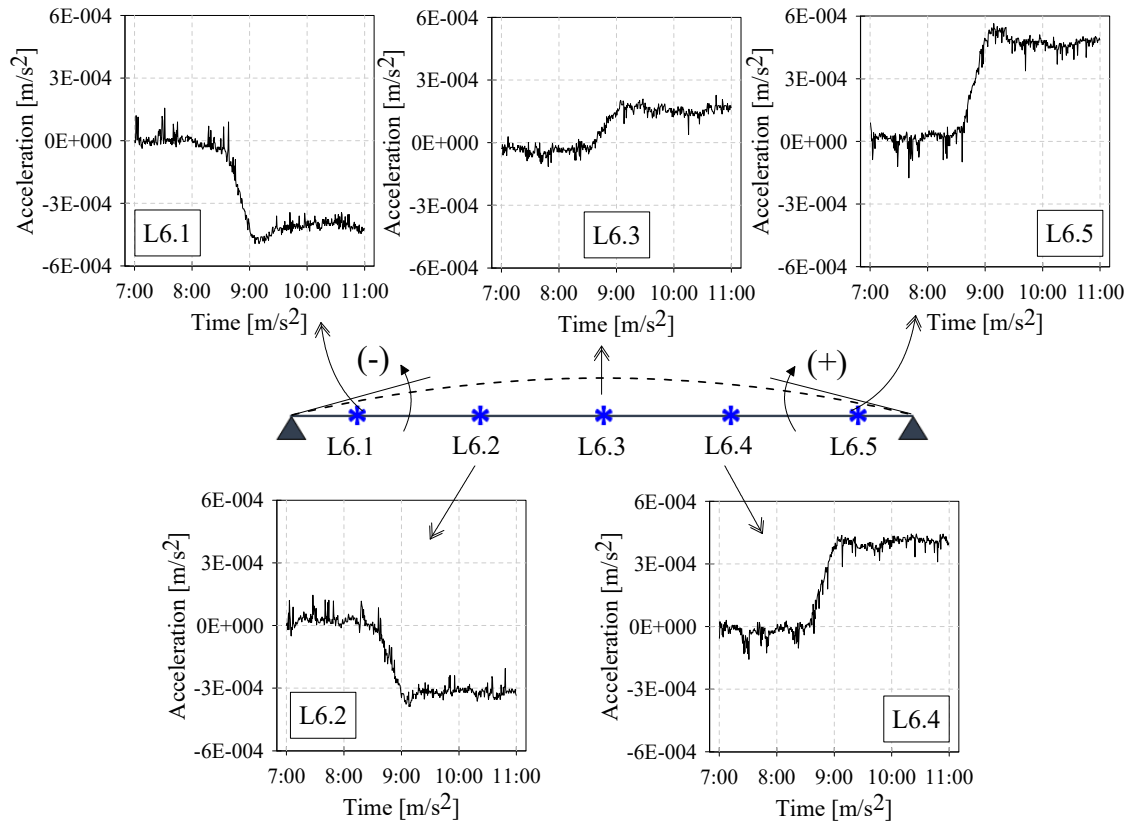


Figure 6.22: Averaged acceleration data along y axis at the strengthening works

of a simply supported span bridge should always show a null tilt value. However, as can be seen from Figure 6.22, L6.3 sensor showed a detectable variation in its average value, indicating an initial non-zero rotation value. This means that, before the reinforcement was installed, a residual deformation under heavy traffic combined with deterioration was recognizable in the analyzed span, confirming the damage scenario detected during the inspections.

In addition, always referring to Figure 6.22, it is possible to observe that the tilt variation due to the strengthening works occurred in the opposite direction with respect to the bridge deformation under traffic loads, indicating that the external pre-stressing has caused a counter-balance in the bridge. Starting from data recorded before and after the reinforcement intervention, it was thus possible calculating the deformation experienced by the bridge under the pre-stressing intervention.

Figure 6.23 shows the bridge deformation, in terms of vertical displacements, experienced by the structure following the strengthening works. The black dotted curve was calculated by linear interpolation of the tilt values obtained averaging acceleration time series in the y direction, after removing the value measured before

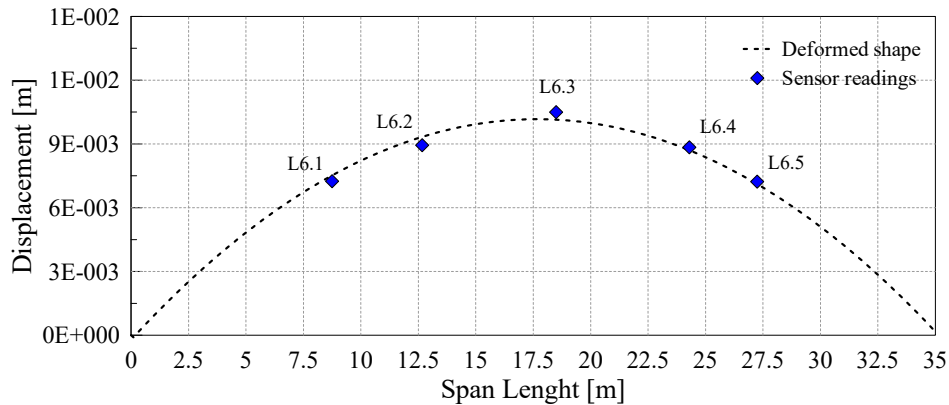


Figure 6.23: Deformed shape of the L6 span after the reinforcement works

the intervention. As can be seen from the graph, following the reinforcement works, the structure experienced a camber of about 1 cm at the centreline of the span, indicating a recovery of the residual deformation.

This means that, before the reinforcement works were carried out, the structure had accumulated a plastic deformation under dead weight as a result of the experimented damage, which was partially recovered following the installation of the additional external pre-stressing tendons.

The results obtained through these further analysis confirmed the considerable variation of the intrinsic characteristics of the structure following the installation of the additional pre-stressed external tendons.

The results produced by the dynamic monitoring system have proved to be reliable and robust as it was possible to automatically detect changes in the stiffness of the structure after the reinforcement intervention.

6.7 Final Remarks

This chapter describes the application of the proposed methodology for identifying changes in the dynamic behavior of a prestressed concrete bridge, following some strengthening works. The analyzed structure is located in northern Italy and has been continuously monitored through a dynamic monitoring system since March 2019, being still monitored. The relevance of this case study lies in the reinforcement works carried out in May 2019, following the identification of a damaged scenario in one of the bridge spans. In order to track the behavior of the structural elements during and after the strengthening works, triaxial accelerometers were installed on all the bridge spans.

The chapter started with the description of the highway bridge and the dynamic

monitoring system installed on it, for the continuous and automated monitoring of the dynamic characteristics of the structure. Subsequently, the inspection campaign carried out in March 2019 is described in detail, highlighting the serious structural deficiencies that have been identified in the sixth span of the left roadway of the bridge.

Afterwards, some preliminary analyses were carried out in order to evaluate the standard behaviour of the structure at the installation of the monitoring system. These preliminary analysis were essential for understanding the state of the structure when the sensors were installed. In particular, at first, the identification of natural frequencies and the corresponding mode shapes has been carried out for all the spans of the bridge. Then, statistical analysis were performed on the time series collected by sensors during the monitoring period. Results from the preliminary analysis highlighted the significant difference between the damaged span and the remaining spans of the bridge both in vibrational and in modal terms. Indeed, natural frequency values associated with the damaged span proved to be considerably lower than the undamaged spans, confirming the hypothesized reduced deck stiffness. At the same time, vibration levels were also obtained for the entire bridge, revealing a marked difference between damaged and healthy spans, being vibration levels for the damaged span significantly higher than the standard behavior.

Subsequently, the main results obtained during the monitoring period were presented. The analysis focused mainly on the reinforcement intervention carried out in May 2019 and entirely recorded by the sensors. This event was extremely relevant as it allowed to verify the effectiveness and robustness of the proposed methodology on a real scenario in which variation of the dynamic characteristics of the structure occurred.

In particular, during the strengthening works, the first level threshold was exceeded by all the sensors installed in the damaged span of the bridge, due to the strong impulse recorded when external tendons were tensioned. Following the first level alert, the second and third checks were automatically activated by the monitoring system and, as a result of the these deeper analysis, both the second and third threshold were exceeded by a group of sensors, indicating a possible structural damage. As a consequence, an alarm message, together with a phone call, was automatically generated.

In conclusion, the reinforcement intervention on one of the spans of the monitored bridge, which showed significant damage evidences, have permitted to prove that the developed and implemented methodology for the automatic and continuous identification of modal parameters make possible a very detailed characterization of the structural intrinsic characteristics over time. Indeed, changes of the modal parameters of the bridge were effectively detected by the system, following the

strengthening works, which caused the stiffening of the structure.

This case study was very important to demonstrate that the proposed methodology for the effective and automatic monitoring of infrastructures presented in this dissertation is really reliable and, at the same time, flexible enough to be used on diverse civil engineering structures.

A very important aspect is that the data coming from the structure in damaged conditions have been observed and this represents a very rare case in the field of SHM of real operating civil structures. Therefore, knowing the outputs of the analyzes obtained when the structure was in a state of advanced and widespread deterioration, the use of supervised learning techniques can be adopted allowing to have indications on the progress of pre-stressing loss for future SHM purposes.

Chapter 7

Conclusion

This chapter is intended to provide a cohesive summary of the main contributions achieved in this work as well as a discussion on possible future research developments.

7.1 Main Outcomes

The present dissertation illustrates the main outcomes and advantages obtained regarding the Structural Health Monitoring of civil engineering infrastructures. In particular, two main topics have been addressed and discussed:

- development and implementation of a generalized methodology to be applied for the structural health monitoring of many structures equipped with many sensors, which allows identifying any evolving damage in their initial stage;
- management of Big Data generated continuously by a large number of devices installed on a large number of structures, using big data analytics for structural diagnosis as well as for data storage and accessibility.

This thesis comprehends an overview of the state of the art related to structural health monitoring methods and application. Particular attention was paid to long-term and automatic monitoring systems, in order to highlight the shortcomings of the literature and outline the area in which the present research fits.

Subsequently, a detailed description of the theoretical background behind some of the main operational modal analysis methods, used for the dynamic identification of civil engineering structures, has been reported. Four methods have been selected and assessed with numerical simulations, in order to choose the method that is better suited to be integrated inside the framework for the real-time and automatic monitoring of full-scale bridge structures, under operating conditions.

The developed and proposed methodology for the continuous and long-term monitoring was therefore detailed. The main goal of the proposed methodology

was to provide a complete data-driven method, able to automatically generate system health indicators without any specific analysis on the monitored structure. In this way, it is possible to apply the developed framework on a large number of structures, always having control of each of them without the need of analyzing structures individually.

The accuracy and reliability of the implemented methodology was evaluated through two significant case studies, where variations in the stiffness of the structural elements were recorded in the monitored period.

In light of this, the developed research permitted to achieve the following main results and conclusions, which are synthesized in the following list.

1. development, implementation and validation of a new methodology for continuous and long-term monitoring of a network of structures, equipped with a large number of sensors, which allows to efficiently obtain reliable system health indicators, used for carrying out a preventive diagnostics of any progressive damage on structural elements. More in detail, the proposed methodology includes the following main outcomes:
 - development, implementation and testing of a data acquisition and storage procedure, in order to efficiently collect data from sensors by discarding those deemed to be lacking in information and therefore limiting the amount of data stored and analyzed.
 - development and implementation of a strategy to efficiently elaborate a large amount of data (big data) in the shortest possible time fully exploiting the resources of the cloud platform;
 - conception and development of a multilevel damage detection procedure, aimed at providing an early-stage alert of anomalous conditions that should trigger more detailed analysis or, if necessary, in situ inspections. In particular, the proposed methodology is based on different levels of alarm (three levels), fully exploiting the potentiality of the monitoring system, where the interaction between different sites of computational capability has been used to produce a reliable alert in case of damage.
 - effective management of Big Data generated continuously by a large number of sensors installed on a large number of structures, ensuring a high level of data quality and accessibility for the assessment of the health status of a system.
2. application of the proposed methodology for the long-term real-time monitoring of a significant number of structures (about 15 bridges) currently in operation;
3. automatic and real-time identification of damages occurred on a box composite highway bridge, strengthened by both internal and external prestressing,

where all the features of the proposed methodology were applied and permitted to prove the effectiveness, feasibility and reliability of the adopted techniques, being able to detect real damages occurred during the monitoring period;

4. automatic and real-time identification of stiffness variation occurred on a prestressed concrete bridge from the early 1965s, where real changes in structural stiffness were identified through a dynamic monitoring system in which the proposed methodology has been adopted.

The illustrated case studies proved that the proposed automated methodology was able to provide a very detailed characterization of the time evolution of the dynamic characteristics of the structures. Thus, this was an important result to demonstrate that the proposed methodology is flexible to be used and generalized for a large variety of civil engineering structures, being at the same time very reliable and effective.

Bibliography

- [1] fib (International Federation for Structural Concrete). *Durability of post-tensioning tendons*. 2001.
- [2] MA-B Abdo and Muneo Hori. “A numerical study of structural damage detection using changes in the rotation of mode shapes”. In: *Journal of Sound and vibration* 251.2 (2002), pp. 227–239.
- [3] RD Adams et al. “A vibration technique for non-destructively assessing the integrity of structures”. In: *Journal of Mechanical Engineering Science* 20.2 (1978), pp. 93–100.
- [4] Randall J Allemang. “The modal assurance criterion—twenty years of use and abuse”. In: *Sound and vibration* 37.8 (2003), pp. 14–23.
- [5] Randall J Allemang and David L Brown. “A correlation coefficient for modal vector analysis”. In: *Proceedings of the 1st international modal analysis conference*. Vol. 1. SEM Orlando. 1982, pp. 110–116.
- [6] Simonetta Baraccani et al. “Structural Interpretation of Data from Static and Dynamic Structural Health Monitoring of Monumental Buildings”. In: *Key Engineering Materials*. Vol. 747. Trans Tech Publ. 2017, pp. 431–439.
- [7] Chiara Bedon et al. “Prototyping and validation of MEMS accelerometers for structural health monitoring—The case study of the Pietratagliata cable-stayed bridge”. In: *Journal of Sensor and Actuator Networks* 7.3 (2018), p. 30.
- [8] Gabriele Bertagnoli et al. “A Large Scale SHM System: A Case Study on Prestressed Bridge and Cloud Architecture”. In: *Dynamics of Civil Structures, Volume 2*. Springer, 2020, pp. 75–83.
- [9] Luca Bertolini. “Steel corrosion and service life of reinforced concrete structures”. In: *Structure and Infrastructure Engineering* 4.2 (2008), pp. 123–137.
- [10] Rune Brincker, Lingmi Zhang, and P Andersen. “Modal identification from ambient responses using frequency domain decomposition”. In: *Proc. of the 18th International Modal Analysis Conference (IMAC), San Antonio, Texas*. 2000.

- [11] Alessandro Cabboi et al. “Automated modal identification and tracking: Application to an iron arch bridge”. In: *Structural Control and Health Monitoring* 24.1 (2017), e1854.
- [12] E Peter Carden and Paul Fanning. “Vibration based condition monitoring: a review”. In: *Structural health monitoring* 3.4 (2004), pp. 355–377.
- [13] Elisa Khouri Chalouhi et al. “Damage detection in railway bridges using machine learning: Application to a historic structure”. In: *Procedia engineering* 199 (2017), pp. 1931–1936.
- [14] Franck Chollet and Haobing Liu. “A (not so) short introduction to Micro Electro Mechanical Systems”. In: *Creative Commons Publisher, version 5* (2012).
- [15] Anil K Chopra. *Dynamics of structures: theory and applications to earthquake engineering*. Prentice Hall, 1995.
- [16] Alfredo Cigada et al. “Mechanical performance and metrological characterization of MEMS accelerometers and application in modal analysis”. In: *Proceedings of the IMAC XXV International Modal Analysis Conference, Orlando, FL, USA*. 2007, pp. 19–22.
- [17] Alfredo Cigada et al. “Vibration testing at Meazza stadium: reliability of operational modal analysis to health monitoring purposes”. In: *Journal of performance of constructed facilities* 22.4 (2008), pp. 228–237.
- [18] Ralph Albert Collacott. *Structural integrity monitoring*. Springer Science & Business Media, 1985.
- [19] A Cunha et al. “Vibration-based SHM of a centenary bridge: a comparative study between two different automated OMA techniques”. In: *preservation* 1 (2011), p. 12.
- [20] AF Daly and W Witarnawan. “Strengthening of bridges using external post-tensioning”. In: *Conference of eastern Asia society for transportation studies (October 1997), Seoul, Korea*. Citeseer. 1997.
- [21] John T DeWolf et al. “Bridge monitoring network-Installation and operation”. In: *Connecticut Department of Transportation, Report No. CT-2217-F-06-10* (2006).
- [22] Scott W Doebling et al. *Damage identification and health monitoring of structural and mechanical systems from changes in their vibration characteristics: a literature review*. Tech. rep. Los Alamos National Lab., NM (United States), 1996.
- [23] David J Ewins. *Modal testing: theory and practice*. Vol. 15. Research studies press Letchworth, 1984.
- [24] David J Ewins and H Saunders. *Modal testing: theory and practice*. 1986.

- [25] Wei Fan and Pizhong Qiao. “Vibration-based damage identification methods: a review and comparative study”. In: *Structural health monitoring* 10.1 (2011), pp. 83–111.
- [26] Charles R Farrar and Keith Worden. “An introduction to structural health monitoring”. In: *Philosophical Transactions of the Royal Society A: Mathematical, Physical and Engineering Sciences* 365.1851 (2006), pp. 303–315.
- [27] Charles R Farrar and Keith Worden. *Structural Health Monitoring.: A Machine Learning Perspective*. John Wiley & Sons, 2012.
- [28] Charles R Farrar et al. *Dynamic characterization and damage detection in the I-40 bridge over the Rio Grande*. Tech. rep. Los Alamos National Lab., NM (United States), 1994.
- [29] CR Farrar and GH James III. “System identification from ambient vibration measurements on a bridge”. In: *Journal of sound and vibration* 205.1 (1997), pp. 1–18.
- [30] Gene F Franklin, J David Powell, Michael L Workman, et al. *Digital control of dynamic systems*. Vol. 3. Addison-wesley Menlo Park, CA, 1998.
- [31] Svend Gade et al. “Frequency domain techniques for operational modal analysis”. In: *1st IOMAC Conference*. 2005.
- [32] Branko Glisic and Daniele Inaudi. *Fibre optic methods for structural health monitoring*. John Wiley & Sons, 2008.
- [33] Luc Hermans and Herman Van der Auweraer. “Modal testing and analysis of structures under operational conditions: industrial applications”. In: *Mechanical systems and signal processing* 13.2 (1999), pp. 193–216.
- [34] Wei-Hua Hu et al. “Analysis and extraction of temperature effect on natural frequencies of a footbridge based on continuous dynamic monitoring”. In: *Proceedings of the 3rd International Operational Modal Analysis Conference. Portonovo, Italy*. 2009, pp. 55–62.
- [35] Wei-Hua Hu et al. “Comparison of different statistical approaches for removing environmental/operational effects for massive data continuously collected from footbridges”. In: *Structural Control and Health Monitoring* 24.8 (2017), e1955.
- [36] Ian Jolliffe. *Principal component analysis*. Springer, 2011.
- [37] JM Ko and YQ Ni. “Technology developments in structural health monitoring of large-scale bridges”. In: *Engineering structures* 27.12 (2005), pp. 1715–1725.
- [38] C Krämer, CAM De Smet, and Guido De Roeck. “Z24 bridge damage detection tests”. In: *IMAC 17, the International Modal Analysis Conference*. Vol. 3727. Society of Photo-optical Instrumentation Engineers. 1999, pp. 1023–1029.

- [39] Jyrki Kullaa. “Damage detection of the Z24 bridge using control charts”. In: *Mechanical Systems and Signal Processing* 17.1 (2003), pp. 163–170.
- [40] Irwanda Laory, Prakash Kripakaran, and Ian FC Smith. “Structural identification through continuous monitoring: data cleansing using temperature variations”. In: *Proceedings of the International Conference on Computing in Civil and Building Engineering*. CONF. University of Nottingham Press. 2010, p. 447.
- [41] NAJ Lieven and DJ Ewins. “Spatial correlation of mode shapes, the coordinate modal assurance criterion (COMAC)”. In: *Proceedings of the sixth international modal analysis conference*. Vol. 1. 1988, pp. 690–695.
- [42] MP Limongelli. “Frequency response function interpolation for damage detection under changing environment”. In: *Mechanical Systems and Signal Processing* 24.8 (2010), pp. 2898–2913.
- [43] Sergiusz Luczak, Waldemar Oleksiuk, and Maciej Bodnicki. “Sensing tilt with MEMS accelerometers”. In: *IEEE Sensors Journal* 6.6 (2006), pp. 1669–1675.
- [44] Jerome P Lynch et al. “Performance monitoring of the Geumdang Bridge using a dense network of high-resolution wireless sensors”. In: *Smart Materials and Structures* 15.6 (2006), p. 1561.
- [45] Johan Maeck, Bart Peeters, and Guido De Roeck. “Damage identification on the Z24 bridge using vibration monitoring”. In: *Smart materials and structures* 10.3 (2001), p. 512.
- [46] Filipe Magalhães, A Cunha, and Elsa Caetano. “Vibration based structural health monitoring of an arch bridge: from automated OMA to damage detection”. In: *Mechanical Systems and Signal Processing* 28 (2012), pp. 212–228.
- [47] Gabriele Marrongelli, Filipe Magalhães, and Álvaro Cunha. “Automated Operational Modal Analysis of an arch bridge considering the influence of the parametric methods inputs”. In: *Procedia engineering* 199 (2017), pp. 2172–2177.
- [48] Nuno Martins et al. “Dynamic monitoring of a stadium suspension roof: Wind and temperature influence on modal parameters and structural response”. In: *Engineering Structures* 59 (2014), pp. 80–94.
- [49] EC Mikulcik and SR Ibrahim. “A method for the direct identification of vibration parameters from the free responses”. In: *Journal of Sound and Vibration* 113.1 (1987), pp. 47–57.
- [50] Mark Moore et al. *Reliability of visual inspection for highway bridges, volume I*. Tech. rep. 2001.

- [51] AK Pandey, M Biswas, and MM Samman. “Damage detection from changes in curvature mode shapes”. In: *Journal of sound and vibration* 145.2 (1991), pp. 321–332.
- [52] Bart Peeters and Guido De Roeck. “One-year monitoring of the Z24-Bridge: environmental effects versus damage events”. In: *Earthquake engineering & structural dynamics* 30.2 (2001), pp. 149–171.
- [53] Bart Peeters et al. “The PolyMAX frequency-domain method: a new standard for modal parameter estimation?” In: *Shock and Vibration* 11.3, 4 (2004), pp. 395–409.
- [54] Brent M Phares et al. “Routine highway bridge inspection condition documentation accuracy and reliability”. In: *Journal of Bridge Engineering* 9.4 (2004), pp. 403–413.
- [55] M Pozzi et al. “MEMS-based sensors for post-earthquake damage assessment”. In: *Journal of Physics: Conference Series*. Vol. 305. 1. IOP Publishing. 2011, p. 012100.
- [56] Giuseppe Quaranta, Walter Lacarbonara, and Sami F Masri. “A review on computational intelligence for identification of nonlinear dynamical systems”. In: *Nonlinear Dynamics* (2020), pp. 1–53.
- [57] Carlo Rainieri and Giovanni Fabbrocino. “Operational modal analysis of civil engineering structures”. In: *Springer, New York* 142 (2014), p. 143.
- [58] RENAN ROCHA RIBEIRO and RODRIGO LAMEIRAS. “AN EVALUATION OF LOW-COST MEMS ACCELEROMETERS FOR SHM: FREQUENCY AND DAMPING IDENTIFICATION OF CIVIL STRUCTURES”. In: (2019).
- [59] M Richardson. *Detection of damage in structures from changes in their dynamic (modal) properties-a survey*. Tech. rep. 1980.
- [60] Mark Richardson and Ron Potter. “Identification of the modal properties of an elastic structure from measured transfer function data”. In: *Proceedings of the 20th International Instrumentation Symposium*. 1974, pp. 1–9.
- [61] OS Salawu. “Detection of structural damage through changes in frequency: a review”. In: *Engineering structures* 19.9 (1997), pp. 718–723.
- [62] CSI SAP2000. “Computers and structures Inc”. In: *Berkeley, CA, USA* (2013).
- [63] Hoon Sohn et al. “A review of structural health monitoring literature: 1996–2001”. In: *Los Alamos National Laboratory, USA* (2003).
- [64] Serdar Soyoz and Maria Q Feng. “Long-term monitoring and identification of bridge structural parameters”. In: *Computer-Aided Civil and Infrastructure Engineering* 24.2 (2009), pp. 82–92.

- [65] Filippo Ubertini, Carmelo Gentile, and Annibale Luigi Materazzi. “Automated modal identification in operational conditions and its application to bridges”. In: *Engineering Structures* 46 (2013), pp. 264–278.
- [66] Graham Upton and Ian Cook. *Understanding statistics*. Oxford University Press, 1996.
- [67] MM Abdel Wahab and Guido De Roeck. “Damage detection in bridges using modal curvatures: application to a real damage scenario”. In: *Journal of Sound and vibration* 226.2 (1999), pp. 217–235.
- [68] Peter Welch. “The use of fast Fourier transform for the estimation of power spectra: a method based on time averaging over short, modified periodograms”. In: *IEEE Transactions on audio and electroacoustics* 15.2 (1967), pp. 70–73.
- [69] Lingmi Zhang, Tong Wang, and Yukio Tamura. “A frequency–spatial domain decomposition (FSDD) method for operational modal analysis”. In: *Mechanical systems and signal processing* 24.5 (2010), pp. 1227–1239.
- [70] Andrew T Zimmerman et al. “Automated modal parameter estimation by parallel processing within wireless monitoring systems”. In: *Journal of Infrastructure Systems* 14.1 (2008), pp. 102–113.

This Ph.D. thesis has been typeset by means of the T_EX-system facilities. The typesetting engine was pdfL^AT_EX. The document class was `toptesi`, by Claudio Beccari, with option `tipotesi=scudo`. This class is available in every up-to-date and complete T_EX-system installation.